Assessment of Cloride and Sulfate Concentrations in Concrete Using Laser-Induced Breakdown Spectroscopy (LIBS)

BY

Abdul-Jabbar A Al-Nehmi

A Thesis Presented to the
DEANSHIP OF GRADUATE STUDIES

KING FAHD UNIVERSITY OF PETROLEUM & MINERALS

DHAHRAN, SAUDI ARABIA

In Partial Fulfillment of the
Requirements for the Degree of

MASTER OF SCIENCE

In

Civil Engineering

October, 2012

KING FAHD UNIVERSITY OF PETROLEUM AND MINERALS

DHAHRAN 31261, SAUDI ARABIA

DEANSHIP OF GRADUATE STUDIES

This thesis is written by **ABDUL-JABBAR A AL-NEHMI** under the direction of his thesis advisor and approved by his thesis committee members, has been presented to and accepted by the Dean of Graduate Studies, in partial fulfillment of the requirements of degree of **MASTER OF SCIENCE IN CIVIL ENGINEERING**

Thesis Committee

Prof. Omar S Baghbrah Al-Amoudi (Advisor)

Prof. Mohammad A Gondal (Co-Advisor)

Prof. Mohammad Maslehuddin (Member)

Dr. Ahmed Saad Al-Qahtani (Member)

Dr. Salah Al-Dulijan (Member)

Dr. Nedal T. Ratrout
(Department Chairman)

16 OCT 2012

Dr. Salam A. Zummo
(Dean of Graduate Studies)

10/11/12

Date

DEDICATED TO

MY BELOVED PARENTS

AND

MY BROTHERS & SISTERS

ACKNOWLEDGMENT

First and foremost, thanks to ALLAH who gave me strength, patience and ability to accomplish this research.

Acknowledgment is due to the King Fahd University of Petroleum & Minerals for supporting this research.

I would like to appreciate and thank my thesis advisor, Prof Omar S. Baghabra Al-Amoudi, for his incessant guidance throughout thesis completion process. He has been available whenever I needed his guidance, assistance. Without his guidance and support, I would have never been able to organize and complete the thesis tasks on time.

I wish to express my sincere appreciation to Prof. Mohammed A.Gondal, my thesis co-advisor, for his leadership, guidance, and wonderful support extended to me during this investigation. Without his guidance and support, I would have never been able to initiate this thesis.

I wish to express my sincere appreciation to Prof. Mohammed Maslehuddin for his leadership, guidance, and wonderful support extended to me during my graduate study.

I also wish to thank the other members of my Thesis Committee, Dr. Ahmed Al-Gahtani and Dr. Salah Al-Dulijan, for their comments and suggestions.

Thanks are also due to the Department of Civil Engineering Department for providing all the available facilities.

I am also grateful to all faculty members for their encouragement and their direct or indirect help, such as Mr. M. Dastageer and Mr. Pillai in the Laser Laboratory as well as Eng. M Shameem and Eng. M. Ibrahim in the Center for Engineering Research Laboratory and others.

Finally, special thanks to all members of my family, my friends and colleagues for their support, prayers and encouragement.

TABLE OF CONTENTS

LIST OF FIGURES

LIST OF TABLES

Thesis Abstract Arabic

ملخص الدراسة

الاســـــــــم: عبدالجبار عبد ربه علي النهمي

عنوان الرسالة: تقييم تركيز الكلورايدات والكبريتات في الخرسانة بإستخدام تقنية تحليل إنهيار الليزر الطيفي (LIBS)

التخصـــــص: هندسة مدنية

تاريخ التخـرج: ذي القعدة 1433 هـ (أكتوبر 2012 م)

إن محتوى الكلورايدات والكبريتات في الخرسانة المسلحة يؤثر بشكل كبير على متانتها وديمومتها. وعادةً ما يتم تحديد تركيز هذه الأيونات بإستخدام التحليل الكيميائي، الإ أن هذه الإجراءات تستهلك الكثير من الجهد والوقت، كما إنها ليست دقيقة جداً. ولذلك، هناك حاجة إلى تطويراختبار غير إتلافي وسريع لتقييم وتركيز الكلورايدات والكبريتات في الخرسانة. إن تحليل انهيار الليزر الطيفي (LIBS) هي تقنية متطوره وسريعة، و تسمح بقياس جميع العناصر تقريباً على سطوح المواد الصلبة أوالسوائل أو الغازات وبدقة عالية.

تهدف هذة الدراسة إلى تقييم إمكانية استخدام LIBS لتقييم وتركيز الكلورايدات والكبريتات في الخرسانة. ولتحقيق هدف الدراسة، تم تحضيرعينات من العجينة الاسمنتية المحتوية على إسمنت النوع الأول (Type I) وإسمنت النوع الخامس (Type V) ، بلإضافة إلى غبار السيليكا (7٪)، والرماد المتطاير (30٪)، وبدرجات تركيز مختلفة من أملاح الكلورايدات والكبريتات. وتم اختبار العينات بإستخدام LIBS، وتقييم تركيز الكلورايدات والكبريتات من منحنى المعايرة المعد وبإستخدام تركيز معروف من هذه الأملاح. وتم مقارنة تركيز النتائج وتقييمها من LIBS مع تلك التي تم الحصول عليها بواسطة التحليل الكيميائي.

وأشارت نتائج هذة الدراسة إلى أن تقنية LIBS كانت ناجحة للغاية في تقدير تركيز الكلورايدات والكبريتات في الخرسانة.

درجة الماجستير في العلوم

جامعة الملك فهد للبترول والمعادن

الظهران - المملكة العربية السعودية

Thesis Abstract

Name: **Abdul-Jabbar A. Al-Nehmi**

Title: **Assessment of Chloride and Sulfate Concentrations in concrete Using Laser-Induced Breakdown Spectroscopy (LIBS).**

Major Field: **Civil Engineering**

Date of Degree: **October 2012**

The chloride and sulfate content in concrete significantly influences its durability. The concentration of these two ions is normally determined by chemical analysis. However, these procedures are exhaustive and time consuming. Therefore, there is a need to develop a non-destructive and quick test to assess the chloride and sulfate concentration in concrete. The laser-induced breakdown spectroscopy (LIBS) is a rapidly developing technique, which allows the measurement of almost all elements on the surface of solids, liquids or gases.

The objective of this study was to assess the possibility of utilizing LIBS for evaluating the chloride and sulfate concentration in concrete. To achieve this objective, cement paste specimens with Type I, Type V, silica fume (7%) and fly ash (30%) were prepared with varying concentrations of chloride and sulfate salts. The specimens were tested using the LIBS technique and the chloride and sulfate concentration was assessed from a calibration curve prepared with known concentrations of these salts. The chloride and sulfate concentration evaluated using LIBS was compared with that obtained by Inductive Couple Plasma (ICP).

Results of this investigation indicated that the LIBS technique was very successful in assessing the chloride and sulfate concentration in concrete.

MASTER OF SCIENCE DEGREE
KING FAHD UNIVERSITY OF PETROLEUM AND MINERALS
DHAHRAN, SAUDI ARABIA

CHAPTER 1

INTRODUCTION

1.1 GENERAL

Deterioration of reinforced concrete structures in the Arabian Gulf has been mainly attributed to chloride-induced reinforcement corrosion. Degradation of concrete due to sulfate attack and/or salt weathering has also been noted in the marine structures and those built on sabkha terrains. Several industrial utilities of Saudi ARAMCO, SABIC, SEC, SWC, etc., and private buildings are exposed to harsh environments and are prone to deterioration and, hence, they require frequent repair and rehabilitation. However, prior to repair, it is essential to assess the causes and extent of deterioration. For example, for the repair of concrete structures suffering from reinforcement corrosion, it is essential to ascertain the chloride concentration profile. Further, the chloride concentration profiles are required to determine the time to initiation of reinforcement corrosion and, hence, the useful service life. The sulfate concentration in concrete is required firstly, to assess that it is less than that specified for cement from the point of view of setting, and secondly to understand the role of sulfate ions on reinforcement corrosion and deterioration of concrete due to sulfate attack.

The existing analytical techniques, such as ICP (Inductive Couple Plasma), XRD (X-Ray Diffraction) and XRF (X-Ray Fluorescence), etc., are very time consuming and the sampling procedure is tedious. Therefore, there is a need to develop a cost effective, fast and reliable test method for the assessment of concrete composition, particularly the concentration of chlorides and sulfates. The laser-induced breakdown spectroscopy (LIBS) technique has been evaluated in this study to determine the chloride and sulfate concentrations.

1.2 ADVANTAGES AND DISADVANTAGES OF LIBS

There are advantages and disadvantages of this technique. First of all, LIBS technique has little sample preparation. This is an advantage because it eliminates possible

contaminations and loss of analyte throughout the sample preparation steps. Besides, LIBS may be easily applied to all forms of samples (i.e., solid, liquid and gas). Even analyses of very hard samples, are permitted. For solid samples, depth profiling and lateral resolution is possible. This advantage arises from the fact that LIBS systems use only small amounts of sample. Craters with a few micrometers of diameters are obtained with suitable optics. With the use of fiber optic cables, LIBS system can be applied as a remote analysis technique. Furthermore, the compact portable LIBS set-ups enable field analysis. One of the major advantages of LIBS is its speed and ability to make multi-elemental analysis. By using suitable spectrograph equipped with a multi-channel detector, analysis of dozens of elements in a single laser shot may take just a second.

Contrary to the advantages of LIBS, there are few disadvantages. Since the energy of laser may vary from one shot to another, the response monitored changes. This 5-10% energy variation may lead to a problem during low level of quantification. Therefore, in order to eliminate this disadvantage, several measurements may be averaged. Also, during the analysis of solids, the surface composition may be different from the bulk composition. Since the crater formed by the focused beam is just a few micrometers in size and depth, the investigated area may not be a representative of the whole sample. As a result of the above facts, the analytical figures of merit are not as good as the other widely used atomic spectroscopic techniques such as ICP. The detection limits are in the range of hundreds of ppb, (μg/l), to ppm, (mg/l), levels, but are improved by new studies [41].

1.3 NEED FOR THIS RESEARCH

The Kingdom of Saudi Arabia spends considerable amount of funds and resources for the repair and rehabilitation of buildings, and industrial and other concrete structures, especially offshore and onshore. The type and extent of repair and rehabilitation processes are dependent on the accurate analysis of the causes of deterioration. For failures due to reinforcement corrosion, the determination of chloride and sulfate concentration profiles is very important in deciding the extent of repair. Damage of reinforced concrete structures, due to corrosion of the reinforcing steel, particularly in

the coastal and off-shore areas (offshore platforms or buildings located in sabkha terrains or near sea shores), or concrete deterioration by the aggressive sulfate and salty waters, would require rapid and on-line testing methods for reliable condition assessment of the concrete structures and quality assurance for repair methods. The available analytical techniques, such as ICP, XRD, XRF, Prompt Gamma Neutron Activation Analysis (PGNAA), etc., are relatively expensive, tedious and time consuming. Further, most of these techniques require obtaining power sample or coring specimens for testing and analysing the chloride and sulfate concentrations. Therefore, there is a need to develop a cost effective, fast and reliable test method for the assessment of concrete composition, particularly the concentration of chlorides and sulfates. The new laser-induced breakdown spectroscopy (LIBS) technique has been utilized for this purpose.

1.4 SCOPE AND OBJECTIVES

The scope of this study was to develop LIBS spectrometer for the detection of trace elements, particularly the chlorides and sulfates, in concrete. Samples of known concentrations of chloride and sulfates were prepared in the form of pellets. Calibration was then carried out based on the measured concentration of these known samples.

Plain (Type I and Type V) and blended (fly ash and silica fume) cement paste specimens were prepared. The mixture composition of these concrete specimens was similar to that commonly utilized by the construction industry. The cement paste specimens were contaminated with varying concentrations of chloride and sulfate salts. These specimens were utilized to determine other elements, such as Si, Al, Ca, Mg, Na, etc.

The overall objective of this study was to evaluate the possibility of utilizing LIBS technique for determining the chloride and sulfate concentrations in specimens.

The specific objectives of the study were as follows:

1. To develop a Laser Induced Breakdown Spectrometer (LIBS) for civil engineering applications;

2. To test the spectrometer for the determination of concrete composition, particularly the chloride and sulfate concentration; and

3. To verify the accuracy of the results obtained by LIBS with the actual concentrations.

CHAPTER 2
LITERATURE REVIEW

2.1 BACKGROUND INFORMATION

The presence and/or diffusion of chloride and sulfate ions in concrete will ultimately lead to its deterioration due to corrosion of reinforcing steel and sulfate attack, respectively. These ions could diffuse from external sources or they may be contributed by the concrete mixture ingredients [1-4]. The diffusion of sulfate ions constitutes a major risk of chemical aggression for concrete. The progressive loss of strength and mass caused by the deterioration of the cement hydration products may endanger the concrete structures [2]. Sulfate ions from external sources, such as sewage treatment plants or sulfate-rich soils, can diffuse into the concrete leading to its degradation. As many industrial and non-industrial installations and utilities are exposed to marine and sabkha environments, the ingress of chloride and sulfate ions is highly probable and deterioration can occur much ahead of the designed service life of a structure. The major contributor to corrosion in the Kingdom of Saudi Arabia is the harsh environment characterized by high humidity, high temperature, and high contents of salt, especially in the coastal regions of Saudi Arabia [5].

In order to evaluate the consequences of chloride-sulfate diffusion on sustainability and durability of concrete structures, the following steps are essential [6-11]:

- The chloride and sulfate concentration profiles have to be measured in order to decide to what extent the contaminated concrete has to be removed.

- The chloride concentration profile is also required to calculate the chloride diffusion coefficient. The determination of chloride diffusion coefficient allows the prediction of useful service life of structures and the optimum duration for their maintenance and/or repair.

Therefore, the detection and monitoring of concrete structures require a detailed knowledge of the spatial distribution of chloride and sulfate contents. This requires extremely sensitive and highly selective detection techniques for monitoring the chloride and sulfate contents. Such techniques should fulfil the following criteria [6-11]:

- Detection of several elements with a single instrument/technique;
- High sensitivity in order to permit precise detection of very low concentrations;
- High selectivity in order to differentiate between the different species present in a multi-component concrete mixture;
- Rapid testing with no sample preparation and chemical requirement;
- Low cost;
- Good temporal resolution to enable on-line monitoring; and
- Good portability for in-situ and remote measurements.

The currently available conventional and analytical methods for inspection of reinforced concrete do not fulfil the above-mentioned criteria. Most of these methods rely on collection of test samples, transporting them to a distant laboratory and, thereafter, preparing them for treatment.

Laser-based sensing techniques [6-11] are superior to the conventional analytical methods because the sample does not require transportation to a remote analyzer. Further, these techniques may be used to analyze samples from locations that are normally inaccessible. The main advantages of laser sensors are being remote in testing with non-intrusive measurements; high sensitivity; high selectivity; large area coverage; and short time measurements, which are not possible with the conventional methods, such as ICP (Inductive Couple Plasma), AA (Atomic Absorption) and PGNAA (Prompt Gamma Neutron Activation Analysis) [6-11].

2.2 PRINCIPLES OF LIBS

Laser-induced breakdown spectroscopy (LIBS) is a totally multi-elemental analytical method based on the measurement of atomic emission lines from laser plasma generated

at a sample surface. Due to its tremendous potential advantages over the conventional elemental and analytical techniques, LIBS related research and applications have been widely investigated since its invention in 1960's. From the previously published papers and books [6-20], it is easy to conclude that LIBS is a versatile, quantitative and multi-elemental analytical approach that can be applied in many areas for the analysis of almost all kinds of samples.

Practically speaking, in LIBS, a short laser pulse is focused on the sample which evaporates a small amount of the material (typically a few micrograms) creating a plasma plume. The light emitted by plasma is spectrally resolved to determine the chemical composition of the targeted material. The light intensity is measured as a function of the wavelength, i.e., the spectrum. Due to the high temperature in the plasma (about 10,000^{o} K), all chemical bonds are broken and the partially ionized atoms are excited. Thus, the information about the elements in the evaporated mass is available. The content of the damaging species can be calculated directly from the elemental content. The intensity of spectral lines of chlorine and sulfur is very weak compared with oxygen or calcium spectral lines.

There is growing interest in the development of sensors for rapid and accurate analytical characterization of chemical species present in rocks, minerals, metallurgy, waste disposal sites, soil and water samples and many other applications [6-11]. More efficient techniques are now replacing the conventional, time-consuming and laborious techniques of wet-chemical analysis. The volume of measurements to be performed in current processing systems has a prohibitive cost in order to acquire samples and to take them to a laboratory for analysis. To overcome the huge costs and other logistic problems, new methods are required, which will perform remote measurements quickly and efficiently. Innovative laser-based techniques are being developed for real time analysis of minerals, rocks, and contaminated samples. In particular, LIBS is a sensitive and selective technique for achieving the objectives for such measurements [6-20]. In this method, a laser source serves to vaporize, atomize and excite the sample material in the course of a laser pulse. The resulting emission is collected by a lens and analysed

with an optical multi-channel analyser (optical spectrometer) or with a scanning monochromator in conjunction with a photomultiplier. LIBS has been used for the analysis of gases, liquids, solids, solid aerosols, liquid aerosols and soils [6-11].

Gondal et al. [9] designed an acoustically resonant CO_2 laser photoacoustic (PA) spectrometer for remote or in-situ monitoring of air pollutants. The system has been applied for the detection of pollutants emitted from the exhaust of a car located at a remote distance. Further, an alarm system based on the PA detection technique has been built for leak detection of toxic gases at industrial complexes. The minimum detectable concentration of C_2H_4 and SO_2 with this system was 50 parts in 10^{12} by volume and 50 parts in 10^9 by volume, respectively.

Differential absorption lidar (i.e. light detection and ranging), "DIAL" system has been applied for the analysis of clouds and for detection of SO_2 and NO_2 pollutants. The maximum range achieved with this system for cloud analysis was 11 km above the earth surface. The lidar data indicated that the thickness varied from 0.8 to 3.6 km at various times [11].

A trace concentration of SO_2 near 225.7 nm transition line has been detected with a master-oscillator power-oscillator (MOPO) laser system for the first time by Gondal et al [10]. A photoacoustic absorption spectrum of SO_2 has been recorded on the $1A_2$–$1B_2$ (π–π^*) transition. Parametric dependence of the photoacoustic signal has been investigated. A detection limit (signal-to-noise ratio of 1) of 1.3 parts in 109 [1.3 ppbv (parts per billion by volume)] for SO_2 has been determined at 1 atmospheric pressure inside a photoacoustic cell.

LIBS system has been applied for the elemental analysis of Arabian crude oil residue samples. The spectra due to trace elements, such as Ca, Fe, Mg, Cu, Zn, Na, Ni, K and Mo, were recorded using this technique. The dependence of time delay and laser beam energy on the elemental spectra was also investigated. The results achieved through this method were compared with conventional technique like inductively-coupled plasma

(ICP) and the results achieved were in agreement with the conventional techniques such as ICP spectrometry. Multi-elemental analysis for trace metals present in the Arabian light crude oil residue sample was carried out using LIBS for the first time. The parametric dependence of LIBS signal and the elemental composition of oil residue sample were investigated. This work demonstrated that LIBS technique, for waste crude oil, was equally applicable and did not need as much sample preparation as other analytical methods, such as ICP and atomic absorption spectrometry [7].

Gondal et al. [6] developed LIBS for the determination of toxic metals in wastewater collected from local paint manufacturing plant. The plasma was generated by focusing a pulsed Nd:YAG laser at 1064 nm on the solid residue from wastewater collected from paint industry. The concentration of different elements of environmental significance, like lead, copper, chromium, calcium, sulfur, magnesium, zinc, titanium, strontium, nickel, silicone, iron, aluminum, barium, sodium, potassium and zirconium, in paint wastewater were 6, 3, 4, 301, 72, 200, 20, 42, 4, 1, 35, 120, 133, 119, 173, 28 and 12 mg kg^{-1}, respectively. The LIBS results were compared with the results obtained using standard analytical technique such as inductively coupled plasma emission spectroscopy. The relative accuracy of LIBS system for various elements as compared with ICP method was in the range of 0.03–0.6 at 2.5% error confidence.

Gondal et al. [8] studied the role of various binding materials, like potassium bromide, poly-vinyl alcohol, starch, silver and aluminum for trace elemental analysis of powder samples using LIBS. The matrix effects using these five binders on LIBS signal intensity was investigated for better performance of LIBS technique as a quantitative analytical tool. The signal intensity of different magnesium (Mg) lines at 518.3, 517.2, 383.8 and 279.5 nm wavelengths were recorded for pellets prepared with known concentrations of Mg in these binders for comparative study of different binders. The influence of laser energy on ablated mass under different binding materials and its correlation with LIBS signal intensity has been explored. Optical scanning microscopy images of the ablated crater were studied to understand the laser ablation process. The study revealed that the binding material plays an important role in the generation of

LIBS signal. The relative signal intensity measured for a standard Mg line (at 518.3 nm) were 735, 538, 387, 227 and 130 for potassium bromide, starch, poly(vinyl alcohol), silver and aluminum as binders, respectively. This indicated clearly that potassium bromide was better as a binder for LIBS studies of powder samples.

LIBS was applied for quantitative elemental analysis of slag samples collected from a local steel plant using an Nd: YAG laser emitting radiation at 1064 nm wavelength. The concentration of different elements of environmental significance, such as cadmium, calcium, sulfur, magnesium, chromium, manganese, titanium, barium, phosphorus and silicon were 44, 2193, 1724, 78578, 217260, 22220, 5178, 568, 2805, 77871 mg/kg , respectively. The concentrations determined with LIBS were compared with the results obtained using ICP emission spectroscopy. The study demonstrates that LIBS could be highly appropriate for rapid online analysis of iron slag waste. Relative accuracy of the LIBS system for various elements in comparison with the method of ICP in the range 0.001 to 0.049 confidence in the error of 2.5%, which is good and acceptable result [12].

Gondal et al. [13] applied LIBS system for the identification of various kinds of plastics for management and recycling of plastic waste. A laser-produced plasma emission was recorded for spectral analysis of the 6 main family of plastics: Low Density Polyethylene (LDPE), High Density Polyethylene (HDPE), Polypropylenes (PP), Polystyrene (PS), Polyethylene Terephthalate (PET) and Polyvinyl chloride (PVC). The plasma was generated by focusing an Nd: YAG laser radiation at wavelength of 1064 nm having laser energy of 40 mJ. The LIBS signal intensity measured for carbon and hydrogen was detrimental for the fingerprinting of various kinds of plastics. The C/H line intensity ratio was 1.68, 1.51, 1.42, 1.16, 1.01 and 0.91 for HDPE, LDPE, PS, PP, PET and PVC, respectively. The detection limits of carbon and hydrogen were found to be approximately 6 micro g/g by applying 20 laser shots. The unique features of LIBS were: it is a simple, rapid, remote, real-time analysis without sampling requirements. The study demonstrated that LIBS could be applied as a best tool for sorting out different kinds of plastics on a fast scale for waste management. The health hazards of different kinds of plastics were also described.

LIBS has been applied for the determination of contaminants present in ore samples by Gondal et al. [14]. The plasma was generated by focusing a pulsed Nd: YAG laser radiation at 1064 nm wavelength on the ore sample collected from one of the open-pit mines located in Saudi Arabia. The concentrations in this ore sample of different elements of environmental significance like Cu, Cr, Ca, Mg, Zn, Ti, Si, Fe and Al were determined by spectral analysis. Parametric dependence for improvement of LIBS sensitivity was carried out. The LIBS results were compared with the results obtained using other analytical techniques such as ICP. Limits of detection (LOD) of the LIBS system were also calculated for the elements under investigation.

A number of international research groups are developing LIBS systems for remote sensing of atmospheric pollution, non-intrusive analysis of hazardous materials, and fiber optics-based systems for in-situ analysis [15-19]. Parts of the findings of these research groups are highlighted below.

Knopp et al. [17] applied LIBS to analyze aqueous solutions of Li^{+}, Na^{+}, Ca^{2+}, Ba^{2+}, Pb^{2+}, Cd^{2+}, Hg^{2+} and Er^{3+} and suspensions of $ErBa_2Cu_3Ox$ particles (d=0.2 µm). An excimer (308 nm) pumped dye laser with laser pulse at 500 nm and pulse energy at $22^{+/-2}$ mJ was used to produce plasma in aqueous solution. Plasma emission lines of the elements were detected by a photodiode array detector. Detection limits of the metal ions were 500 mg/l for Cd^{2+}, 12.5 mg/l for Pb^{2+}, 6.8 mg/l for Ba^{2+}, 0.13 mg/l for Ca^{2+}, 13 µg/l for Li^{+} and 7.5 µg/l for Na^{+}. No mercury and erbium emission could be detected, even at Hg^{2+} and Er^{3+} concentrations of up to the g/l range. On the other side, for Er in suspensions of $ErBa_2Cu_3Ox$ particles, a more than 10^3 times higher sensitivity was found than for dissolved Er^{3+}. This result gave a possibility to analyze colloid-borne metal ions with an increased sensitivity.

Noll et al. [18] used LIBS as an online monitoring method to measure alkali metals, which influence energy and mass flow in the furnace. Direct analysis of liquid steel reduces processing times in secondary metallurgy. By using sensitivity-enhanced LIBS,

limits of detection of approximately10 µg/g and below were achieved for light and heavy elements in liquid steel. The process control in steel production relies on the results from the chemical analysis of the slag. A prototype of an analytical system was developed using LIBS to analyze slag samples two times faster than with conventional methods. The cleanness of steel was a key issue in the manufacturing of spring steel, thin foils and wires. Microscopic inclusions had to be determined quickly. A scanning microanalysis system based on LIBS was developed with measuring frequencies up to 1 kHz and a spatial resolution of <15 µm. For the final inspection of the steel grade of pipe fittings, an inspection machine using LIBS was developed and introduced into routine industrial used to detect material mix-ups.

Solle et al. [19] studied the influence of the ambient pressure (50 mTorr in air to begin to simulate the Moon or asteroids, 7 Torr of CO_2 for Mars, and atmospheric pressure in air for the Earth) on the calibration curves prepared from certified soil and clay pellets. The results show that useful calibration curves can be obtained at reduced pressure without temporal resolution of the emission signal. The best linear regression coefficient and the best repeatability are obtained at 7 Torr of CO_2 for Martian conditions. LIBS method was used at reduced pressure (7 Torr CO_2 to simulate the Martian atmosphere) and near vacuum (50 mTorr in air to begin to simulate the Moon or asteroids' pressure) as well as at atmospheric pressure in air (for Earth conditions and comparison). In-situ corresponds to distances on the order of 150 mm in contrast to stand-off analysis at distance of many meters. The influence was shown of the ambient pressure on the calibration curves prepared from certified soil and clay pellets. An Echelle spectrograph was used to detect simultaneously all the elements commonly observed in the terrestrial soil.

Hussian et al. [15] developed LIBS system locally for the determination of toxic metals in liquid samples and the system was tested for the analysis of wastewater collected from dairy products processing plant. The plasma was generated by focusing a pulsed Nd: YAG laser at 1064 nm on wastewater samples. Optimal experimental conditions were evaluated for improving the sensitivity of LIBS system through parametric

dependence investigations. LIBS results were then compared with the results obtained using standard analytical technique, such as ICP. The values obtained with LIBS setup were in well agreement with the ICP results. The accuracy of an analytical method was defined as how close the measured experimental values to accepted values measured with standard technique like ICP. The relative accuracy was in the range of 0.01–0.4, which is quite acceptable for any good instrument.

Hussian et al. [16] used LIBS to detect trace metals present in oil spill contaminated soil samples. The concentrations of trace metals present in oil spill samples were estimated and results achieved were in good agreement with the conventional technique, such as ICP. The concentration measured and verified by ICP method for Ba (~5 ppm) and Cr (~6 ppm) were higher than the permissible safe limits. The parametric dependence of signal intensity for improvement of the sensitivity of LIBS spectrometer was also carried out.

The group at IFAM-CNR [20] has been conducting extensive research for the development of a LIBS-based system for the analysis of polluted water with the main emphasis on developing diagnostic devices for in-situ continuous monitoring. The method presented, based on an algorithm developed and patented by IFAM-CNR, allowed the matrix effects to be overcome, yielding precise and accurate quantitative results on elemental composition of materials without the use of calibration curves. Some applications of the method were illustrated for quantitative analysis of the composition of metallic alloy and quantitative determination of the composition of the atmosphere.

There are many groups interested in the development of LIBS systems for field studies [21-35]. Anderson et al. [21] in Sweden have evaluated the influence of sewage sludge applications to soil on trace element enrichment of soils and plants and applied LIBS for the detection of heavy metals in soil samples, and a detection limit of 200 ppb was achieved.

Kagowaet et al. [22] studied the characteristics of the plasma, namely the spatial distribution of the emission intensity, the time behaviour of the spatial displacement and the excitation temperature, under various conditions of the surrounding gas (pressure range between 0.02 and 6 torr in He, Ar, N_2 and CO_2). Most of the experimental results were explained fairly well on the basis of a hypothetical model in which the shock wave plays an important role in forming the luminous plasma. It was found that argon would be most suitable as the surrounding gas when the plasma is used for practical spectrochemical analysis.

St-onge et al. [26] used laser-induced plasma spectrometry (LIPS) for the quantitative analysis of Al, Cu, Fe, Pb and Sn components in solid zinc alloys. Laser-induced plasmas were characterized using spectroscopic diagnostic techniques that yield the excitation temperature and density. Optimal experimental conditions for analysis were evaluated including time gating parameters and distance from focusing lens to target where it was found that the focus of the laser beam should be positioned behind the target in order to prevent secondary air plasmas from forming in front of the target.

Panne et al. [35] used laser-induced plasma spectrometry (LIPS) for the analysis of glass and glass melts during the verification process of fly and bottom ashes. The LIPS analysis of glass main components (Si, Al, and Ca) in a verification process of fly and bottom ashes, a normalization procedure for line ratios was presented. As a result of variations in the material laser interaction, strong pulse-to-pulse fluctuations of the plasma electronic excitation temperature and electron density influencing the relative intensities of single emission lines were observed. For sample, with high aluminum concentrations, problems with self-reversal effects were detected by utilizing a simple numerical indicator.

Samek et al. [27] applied LIBS for the detection of hazardous metallic contents in liquids. Most of the measurements were conducted using a fiber assembly that was capable of both delivering the laser light and collecting the light emitted from the micro plasma, up to about 30 min from the target area. Alternatively, a telescopic arrangement

for line-of-sight measurements was employed, with a range of 3 to 5 m. For internal standardization and the generation of concentration calibration curves, reference lines of selected elements were used. In the majority of cases, calibration against the matrix element, hydrogen was employed using the Hα, Hβ, and Hγ lines, but also spiking with selected reference species was utilized. In order to provide high reliability and repeatability in the analyses, plasma parameters were measured such as electron density, plasma temperature, and line-shape functions, and determined their influence on the measurement results. Numerous elements, including a range of toxic heavy metals, have been measured over a wide range of concentrations (Al, Cr, Cu, Pb, Tc, U, and others). Limits of detection were usually in the range of a few parts per million; for elements.

Fink et al. [32] applied LIPS for the analysis of recycled thermoplasts from consumer electronic. An experimental setup for direct elemental analysis of recycled thermoplasts from consumer electronics by LIPS or LIBS was realized. The combination of an echelle spectrograph, featuring a high resolution with a broad spectral coverage, with multivariate methods, such as PCR (Principal Component Regression), PLS (Partial Least Squares), and variable subset selection via a genetic algorithm, resulted in considerable improvements in selectivity and sensitivity for this complex matrix. The limits of detection were in the ppm range with normalization to carbon as internal standard. Several experiments at an extruder within a recycling plant demonstrated successfully the capability of LIPS for different kinds of routine on-line process analysis.

Panne et al. [31] used LIPS for remote analysis of a mineral melt. The performance of a customized mobile LIPS system, based on a Nd:YAG laser for plasma ignition and an echelle spectrometer with an intensified charge-coupled device (CCD) camera, was tested during a field campaign for in-situ and on-line process analysis of major constituents in a mineral melt of 1600 °C. After an optimization of the instrumental parameters, such as irradiance, gate width, and delay of the integration time relative to the laser pulse, LIPS allowed the on-line identification of all elements relevant for mineral wool production (i.e., Ti, Fe, Mn, Mg, Ca, Si, Na, and Al) directly from the

melt in a rather harsh industrial environment. Validation of the LIPS analysis was performed via manual sampling and X-ray fluorescence (XRF) analysis.

Kumar et al. [33] used LIBS for the first time to distinguish normal and malignant tumor cells from histological sections. The concentration of trace elements in normal and tumor cells was significantly different. For comparison, the tissue samples were also analyzed by an inductively coupled plasma emission spectroscopy (ICPES) system. The results from the LIBS measurement and ICPES analysis were in good agreement.

Radivojevic et al. [34] applied a new setup of LIPS in the vacuum ultraviolet (VUV) for microanalysis. The system features an integrated ablation and detection module with a newly-designed VUV echelle system that allowed a full spectral coverage between 150 and 300 nm with a resolving power $\lambda/\Delta\lambda$, which is the ability of a spectrometer to separate two adjacent peaks in a spectrum, between 11,000 and 15,000. At present, the ablation module permits a microanalysis with a crater size of 25 μm and a nominal depth resolution with an ablation rate of 150 nm/pulse. The VUV performance was demonstrated for bulk analysis of steel; detection limits for sulfur, carbon, and phosphorus were in the lower milligram per kilogram range.

Ismail et al. [25] studied limits of detection for several elements in aluminium and steel alloys, at atmospheric pressure in air, by the use of single and collinear double pulse configurations of LIBS. Calibration plots were constructed for Mg, Al, Si, Ti, Cr, Mn, Fe, Ni, and Cu using a set of certified aluminium alloy samples and a set of certified steel samples for this purpose. The investigation included optimization of the experimental conditions to furnish the best signal to noise ratio. Inter-pulse delay, gate width, and acquisition delay were studied. The detection limits for the elements of interest were calculated under the optimum conditions for the double-pulse configuration and compared with those obtained under the optimum conditions for single-pulse configuration. Significantly improved detection limits were achieved, for all the elements investigated, and in both aluminium and steel, by the use of double-

pulse configuration. The extent of the improvement was larger for aluminium alloys than for steel.

Adamson et al. [23] used LIBS at a water/gas interface. A study of bath gas-dependent molecular species was conducted at the interface of a bulk pure water sample and three bath gases: air, nitrogen, and argon. The temporal evolution of the laser-created plasmas as well as their dependence on incident laser pulse energy has been studied. Specifically, the emission from the two strongest observed hydrogen transitions and specific vibrational band emissions from two molecular transitions in OH and NH were studied to determine the experimental parameters necessary for optimal signal-to-background, signal-to-noise, and total absolute emission intensity. As well, plasma parameters, such as the excitation temperature and electron density, were calculated from the ratio of hydrogen transition emission intensities and the stark broadening of those transitions. The extreme longevity (out to 40 μs) of emission from the hydrogen-containing molecules could provide a sensitive probe of the liquid matrix allowing a measurement to be made at far-extended gate delay times where contributions from background continuum emission and other sources of noise may be eliminated.

Mateo et al. [28] used LIBS for the analysis of ceramic raw materials (brick clays and kaolin) submitted to laser ablation in the form of pressed pellets. Standard single-pulse LIBS technique and orthogonal reheating double-pulse LIBS provided spectrographic study. It was found that both methods are comparable in terms of analytical performance if adequate experimental parameters and signal detection systems are used. Silicate raw materials for brick-and-tile industry in the form of pressed pellets were examined by LIBS. Two different LIBS systems were applied to analyze the elemental composition and to carry out the calibration curves. The observation by optical microscopy of silicate material behavior during laser ablation leads to the necessity to apprehend the examined samples as complex materials instead of the set of contained elements. For that reason, it was found to be more precise to use the group of most important constituents of the material to construct the calibration curve. The best solution with respect to analytical performance was the double-pulse LIBS with Echelle

spectrograph. On the other hand, the double-pulse method demanding two lasers in orthogonal configuration was not convenient for fast and simple in-situ analysis. Preferable system to be applied directly to the industry was single pulse LIBS with high-resolution multi-elemental detection device.

Ctvrtnickova et al. [29,30] developed LIBS for multi-layered samples. In a typical LIBS experiment, an optical restriction consisting of a pinhole placed between the dichroic mirror and the collecting lenses was used. The optical approach allowed observing only the light emission coming from the central region of the plume. The micro-plasma was created on the sample by a pulsed Nd:YAG laser operating at 1064 nm with a homogeneous distribution of energy across the beam. Light emitted by the micro-plasma was detected with an intensified charge-coupled device (ICCD) multi-channel detector. The effect of pinhole diameter and the delay time influence on depth analysis were assessed. An ablation range of only a few nanometers per pulse has been achieved. Depth profiles of various metals (Cr, Ni, Cu) from multi-layered samples were generated by LIBS and depth resolution at different delay times using various pinhole diameters was calculated and compared.

Gondal et al. [36] have recently used a new atomic line at 594.8 nm of neutral chlorine (Cl I) as a marker to quantify the amount of chloride present in the concrete samples using LIBS. Although the relative intensity of the 594.8 nm line is 1000-fold less intense than that of the most commonly used atomic line of Cl I at 837.5 nm reported in the literature, the limit of detection of chlorine achieved with set-up in the concrete sample using the new line was comparable with the 837.5 nm. This clearly indicates that the sensitivity of the LIBS system for detection of chlorine in concrete sample using 594.8 nm was at least 1000-fold intense more than the one using 837.5 nm, which can be attributed to the characteristic of less self-absorption. LIBS data for different concentration of chloride content in concrete samples were also carried out and a calibration curve was drawn.

Gondal et al. [37] have recently developed a dual-pulsed laser-induced breakdown spectrometer for the detection of chloride contents in concrete using two atomic transition lines of neutral chlorine (ClI) at 594.8 and 837.5 nm. A calibration curve was also established using standard samples containing chloride with known concentrations in the concrete. The dual-pulsed LIBS system demonstrated a substantial improvement in the signal level at both wavelengths (594.8 and 837.5 nm). However, the new atomic transition line at 594.8 nm shows a significant improvement compared to the line at 837.5 nm in spite of the fact that the relative intensity of the former is 0.1% of the latter.

Gondal et al. [38] employed a dual pulsed LIBS system for the detection of sulfur in concrete structures. The detection of weak spectral line of sulfur in concrete using the SII (i.e. ionized sulfur) peak was attained at 545.38 nm as a marker for quantifying sulfur content in the concrete. The atomic emission lines of sulfur lying in the 200–900 nm region do mostly exist in singly ionized states and, hence, inherently very weak. The limit of detection achieved with dual pulsed LIBS system was approximately 38 μg/g. The dual pulsed LIBS system and the fine maneuvering of the gate parameters and inter-pulse delay yielded improvement in the sensitivity, and resulted in a systematic correlation of the LIBS signal with the concentration of sulfur in the concrete sample. In order to quantify the sulfur content in concrete, a calibration curve was also drawn by recording the LIBS spectra of sample having sulfur in various concentrations.

Weritz et al. [45] used LIBS for the investigation of the sulfur content of concrete. Sulfur compounds were a natural but minor component in building materials. The sulfur spectral line at 921.3 nm was used for quantitative determination. The comparison of measurements accomplished under air, argon and helium atmosphere has determined the optimum ambient atmosphere. Reference samples have been produced and calibration curves have been determined, and the results of LIBS measurements were compared with results from chemical analysis. Defining a limit for the intensity ratio of calcium and oxygen spectral lines reduced the influence of the heterogeneity of the material, so that only spectra with a high amount of cementitious material were evaluated. Depth

profiles and spatial-resolved sulfur distributions were measured on concrete cores originating from a highly sulfate contaminated clarifier.

CHAPTER 3

METHODLOGY OF RESEARCH

3.1 LASER INDUCED BREAKDOWN SPECTPOSCOPY (LIBS)

LIBS technique uses a high peak power laser to disintegrate a sample of a desired material into excited atoms and ions resulting in plasma formation. During the early stages of the plasma development (less than 10 microseconds), the plasma temperature goes up to 10,000° to 25,000°K. At this very high temperature, the plasma has sufficient energy to break molecular bonds to form constituent atoms and excite electrons of neutral atoms and ions into excited electronic states. Hence, all chemical bonds are broken resulting in highly excited, and unstable atoms, ions and free electrons. The free electrons are absorbed by the atoms and ions in the plasma, resulting in a continuum emission. As the plasma cools, characteristic photons are emitted as the excited ions and atoms stabilize, resulting in the formation of the ionic and atomic emission lines of the elements, i.e. the spectrum. Each element has a unique spectrum of atomic and ionic emission lines. The emitted light from the laser-induced plasma can be collected and used to provide information on the elemental composition of the material by means of spectroscopy [43].

There are several key advantages to LIBS that can be beneficial for an on-line monitoring and diagnosis. LIBS is a non-contact, minimally destructive test. It requires the light collected from the plasma created by the laser and destroys an insignificant amount of particles (i.e. in the tens of nanograms). Because LIBS is an optical technique, it can be used for deployment in hostile environments. After sufficient calibration, LIBS requires no sample preparation, which makes it a candidate for development of a portable system, easily deployed for field use [43].

LIBS operates by focusing the laser onto a small area at the surface of the specimen, which can be a gas, liquid, aerosol or solid. When the laser is discharged, it ablates a very small amount of material, in the range of 1 μg, which instantaneously superheats generating a plasma plume with temperatures of ~10,000°K, as illustrated in Figure 3.1.

At these extreme temperatures, the ablated material dissociates (breaks down) into excited ionic and atomic species. During this time, the plasma emits a continuum of radiation which does not contain any useful information about the species present. However, within a very small timeframe (microseconds), the plasma expands at supersonic velocities and cools. At this point, the characteristic atomic emission lines of the elements can be observed [24].

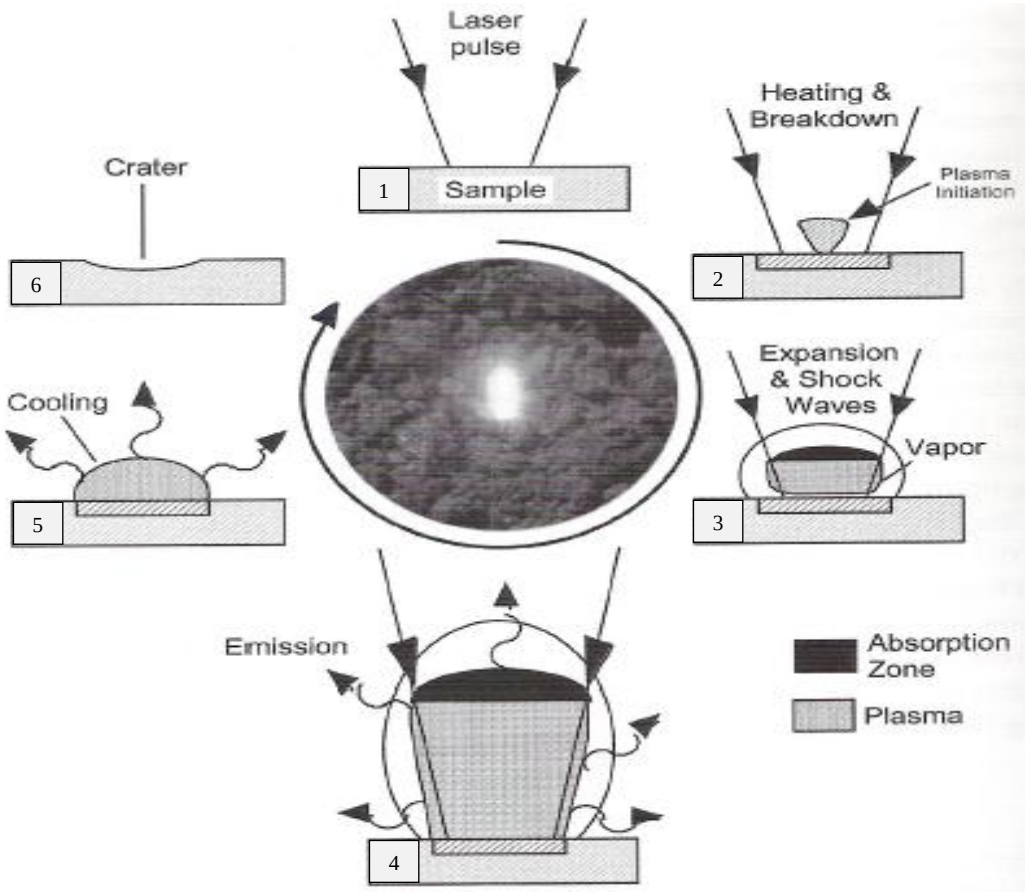

Figure 3.1: Life cycle diagram showing main events in the LIBS process [24].

The radiation of plasma is collected by lenses or fiber optics. The signal is sent to a spectrograph with a gated detector such as a photomultiplier tube (PMT) an intensified optical multichannel analyzer (OMA) or an intensified charge-coupled device (ICCD), as shown in Figure 3.2. A digital delay generator is used to gate the detector. The detector remains off for a certain amount of time after receiving a trigger pulse from the

laser, until a signal from the delay generator is received (t_d), as shown in Figure 3.3. In Figure 3.3, t_d represents the delay from the initiation of the laser to the opening of the detector window; t_b represents the length of that window [40]. A computer is used for data storage [39,40].

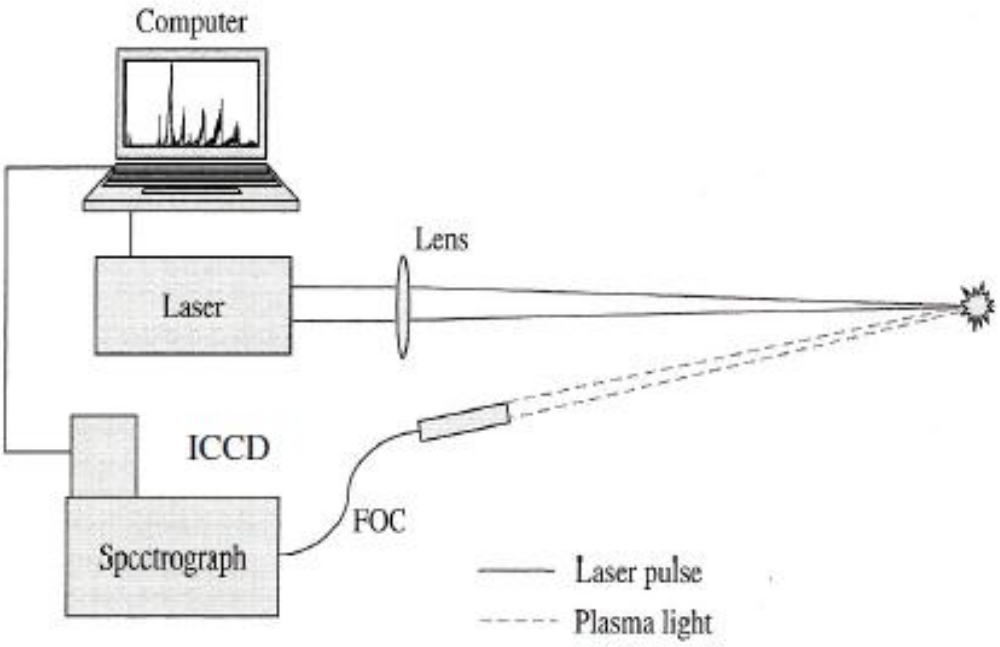

Figure 3.2: A schematic of a simple apparatus for LIBS illustrating the principal components [39].

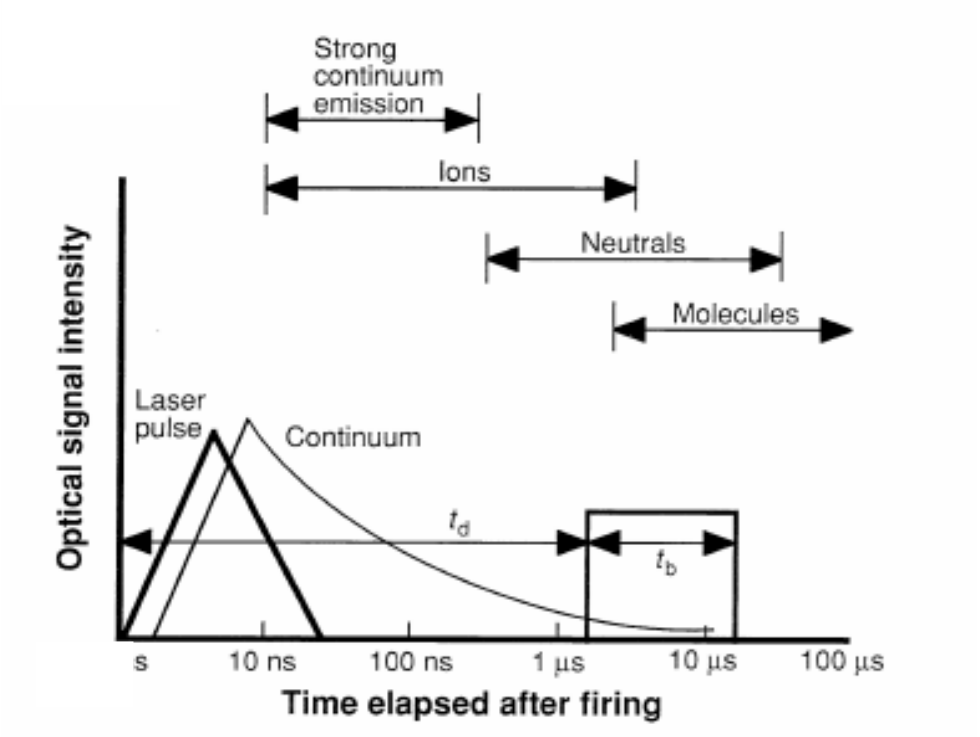

Figure 3.3: The important time periods after plasma formation [40].

The basic physical and chemical processes involved in LIBS are not very simple. The initiation, formation and decay of the plasma are complex processes. Absorption of the incident laser radiation occurs through the mechanism of inverse bremsstrahlung ("radiation", i.e. "braking radiation" or "deceleration radiation" which is electromagnetic radiation produced by the deceleration of a charged particle when deflected by another charged particle, typically an electron by an atomic nucleus), involving three-body collisions between photons, electrons, and atoms or molecules [40]. In gases and liquids, the plasma creates a shock wave in the surrounding medium transferring energy by means of conduction, radiation and the shock wave. When the experiment deals with a sample surface in a vacuum, the plasma expands freely away from the surface at different speeds. Excitation of specific energy levels in different atoms is likewise complex, and depends on factors such as the thermodynamic equilibrium and interactions with other atoms and molecules generally lumped under the category of matrix effects. After the laser pulse has terminated (typically within 10 ns), the plasma decays over an interval of one to several microseconds, depending on

the laser energy deposited. In vacuum, the temporal process is shortened. Most LIBS experiments involve repetitive plasmas with frequencies of 10 Hz or greater [40].

3.2 LIBS INSTRUMENTATION

A typical LIBS system consists of a pulsed laser, a focusing lens, collection of lenses and a spectrometer with a wide spectral range and a high sensitivity, fast response rate, time-gated detector, as shown in Figure 3.4.

In the following sub-sections, each part of the typical LIBS system used in this investigation is explained in detail.

3.2.1. LASERS

The word **LASER** is an acronym for **L**ight **A**mplification by **S**timulated **E**mission of **R**adiation. A laser is a quantum-mechanical device that creates and amplifies a narrow, intense beam of coherent light. A laser consists of an active lasing medium, a high reflective mirror and a partially transmissive mirror (output coupler), as shown in Figure 3.5 [41].

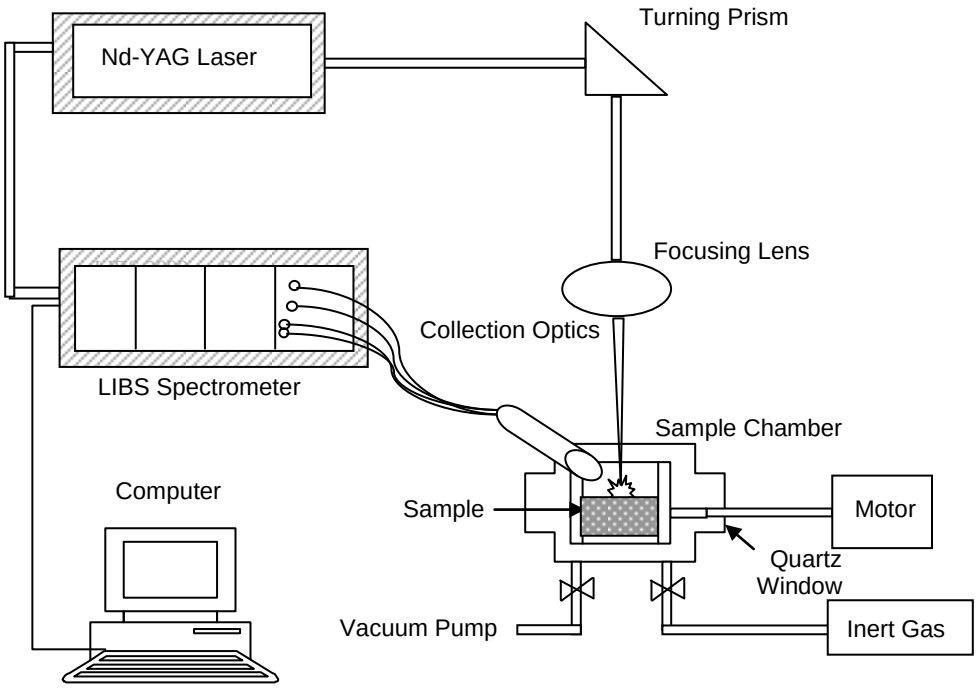

Figure 3.4: Schematic diagram LIBS system.

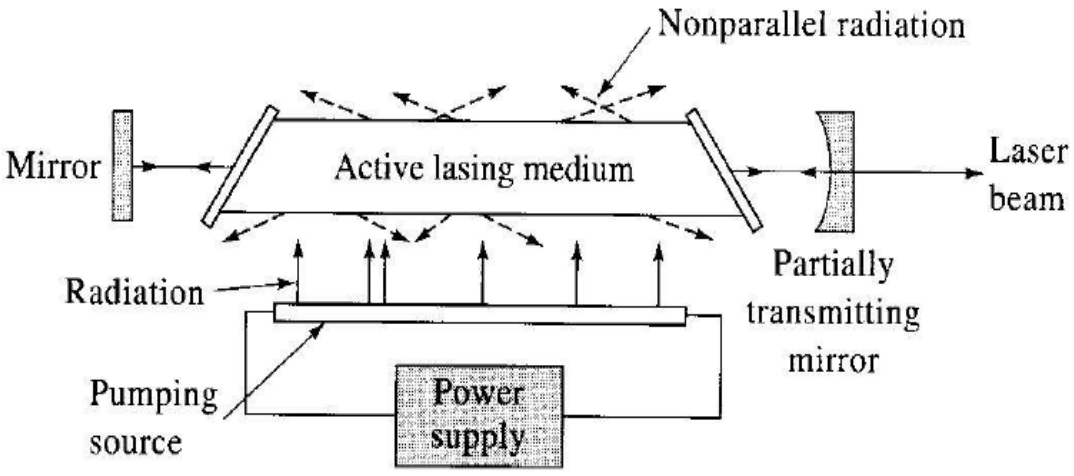

Figure 3.5: A laser and its components [41].

The active lasing medium is the heart of the laser and may be in the form of gas, liquid, solid or free electrons (see Figure 3.5). This lasing medium is energized or pumped by an external energy source (electricity or flash lamps). Consequently, electrons in the active medium are excited to higher energy levels. Population inversion is successful if the number of particles in one excited state exceeds the number of particles in some lower-energy state. Thus, stimulated emission is observed and light is amplified [41].

An optical cavity consists of a pair of mirrors arranged such that light is reflected back and forth by passing through the active medium. Throughout each passage, the intensity of light is amplified by the generation of additional photons. One of the mirrors in the optical cavity is partially transparent and is called the output coupler. The output laser beam is emitted through this mirror. Lasers are generally classified according to laser material and pump material [41], as shown in Figure 3.5.

3.2.2 FOCUSING AND COLLECTION OPTICS

Focusing optics bring the parallel beam from the laser to a focused spot. Since the size of the spot and depth of focus depends on the focusing optics, choosing the right lens type is important. The collimating optics are used to bring the plasma light to a parallel beam and then bring it again to a focused spot. Thus, the plasma light is focused onto the entrance slit of the detector with the use of a pair of lenses [41].

3.2.3 SPECTROGRAPH AND DETECTOR

Regardless of the sample type being analyzed, the plasma light is analyzed in the same way. Typically, emission from the atoms and ions in the plasma is collected by a lens or fiber optics and sent to a spectrograph and a detector. LIBS is usually composed of either a monchromator (i.e. Czerny-Turner type) or a polychromator (i.e. Echelle type) and a photomultiplier tube or an intensified charged coupled device detector (CCD) combination. The use of Echelle type polychromators is ever increasing whilst Czerny-Turner is the most widely used monochromator type. A system based on an Echelle spectrograph offers a combination of high resolution and wide wavelength range by using a grating with a large groove spacing.

In an Echelle spectrograph, there are two dispersing elements: (a) an echelle grating, or a diffraction grating and (b) a low-dispersion grating, or a prism, as shown in Figure 3.6. A diffraction grating has widely-spaced grooves. The light is diffracted in a standard grating at normal incidence to the face of grooves. Therefore, a series of overlapping spectra with high resolution are produced. A low dispersion grating, or a prism, placed perpendicular to the Echelle is used for separating out the overlapping spectra [41].

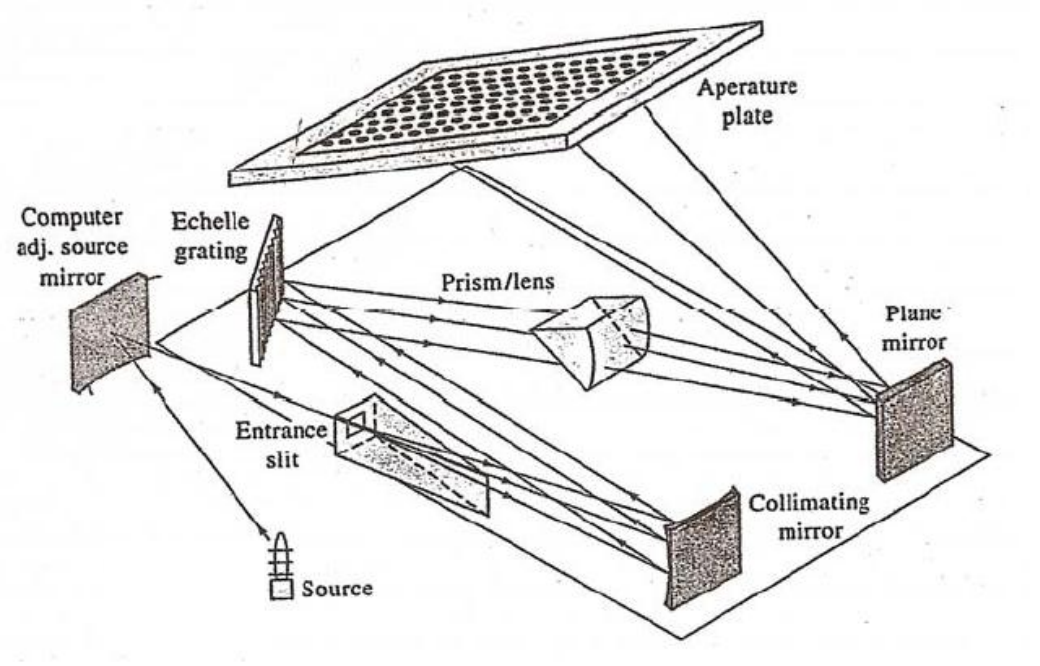

Figure 3.6: An echelle polychromator system [41].

The grating is used over a smaller range of angles so that it can be blazed with a well-shaped groove to be more efficient in a very wide range of wavelengths. This is the main advantage of an Echelle spectrograph. The plasma light is imaged on the entrance slit of a scanning monochromator or a spectrograph to be resolved spectrally with a photomultiplier tube (PMT), photodiode array (PDA) or intensified charged coupled device (ICCD) [41].

A charged coupled device (CCD) with an image intensifier tube is called intensified charged coupled device (ICCD) and is usually attached to a spectrograph, as shown in Figure 3.7. An image intensifier tube is an electronic tube consisting of a photocathode, micro-channel plate (MCP) and an anode (phosphor screen). In an image intensifier tube, the photons arrive at the photocathode that is located in the image (focal) plane of the tube [42].

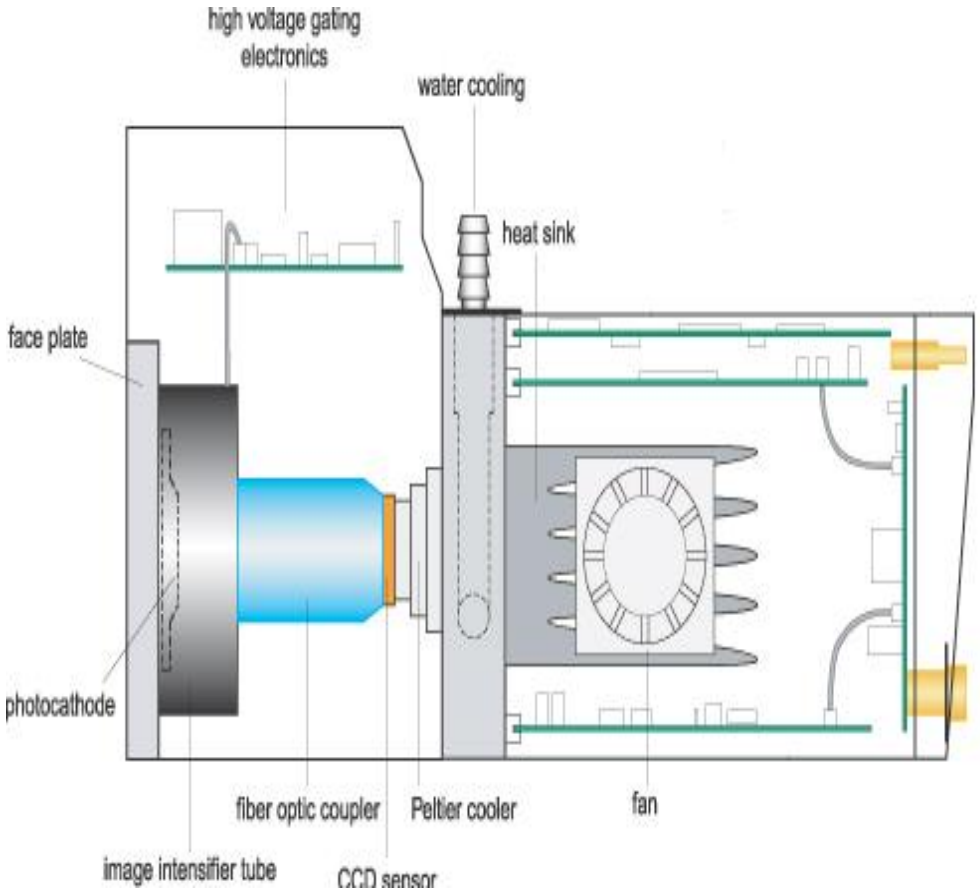

Figure 3.7: ICCD detector [42].

At the cathode, the photons are converted into electrons that are then sent into the vacuum of the image intensifier. The electrons are accelerated to the MCP because of the negative charge of the photocathode. The MCP is a multichannel plate: each channel multiplies the number of incoming electrons. The out-coming electrons are

accelerated towards the anode, which is a phosphor screen in which the electron energy is converted into photons. The image is thus intensified and then transferred to the CCD of the camera either by a fiber optic coupling or by a lens coupling. The main advantage of an ICCD camera is to image acquisition at very low light levels at relatively high speed [42].

3.3 DEVELOMENT OF KFUPM LIBS SYSTEM

The LIBS system developed at KFUPM for concrete assessment consisted of Ocean Optics LIBS 2000^{+} spectrometer, a sample chamber, Ocean Optics Introduces Laser Induced Breakdown Spectroscopy (OOILIBS) software and a Nd: YAG Laser (Spectra Physics, Model GCR100). A schematic diagram of the LIBS experimental set-up developed locally for the analysis of cement and concrete is presented in Figure 3.4. The Nd: YAG laser could deliver a maximum pulse energy of one joule with a laser pulse width of 8 ns and operated at 10 Hz pulse repetition rate, operating in Q-switched mode. In this study, 1064 nm radiation emitted at the fundamental frequency of Nd: YAG laser was applied for the production of plasma sparks at the cement sample surfaces. The laser energy was measured with a calibrated energy meter (Ophir Model 300) for the study of dependence of LIBS signal on incident laser energy.

The pulse energy utilized in these experiments was in the range of 20-60 mJ. The light from the plasma spark was collected by a collimating lens using an UV graded fused silica 1 meter, multimode sampling fiber with SMA connectors and was transferred to LIBS 2000^{+} spectrometer (Ocean Optics). The LIBS 2000^{+} had four spectrometer modules to provide high resolution (FWHM 0.1 nm) in the 200 nm to 620 nm wavelength region. The detector had a gated CCD camera, which made it possible to measure LIBS spectra over a broad spectral range simultaneously with high spectral resolution.

The emission was observed at a 45^{o} angle to the laser pulse and the software built in the spectrometer read the data from the chip and reconstructed the spectrum. For each LIBS analysis, the sample was placed on a stainless steel disc shaped (20 mm diameter by 10 mm long) platform mounted on a disk holding the sample. Twenty laser pulses were

directed into the cup to complete one measurement. The table was rotated using a step motor having 12 revolutions per minute. The concentrations of different elements present in cement samples were also measured with a calibrated ICP spectrometer to verify the results achieved with our LIBS method.

The laser beam was focused on the surface of the sample to produce a laser spark (plasma). The sample was mounted on a rotary holder to irradiate it uniformly at different spots. However, the samples were analysed from pre-determined fixed spots without rotation of the sample. The atomic emission lines were recorded using an optical spectrometer. The data was recorded on a PC and the spectra were compared according to standard spectra libraries [15-16].

The developed LIBS spectrometer was tested for the analysis of some solid samples for the detection of trace elements. Samples of known concentrations of chloride and sulfate ions were prepared in the form of pellets. The calibration would then be carried out based on the measured concentration of these known samples.

Special software was developed for data acquisition and analysis; this software was useful for the identification and quantification of the elements of interest.

3.4 MATERIALS

Type I and Type V Portland cements produced by Al-Yamamah Saudi Cement Company were used. Both cements complied with the specification requirements of ASTM C 150. The chemical composition of Type I and Type V cements is shown in Table 3. 1.

Distilled water was used for preparing all the paste specimens.
Analar (i.e. pure) sodium sulfate and sodium chloride were used for preparing the contaminated cement pastes.

Table 3.1 shows the chemical composition of Portland cements, fly ash and silica fume. Fly ash was used as 30% replacement of cement while silica fume was used as 7% replacement of cement, as shown in Table 3.2.

Cement paste specimens with Type I and Type V cements, silica fume (7%) and fly ash (30%) were prepared with varying concentration of chloride (0.0, 0.2, 0.4, 0.8, 1.0, 1.5, 3.5 and 5.0% by the weight of cementitious materials) and sulfate (0.0, 0.2, 0.4, 0.8, 1.5, and 3.0% by the weight of cementitious materials), as shown in Table 3.2.

Table 3.1: Chemical composition of Portland cement, silica fume and fly ash.

Constituent (wt%)	Type-I Cement	Type-V Cement	Silica Fume	Fly Ash
SiO_2	21.30	21.20	92.50	42.14
Al_2O_3	5.10	4.20	0.72	19.38
Fe_2O_3	3.56	4.48	0.96	4.60
CaO	64.50	64.77	0.48	26.96
MgO	2.10	2.00	1.78	1.78
SO_3	1.89	1.71	-	2.43
K_2O	0.34	0.33	1.84	1.13
Na_2O	0.29	0.28	0.50	1.90
Insoluble residue	0.14	0.15	-	-
L.O.I	0.70	0.80	1.55	0.40
C_3S	55.90	63.00	-	-
C_2S	19.00	13.30	-	-
C_3A	7.50	3.56	-	-
C_4AF	10.83	13.63	-	-

Table 3.2: Details of plain and blended cement paste specimens.

Mix Type	Mix No	% Cementitious Materials	Chloride % by Weight of Cementitious Materials	Sulfate % by Weight of Cementitious Materials
Plain cement	1	Type I cement (100%)	0.0 0.2 0.4 0.8 1.0 1.5 3.5 5.0	0.0 0.2 0.4 0.8 1.5 3.0
	2	Type V cement (100%)		
Blended cement	3	Type I cement (93%) + silica fume (7%)		
	4	Type I cement (70%) + fly ash (30%)		

3.5 MIX PROPORTIONS

Based on the mix design parameters of the paste, such as water-cementitious materials ratio, cementitious materials content, silica fume, fly ash, salts (NaCl, Na_2SO_4), paste specimens cubes (25*25*25 mm) and small cubes (25 *25*8 mm) were prepared, as shown in Tables 3.3 through 3.12. All of these specimens were made with distilled water and plain (Type I and Type V) and blended (fly ash and silica fume) cements while the water to cementitious materials ratio was kept invariant at 0.4 and the mixing temperature was maintained at 22 ± 3^0C. Figure 3.8 shows the moulds utilized for the preparation of paste specimens.

Table 3.3: Plain cement pastes (made with Type I and Type V) mixed with chloride or sulfate.

Mix. No	Mix Details	Cement g	Water g	W/C	Chloride %	Chloride g	Sulfate %	Sulfate g
M1	I-C_0-S_0	750	300	0.4	0	0	0	0
M2	I-$C_{0.2}$-S_0	750	300	0.4	0.2	2.47	0	0
M3	I-$C_{0.4}$-S_0	750	300	0.4	0.4	4.94	0	0
M4	I-$C_{0.8}$-S_0	750	300	0.4	0.8	9.87	0	0
M5	I-C_1-S_0	750	300	0.4	1	12.34	0	0
M6	I-$C_{1.5}$-S_0	750	300	0.4	1.5	18.51	0	0
M7	I-$C_{3.5}$-S_0	750	300	0.4	3.5	43.18	0	0
M8	I-C_5-S_0	750	300	0.4	5	68.83	0	0
M9	I-C_0-$S_{0.2}$	750	300	0.4	0	0	0.2	2.22
M10	I-C_0-$S_{0.4}$	750	300	0.4	0	0	0.4	4.44
M11	I-C_0-$S_{0.8}$	750	300	0.4	0	0	0.8	8.87
M12	I-C_0-$S_{1.5}$	750	300	0.4	0	0	1.5	16.64
M13	I-C_0-S_3	750	300	0.4	0	0	3	33.28
M14	V-C_0-S_0	750	300	0.4	0	0	0	0
M15	V-$C_{0.2}$-S_0	750	300	0.4	0.2	2.47	0	0
M16	V-$C_{0.4}$-S_0	750	300	0.4	0.4	4.94	0	0
M17	V-$C_{0.8}$-S_0	750	300	0.4	0.8	9.87	0	0
M18	V-C_1-S_0	750	300	0.4	1	12.34	0	0
M19	V-$C_{1.5}$-S_0	750	300	0.4	1.5	18.51	0	0
M20	V-$C_{3.5}$-S_0	750	300	0.4	3.5	43.18	0	0
M21	V-C5-S0	750	300	0.4	5	68.83	0	0
M22	V-C_0-$S_{0.2}$	750	300	0.4	0	0	0.2	2.22
M23	V-C_0-$S_{0.4}$	750	300	0.4	0	0	0.4	4.44
M24	V-C_0-$S_{0.8}$	750	300	0.4	0	0	0.8	8.87
M25	V-C_0-$S_{1.5}$	750	300	0.4	0	0	1.5	16.64
M26	V-C_0-S_3	750	300	0.4	0	0	3	33.28

Table.3.4: Blended cement pastes (Type I cement mixed with silica fume).

Mix. No	Mix Details	Cement G	Water/ Cement	Water g	Silica Fume g	Chloride %	Chloride g	Sulfate %	Sulfate g
M27	I_{SF}-C_0-S_0	697.5	0.4	300	52.5	0	0	0	0
M28	I_{SF}-$C_{0.2}$-S_0	697.5	0.4	300	52.5	0.2	2.47	0	0
M29	I_{SF}-$C_{0.4}$-S_0	697.5	0.4	300	52.5	0.4	4.94	0	0
M30	I_{SF}-$C_{0.8}$-S_0	697.5	0.4	300	52.5	0.8	9.87	0	0
M31	I_{SF}-C_1-S_0	697.5	0.4	300	52.5	1	12.34	0	0
M32	I_{SF}-$C_{1.5}$-S_0	697.5	0.4	300	52.5	1.5	18.51	0	0
M33	I_{SF}-$C_{3.5}$-S_0	697.5	0.4	300	52.5	3.5	43.18	0	0
M34	I_{SF}-C_5-S_0	697.5	0.4	300	52.5	5	61.69	0	0
M35	I_{SF}-C_0-$S_{0.2}$	697.5	0.4	300	52.5	0	0	0.2	2.22
M36	I_{SF}-C_5-$S_{0.4}$	697.5	0.4	300	52.5	0	0	0.4	4.44
M37	I_{SF}-C_5-$S_{0.8}$	697.5	0.4	300	52.5	0	0	0.8	8.87
M38	I_{SF}-C_5-$S_{1.5}$	697.5	0.4	300	52.5	0	0	1.5	16.64
M39	I_{SF}-C_5-S_3	697.5	0.4	300	52.5	0	0	3	33.28

Table 3.5: Blended cement pastes (Type I cement mixed with fly ash).

Mix. No	Mix details	Cement G	Water/ Cement	Water g	Fly Ash g	Chloride %	Chloride g	Sulfate %	Sulfate g
M40	I_{FA}-C_0-S_0	525	0.4	300	225	0	0	0	0
M41	I_{FA}-$C_{0.2}$-S_0	525	0.4	300	225	0.2	2.47	0	0
M42	I_{FA}-$C_{0.4}$-S_0	525	0.4	300	225	0.4	4.94	0	0
M43	I_{FA}-$C_{0.8}$-S_0	525	0.4	300	225	0.8	9.87	0	0
M44	I_{FA}-C_1-S_0	525	0.4	300	225	1	12.34	0	0
M45	I_{FA}-$C_{1.5}$-S_0	525	0.4	300	225	1.5	18.51	0	0
M46	I_{FA}-$C_{3.5}$-S_0	525	0.4	300	225	3.5	43.18	0	0
M47	I_{FA}-C_5-S_0	525	0.4	300	225	5	61.69	0	0
M48	I_{FA}-C_0-$S_{0.2}$	525	0.4	300	225	0	0	0.2	2.22
M49	I_{FA}-C_5-$S_{0.4}$	525	0.4	300	225	0	0	0.4	4.44
M50	I_{FA}-C_5-$S_{0.8}$	525	0.4	300	225	0	0	0.8	8.87
M51	I_{FA}-C_5-$S_{1.5}$	525	0.4	300	225	0	0	1.5	16.64
M52	I_{FA}-C_5-S_3	525	0.4	300	225	0	0	3	33.28

Table 3.6: Plain cement pastes (Type I mixed with chloride and sulfate).

Mix. No	Mix Details	Cement g	Water g	Water/ Cement	Chloride %	Chloride g	Sulfate %	Sulfate g
M_{61}	I-$C_{0.4}$-$S_{0.2}$	750	205	0.27	0.4	4.94	0.2	2.22
M_{62}	I-$C_{0.4}$-$S_{0.4}$	750	205	0.27	0.4	4.94	0.4	4.94
M_{63}	I-$C_{0.8}$-$S_{0.2}$	750	205	0.27	0.8	9.87	0.2	2.22
M_{64}	I-$C_{0.8}$-$S_{0.4}$	750	205	0.27	0.8	9.87	0.4	4.94

Table 3.7: Plain cement pastes (Type V mixed with both chloride and sulfate).

Mix .No	Mix Details	Cement g	Water g	Water/ Cement	Chloride %	Chloride g	Sulfate %	Sulfate g
M_{65}	V-$C_{0.4}$-$S_{0.2}$	750	205	0.27	0.4	4.94	0.2	2.22
M_{66}	V-$C_{0.4}$-$S_{0.4}$	750	205	0.27	0.4	4.94	0.4	4.94
M_{67}	V-$C_{0.8}$-$S_{0.2}$	750	205	0.27	0.8	9.87	0.2	2.22
M_{68}	V-$C_{0.8}$-$S_{0.4}$	750	205	0.27	0.8	9.87	0.4	4.94

Table 3.8: Blended cement pastes (Type I and silica fume mixed with both chloride and sulfate).

Mix. No	Mix Details	Cement g	Water/ Cement	Water g	Silica Fume g	Chloride %	Chloride g	Sulfate %	Sulfate g
M_{73}	I_{SF}-$C_{0.4}$-$S_{0.2}$	697.5	0.27	205	52.5	0.4	4.94	0.2	2.22
M_{74}	I_{SF}-$C_{0.4}$-$S_{0.4}$	697.5	0.27	205	52.5	0.4	4.94	0.4	4.94
M_{75}	I_{SF}-$C_{0.8}$-$S_{0.2}$	697.5	0.27	205	52.5	0.8	9.87	0.2	2.22
M_{76}	I_{SF}-$C_{0.8}$-$S_{0.4}$	697.5	0.27	205	52.5	0.8	9.87	0.4	4.94

Table 3.9: Blended cement pastes (Type I and fly ash with both chloride and sulfate).

Mix .No	Mix Details	Cement g	Water/ Cement	Water g	Fly Ash g	Chloride %	Chloride g	Sulfate %	Sulfate g
M69	I_{FA}-$C_{0.4}$-$S_{0.2}$	525	0.27	205	225	0.4	4.94	0.2	2.22
M70	I_{FA}-$C_{0.4}$-$S_{0.4}$	525	0.27	205	225	0.4	4.94	0.4	4.94
M71	I_{FA}-$C_{0.8}$-$S_{0.2}$	525	0.27	205	225	0.8	9.87	0.2	2.22
M72	I_{FA}-$C_{0.8}$-$S_{0.4}$	525	0.27	205	225	0.8	9.87	0.4	4.94

Table 3.10: Plain cement pastes (Type I mixed up with both chloride and sulfate).

Mix. No	Mix Details	Cement g	Water g	Water/ Cement	Chloride %	Chloride g	Sulfate %	Sulfate g
M_{53}	I-C_2-$S_{0.5}$	250	75	0.3	2	8.2251	0.5	1.84875
M_{54}	I-C_2-S_1	250	75	0.3	2	8.2251	1	3.6975
M_{55}	I-C_3-S_2	250	75	0.3	3	12.3376	2	7.395
M_{56}	I-C_3-S_3	250	75	0.3	3	12.3376	3	11.0925

Table 3.11: Blended cement pastes (Type I and silica fume mixed with both chloride and sulfate).

Mix. No	Mix Details	Cement g	Water/ Cement	Water g	Silica Fume g	Chloride %	Chloride g	Sulfate %	Sulfate g
M_{57}	I_{SF}-C_2-$S_{0.5}$	232.5	0.3	75	17.5	2	8.2251	0.5	1.84875
M_{58}	I_{SF}-C_2-S_1	232.5	0.3	75	17.5	2	8.2251	1	3.6975
M_{59}	I_{SF}-C_3-S_2	232.5	0.3	75	17.5	3	12.3376	2	7.395
M_{60}	I_{SF}-C_3-S_3	232.5	0.3	75	17.5	3	12.3376	3	11.0925

Table 3.12: Blended cement pastes (Type I and fly ash mixed with both chloride and sulfate).

Mix. No	Mix Details	Cement g	Water/ Cement	Water g	Fly Ash g	Chloride %	Chloride g	Sulfate %	Sulfate g
$M_{57\text{-}R}$	I_{SF}-C_2-$S_{0.5}$	175	0.3	75	75	2	8.2251	0.5	1.84875
$M_{58\text{-}R}$	I_{SF}-C_2-S_1	175	0.3	75	75	2	8.2251	1	3.6975
$M_{59\text{-}R}$	I_{SF}-C_3-S_2	175	0.3	75	75	3	12.3376	2	7.395
$M_{60\text{-}R}$	I_{SF}-C_3-S_3	175	0.3	75	75	3	12.3376	3	11.0925

Figure 3.8: Moulds and samples utilized for preparing the paste specimens.

3.6 SPECIMEN PREPARATION

3.6.1 MIXING OF SPECIMENS

The paste constituents were weighed in sensitive balances; one for the paste materials and another for the contaminants (i.e. chloride and sulfate salts), as shown in Figure 3.9. These constituents were and mixed in a Hobart mixer, as shown in Figure 3.10, for approximately 1.5 to 3 minutes to obtain a homogeneous mixture with uniform consistency.

Casting of specimens was carried out in 76 batches. Before casting, the moulds were oiled and thereafter filled with paste in three layers. After placement of each layer, the mould was vibrated to ensure proper consolidation. After casting, the specimens were covered with plastic sheet to avoid loss of water due to evaporation. The specimens were demolded after 24 hours of casting and then put in containers to cure at a temperature of 22 ± 3°C and curing was continued for thirteen more days at the laboratory, as shown in Figure 3.11.

Figure 3.9: Weighting balances used to weigh cement (left) and salts (right)

Figure 3.10: Mixer used to prepare the pasts specimens.

3.6.2 CURING

After demolding, the specimens were kept in desiccator in the laboratory, as shown in Figure 3.11. The casting and curing was continued for two weeks in the labaratory (22 ± 3°C).

Figure 3.11: Curing of paste specimens.

3.7 EXPERIMENTAL SET-UP DETAILS

3.7.1 SINGLE PULSED LIBS

A schematic diagram of the LIBS experimental set-up developed locally for the analysis of cement paste samples and concrete is presented in Figures 3.12 and 3.13. Nd: YAG laser can deliver a maximum pulse energy of one joule with a laser pulse width of 8 ns and operates at 10 Hz pulse repetition rate, operating in Q-switched mode. In this study, 1064 nm radiation emitted at the fundamental frequency of Nd: YAG laser was applied for the production of plasma sparks at the cement paste sample surfaces. The laser

energy was measured with a calibrated energy meter (Ophir Model 300) for the study of dependence of LIBS signal on incident laser energy. A pictorial view of the experimental set-up is shown in Figure 3.13.

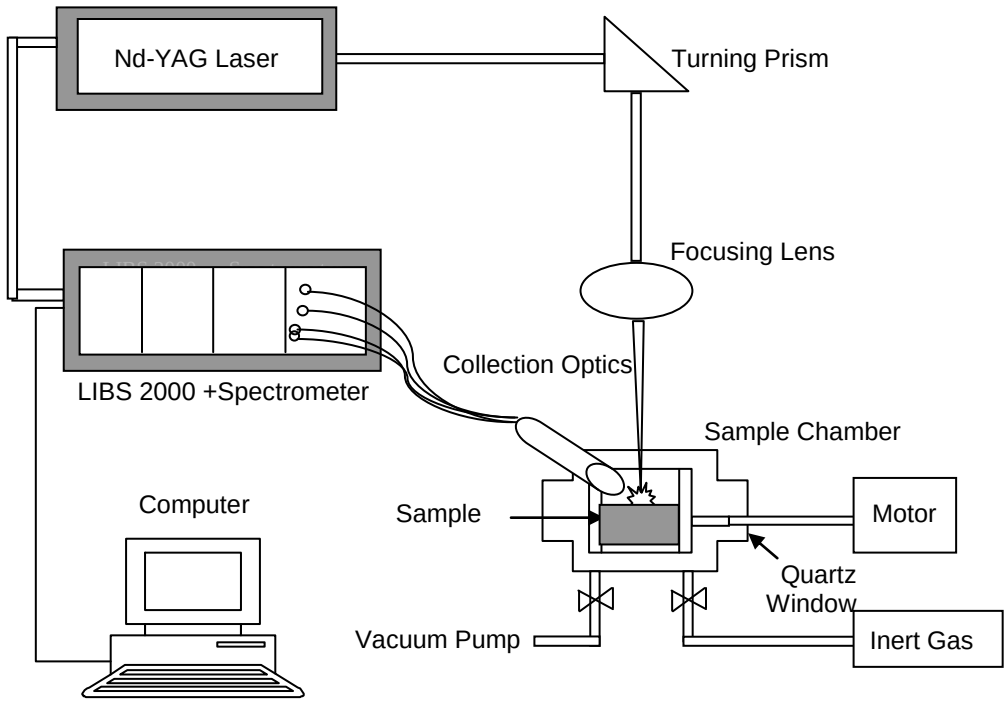

Figure 3.12: Schematic diagram of experimental set up of single pulsed LIBS system.

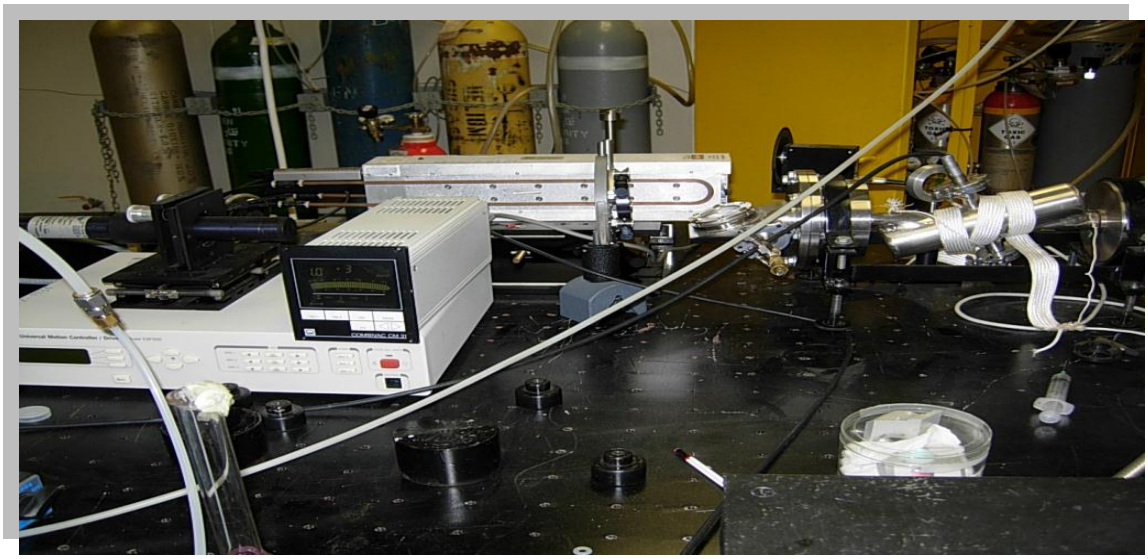

Figure 3.13: Pictorial view of single pulsed LIBS system.

3.7.2 DUAL PULSED LIBS

The experimental set-up for the dual pulsed LIBS system is shown in Figures 3.14 and 3.15. In this system, two Q-switch pulsed Nd: YAG lasers (Sky lasers) of which the fourth harmonic (266 nm) serves as laser 1 and the fundamental (1064 nm) serves as laser 2 as shown in Figures 3.14. The two lasers were so precisely aligned that the two laser spots fall on the same spot on the sample surface and this aligned laser spots should be at the line of sight of the fiber optic detection lens. The adjustable infrared (IR) and ultraviolet (UV) lens assembly is used to focus the laser beams on the sample surface. The LIBS signal was collected by the fiber bundle assembly and fed into the seven channels of the LIBS spectrometer (Ocean Optics LIBS 2500 plus). The flash lamps and the Q-switches of both lasers are externally controlled by the LIBS system in the sequence shown in the Figure 3.14. Laser 1 produces laser induced plasma at the sample surface and after an appropriate time delay after the firing of laser 1, the second laser was fired, which is controlled by the built software in spectrometer of the LIBS system. The second laser was allowed to pass through plume created by the first laser and hit on the sample surface which enhanced the normal LIBS process.

Chloride samples were prepared by adding the appropriate amount of sodium chloride to the cement paste to maintain the desired chloride concentration and the sample surface was kept uniform and all the paste pallets were of same thickness. The sodium chloride used for this work was of research grade (i.e. analar) free from other impurities. In order to avoid the pitting on the surface by the high energy laser pulses, the sample was kept on the motor controlled X-Y translator system and the sample was kept

moving throughout the experiment. A pictorial view of the experimental set-up is shown in Figure 3.15.

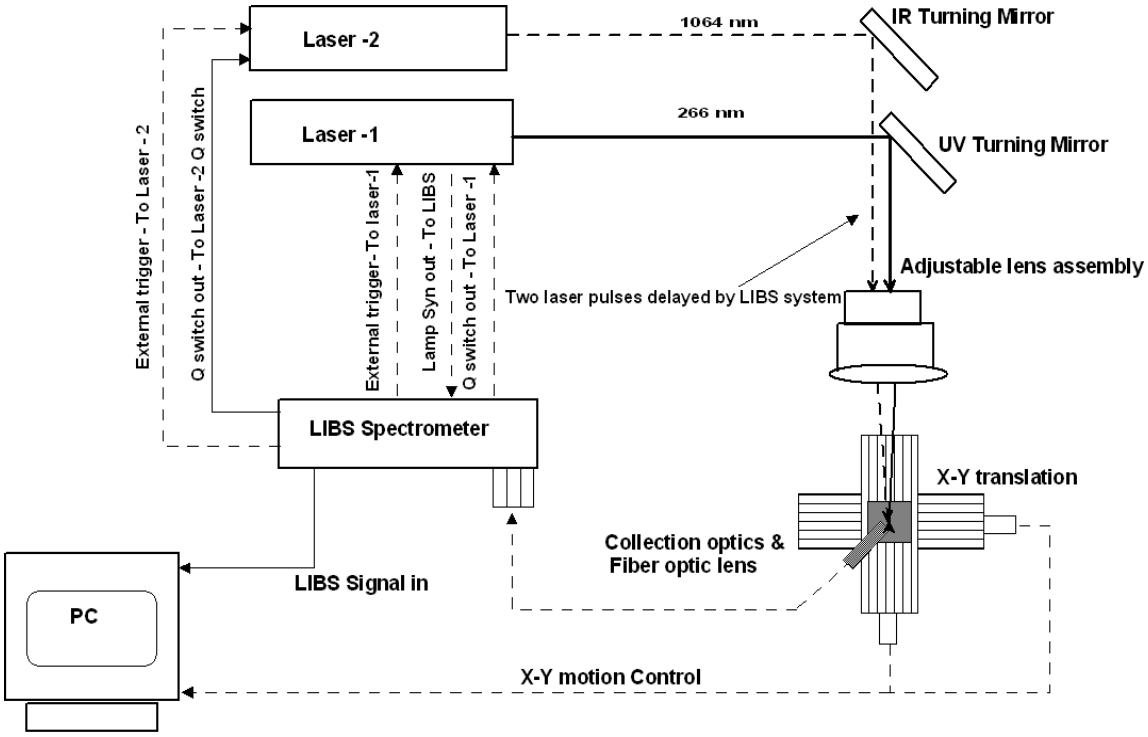

Figure 3.14: Experimental set-up of dual pulsed LIBS system.

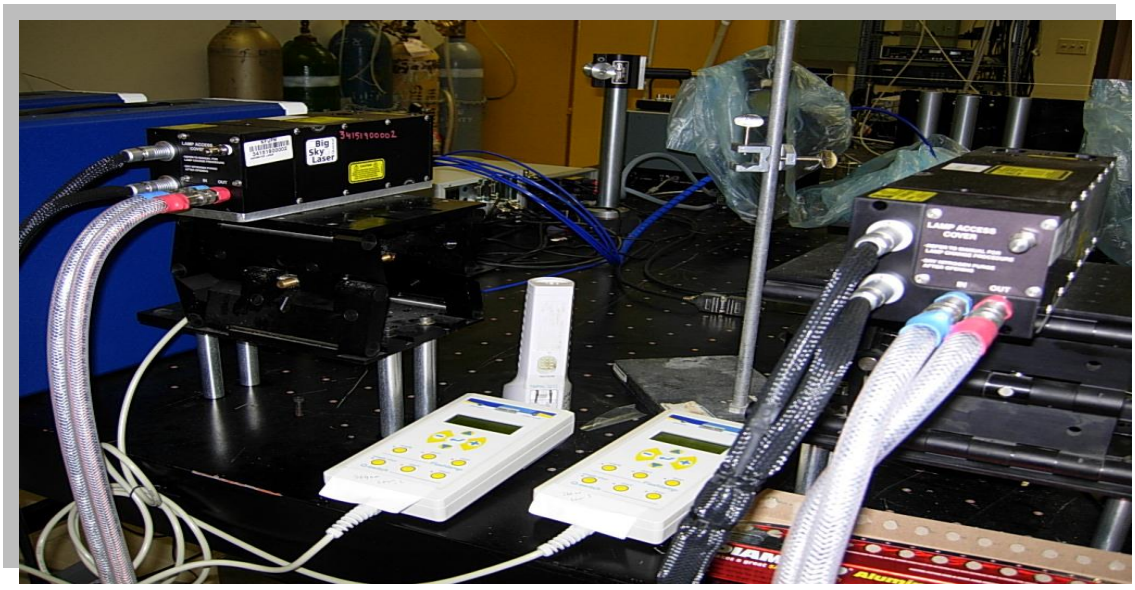

Figure 3.15: Pictorial view of dual pulsed LIBS system.

CHAPTER 4

RESULTS AND DISCUSSION

4.1 LIBS TESTING ON DIFFERENT KINDS OF CEMENTS

The important experimental parameters, which can affect the limit of detection (LOD) in LIBS, are laser energy, gate delay time, focusing lens for incident laser radiation, collecting lens for laser produced emission and target rotation speed. The effects of these parameters are addressed in the following sections.

4.1.1 DEPENDENCE OF LIBS INTENSITY ON INCIDENT LASER ENERGY

The laser energy can affect the properties of the induced plasma and eventually the figure of merit of LIBS measurement. The signal of the analyte or component line was proportional to the laser energy [7, 8], while the laser produced plasma was in the optically thin region. The emission spectra of paste samples were recorded at different laser energies to study the effect of the laser energy on the line emission intensity. Plasma emission spectra were recorded for most of the elements under investigation at different laser energies with a fixed time delay between laser incidence and collection of emitted light from plasma.

To study the effect of laser energy on the intensity for 585.7 nm emission line of Cl (signature of ClI), the laser produced plasma emission spectra from different cement paste samples were recorded in the 200 to 650 nm region at laser energies of 20, 30, 40, 50 and 60 mJ per pulse. A time delay of 5.0 μs was selected because this was experimentally found to produce the maximum signal intensity of the LIBS signal for Cl. Figure 4.1 shows a typical trend of dependence of laser produced plasma intensity on incident laser energy for Cl in a test sample. The line intensity variation versus incident laser energy was plotted in Figure 4.1. It is clear from the data in the figure that the line intensity increases linearly with a rise in the incident laser energy from 20 to 60 mJ. The least square fit value of R^2 = 0.9995 shows vividly the linear dependence. However, one can detect enough intensity at 40 mJ so that incident laser pulse energy of

40 mJ was enough for detection of different elements present in the cement samples under investigation.

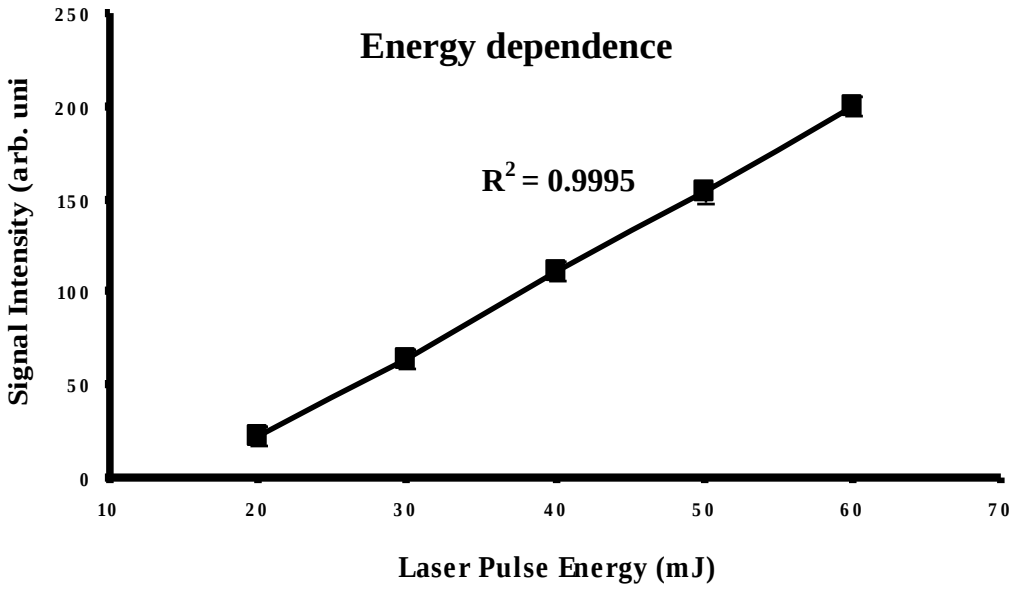

Figure 4.1: Dependence of the intensity of the Cl (585.7 nm) emission line on laser energy.

4.1.2 LIBS SIGNAL INTENSITY DEPENDENCE ON TIME DELAY

The LIBS spectrum shows also time dependence. In order to study the behavior of time evolution, delay times between incident laser pulse and recording of plasma emission was studied carefully. The delay times were controlled by a Q-switch trigger pulse (i.e. external Q-switch) to the laser and the trigger pulse to gate the CCD camera. A series of measurements were made to find the optimum delay time between the laser pulse and the beginning of the LIBS spectra acquisition. The delay times were chosen according to the detection of maximum LIBS signal intensity for each element and the delay time measured during the experiments were presented in Table 4.1. Figure 4.2 depicts the dependence of LIBS signal intensity on time delay between the laser pulse and the CCD camera recording of LIBS signal. From this figure, it is clear that the best signal intensity occurs at a time delay of 5 μs.

Measurements were carried out to find the optimum time delay between the laser pulse and the beginning of the LIBS spectrum acquisition. The delay times were chosen according to the detection of maximum LIBS signal intensity for each element present in the cement paste samples. a Q-switch trigger pulse (i.e. enternal Q-switch) to the laser and the trigger pulse to gate the CCD camera A typical plot of dependence of LIBS signal peak intensity (at a wavelength of 585.7nm) on delay time for Cl is depicted in Figure 4.2. It is clear from the data in this figure that the maximum LIBS signal is recorded at around 5 μs of delay for Cl. Other elements under investigation show the maximum spectral line intensity between 3.0 and 7.0 μs delay time.

Table 4.1: Elements detected in cement samples and comparison of LIBS with ICP Techniques.

Element	**Wave-length (nm)***	**Cement Type I**		**Cement Type V**		**Cement Type I + SF**		**LOD (ppm)**	**Delay (μS)**
		LIBS (ppm)	**ICP (ppm)**	**LIBS (ppm)**	**ICP (ppm)**	**LIBS (ppm)**	**ICP (ppm)**		
Al	394.4	34500	34100	24350	24200	521.4	474	8.0	4.5
Ba	493.4	6280	6080	6731	6620	Nd	Nd	5.0	5.0
Ca	396.1	433500	433000	443480	443000	2090	2043	6.0	5.0
Cr	427.3	96.58	87.8	Nd**	Nd**	Nd**	Nd**	4.0	5.5
Fe	526.9	20230	19300	21980	21200	396	366	7.0	3.5
Mg	518.2	8017	7470	13905	13400	2801	2700	2.0	4.5
Mn	403.4	226.6	206	306.9	279	510.1	475	4.0	4.5
Na	588.9	3211	3010	3977	3680	2852	2760	3.0	3.5
P	438.51	Nd**	Nd**	Nd**	Nd**	825.3	783	7.0	4.5
S	373.81	11320	11000	8480	8080	304.7	277	10.0	4.0
Si	390.5	92020	88200	81600	81200	351590	349000	11.0	4.5
Cl	585.7	1825	1720	1590	1520	6690.7	6595	12	5.0

*From Reference No. [44].

Nd**: Not detected.

Different stoichiometric samples of each element are prepared for the construction of the calibrations curves. This task is essential for accurate measurement of concentration of trace elements present in different cement paste samples. The concentrations of the prepared samples are also verified by a calibrated Inductively Coupled Plasma (ICP) spectrometer.

In this experimental work, known concentrations 100,000 ppm, 10,000 ppm, 1000 ppm, and 100 ppm of Cl, Mg, Ca, Zn, Fe, Cu ,Cr, Mn, Al, S and other elements under investigation were prepared in the test sample matrix. LIBS spectra are recorded for these four concentrations of each element. All these spectra are recorded with an average of 20 laser shots, at three different locations on the sample surface. Average spectra were recorded for each data point. Further, to confirm results, the initial calibration is performed on cement samples with well-defined sodium-chloride additions. The detection limits for LIBS analysis of pellets sample under investigation are calculated by using the standard equation (Radziemski and Cremers 1989). The results achieved from cement samples are comparable to the results obtained by the ICP analysis. The limits of detection for the elements under investigation are given in Table 4.1.

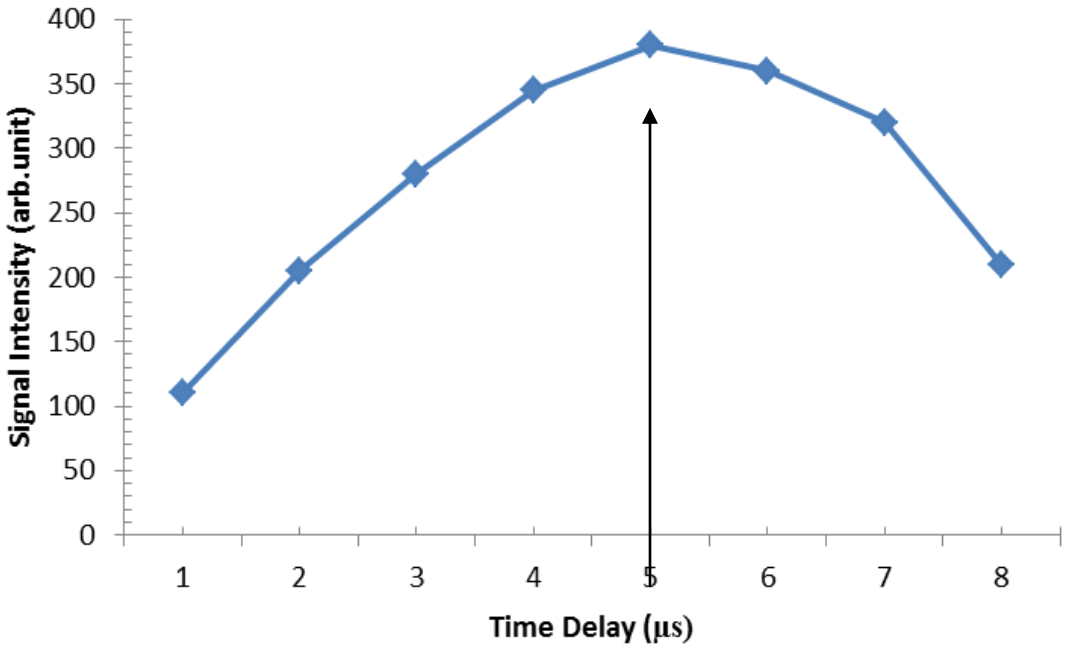

Figure 4.2: Time delay and signal intensity for Cl 585.7 nm line.

4.2 LIBS ANALYSIS OF CEMENT PASTE SAMPLES

The main parameters that could affect the precision and limit of detection were delay time, laser pulse energy, number of shots accumulated, the distance between the plasma and optical fiber. All these parameters were carefully optimized prior to performing the analysis of the test samples. Figures 4.3, 4.4, 4.5 and 4.6 depict the emission spectra of samples prepared with Type I, Type V and Type I with SF and Type I plus fly ash cements, respectively, recorded with the set-up at a time delay of 5.0 μs in the spectral region of 200 to 650 nm. The laser pulse energy was fixed at 40 mJ for recording these spectra. The distance between the optical fiber and the plasma emission was kept at 10 mm. The average spectra due to 20 laser shots were recorded for each data point. It was to be noted that averaging the 20 laser shots spectra tended to reduce the background noise to a great extent when compared to the single laser shot spectrum of the sample.

The detection limits for LIBS analysis of pellet samples under investigation were calculated using the standard equation [41] because the detection limit is a very important parameter for any spectrometer and for analysis of samples under investigation. Detection limit here means the lowest concentration that can be detected with LIBS. The limit of detection (LOD) was estimated using the following equation (1) [41].

$$\mathrm{LOD} = \mathbf{2\sigma_B/S} \quad \ldots\ldots\ldots\ldots\ldots\ldots\ldots\ldots\ldots\ldots\ldots\ldots \quad (4.1)$$

Where $\boldsymbol{\sigma_B}$ is the standard deviation of the background measurements, and **S** is the sensitivity which is given by the ratio of the intensity to the concentration. The limit of detection of the system was 0.00385% equivalent to 38 mg/g. The results achieved from cement paste samples were comparable to the results obtained by the ICP analysis. The limits of detection for the elements under investigation are given in Table 4.1.

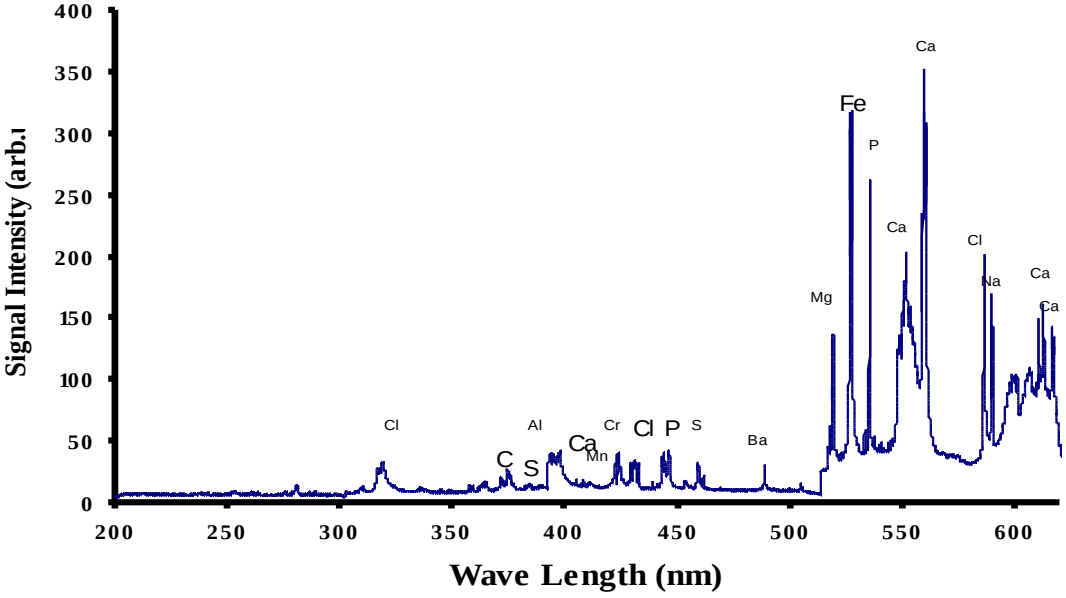

Figure 4.3: Typical LIBS spectra of Type I cement sample in the region of 200 to 650 nm recorded at delay time of 5.0 µs and laser pulse energy of 40 mJ.

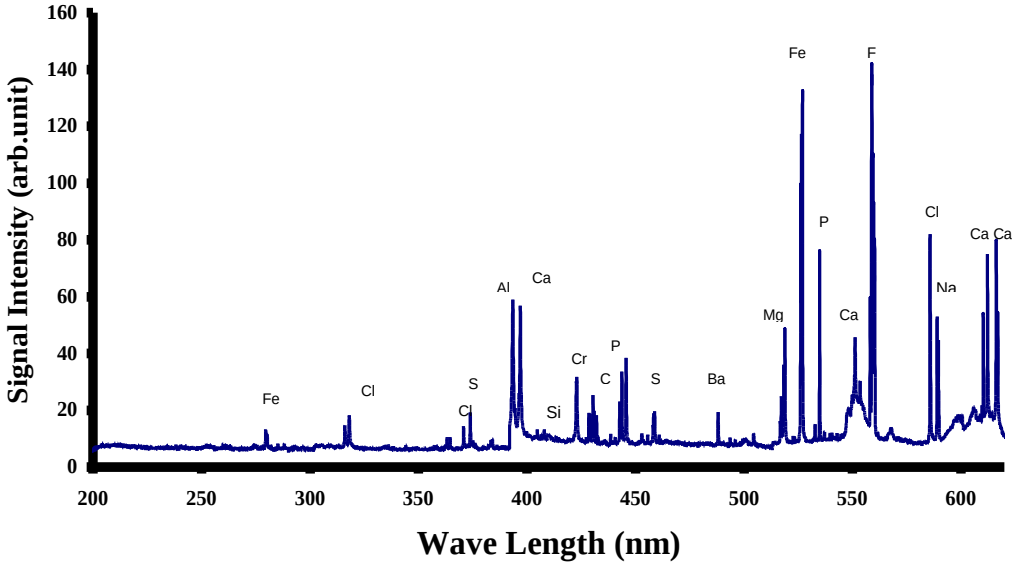

Figure 4.4: Typical LIBS spectra of Type V cement in the region of 200 to 650 nm recorded at delay time of 5.0 µs and laser pulse energy of 40 mJ.

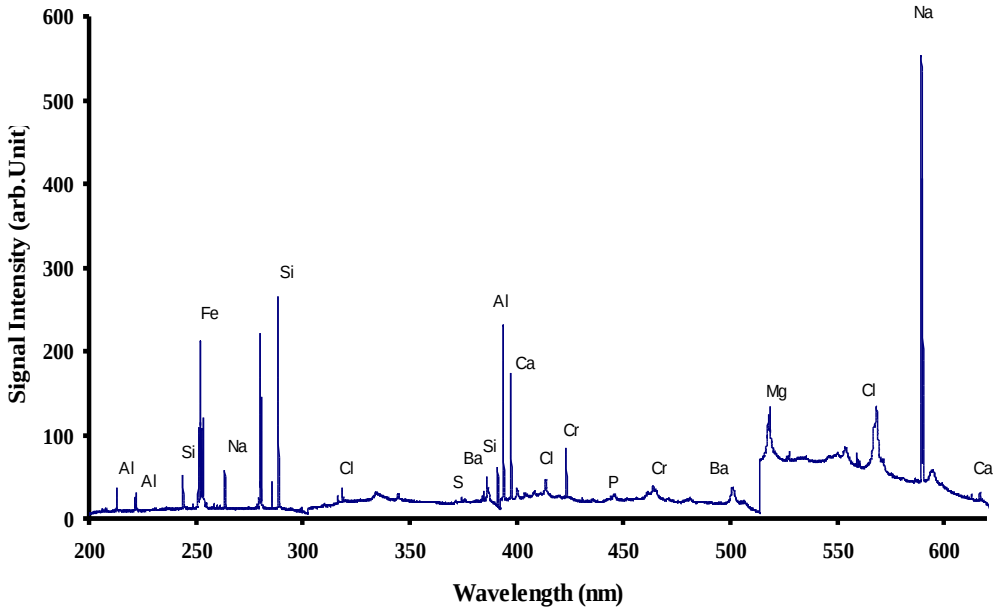

Figure 4.5: Typical LIBS spectra of cement Type I + SF cement in the region of 200 to 650 nm recorded at delay time of 5.0 µs and laser pulse energy of 40 mJ.

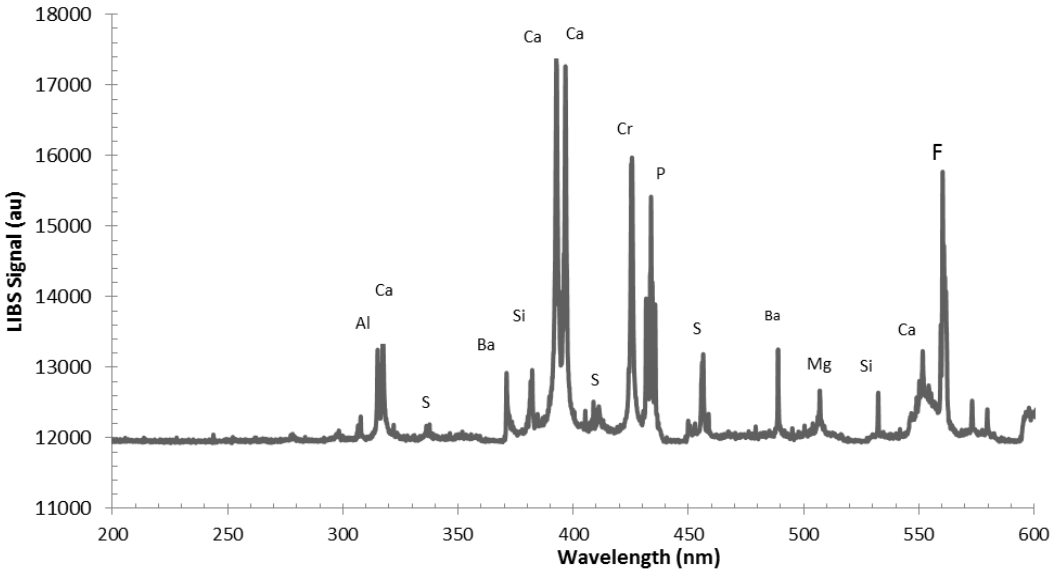

Figure 4.6: Typical LIBS spectra of cement Type I + FA cement in the region of 200 to 600 nm recorded at delay time of 5.0 µs and laser pulse energy of 40 mJ.

The elements present in the above-mentioned cement samples were identified and marked in the figures. The major elements detected in the samples were calcium, aluminum, chromium, magnesium, sodium, silicon, iron, chlorine, sulfur, phosphourus and manganese. All the spectral lines for the above-mentioned elements recorded with the LIBS set-up were identified using the NIST atomic spectral data base [44] and other references [37, 38, 39, and 45].

The elements detected and the corresponding concentrations are listed in Table 4.1. The concentration for each element as listed in Table 4.1 was confirmed by the analysis using Inductive coupled plasma (ICP) technique. Comparison of the values obtained with the LIBS set-up with the ICP results indicates a good agreement between the two techniques.

4.3 PRECISION AND ACCURACY OF CEMENT PASTE RESULTS

The precision of any analytical instrument is defined as the repeatability of the analyte measurement, and was usually estimated in LIBS with the relative standard deviation (RSD) as follows [7]:

$$\text{RSD} = \text{standard deviation} / \text{mean} \quad \ldots\ldots\ldots\ldots\ldots\ldots\ldots\ldots\ldots\ldots \quad (4.2)$$

For cement paste samples, the precision of LIBS measurements depended on the complexity and homogeneity of the sample, and the reproducibility of the laser shots. Typical values for LIBS were in the range of 1 to 5%. For precision of the results for three paste samples (cement Type I, cement Type V and cement Type I with silica fume and fly ash), the same method was adopted as applied for the analysis of samples like paint and cement [7], the precision was found to be 2 to 4%.

The precision of an analytical method is defined as the measured experimental values as compared to the accepted “actual” values [7]. Generally speaking, the accuracy of any measurement or analytical technique was defined as the percentage difference between

the experimental values measured with LIBS and the actual values measured with a standard method like ICP technique.

Results regarding concentration of contaminants, like Cl and S and other trace metals, were discussed in an earlier publication [38]. For three cement samples (cement Type I, cement Type V and cement Type I with silica fume) studied in this work as shown in Table 4.1, the residual error between values obtained by two methods (ICP and LIBS) are presented in Table 4.1. Further, the values for different elements were compared with the values obtained by ICP.

Briefly, the concentrations of various elements present in cement samples can be measured accurately using LIBS system. The accuracy of the system in terms of qualitative as well as quantitative analysis was obvious from the comparison of LIBS results with those obtained by ICP in Table 4.1. The contaminants and concentrations detected with the set-up of dual pulsed laser are shown in Table 4.1. It was also shown that the LIBS measurements are a suitable for the determination of chloride and sulfate contents in any paste sample.

4.4 CHLORIDE DETECTION

The dual pulsed LIBS spectra showing different elemental composition of the cement paste with Cl (3.5%) by the weight of cementitious materials and between 280 and 480 nm regions is shown in Figure 4.7. Concrete has many chemicals added to it beside the basic ingredients, aggregate, cement and water. The chemicals may include one or more of the following, e.g. retarders to control the setting time, plasticizers for workability, and slump retention admixtures for ready-mixed concrete and mineral admixtures, like silica fume, fly ash or slag for durability enhancement. Chemical and physical properties of ingredients decide the concrete properties, both in plastic and hardened forms. In the case of concrete, the major ingredient that decides the physical, chemical and the engineering properties of the concrete is Portland cement. Typical composition of Portland cement is as follows: tricalcium silicate (C_3S), dicalcium silicate (C_2S), tricalcium aluminate (C_3A) and tetracalcium aluminoferrite (C_4AF), which are basically the oxides of calcium, silicon, aluminum and iron. The composition of cement was

varied depending on the application. Typical cement contains 50–70% of C_3S, 15–30% of C_2S, 5–10% of C_3A, 5–15% of C_4AF, and 3–8% of other additives or minerals [37].

In the LIBS spectrum, the atomic transitions of the neutral and ionized atoms are recorded. In the case of multi-elemental composite like cement paste samples; one cannot expect all the characteristic atomic lines of any element in the spectroscopic detection system. The self- absorption or the re-absorption poses a great technical difficulty. In a multi-element system, if the emitted light from certain element with a particular wavelength matches the absorption region of another element in the same sample, the emitted light is reabsorbed by the sample, irrespective of the high emission intensity of the first element [41].

In the case of chlorine, there are many atomic emission lines of varying intensities present in the UV-visible (UV-VIS) region for both neutral and singly-ionized chlorine. However, in the case of multi-elemental composite like concrete, the re-absorption problem poses greater difficulty as there are many elements reabsorb the atomic emission lines of chlorine. In the case of concrete, more than 60 % of the material is calcium oxide (CaO) and the Ca atom has very strong absorption lines, which can easily reabsorb the emission lines of all other elements including chloride. The strong atomic emission line at 837.5 nm has been used as a marker for the detection of chloride in cement as it is one of the strongest emission lines of the neutral chlorine atom [41]. Hence, in the case of calcium, only a few neutral and singly-ionized atomic lines were observed in spite of the fact that calcium was the most abundant element in the cement paste samples and also calcium had many strong lines in the region covered in Figure 4.7 [41]. In the case of silicon, it did not have any strong transitions in the region covered in Figure 4.7 except the one at 288.15 nm, which was characteristically one of the strongest persistent lines of silicon. Besides these two elements, the lines of aluminum, iron, carbon, oxygen and sodium were identified, where the sodium comes from the sodium chloride present in the cement paste samples. The elemental identification and the atomic transitions of these lines are listed in Table 4.2.

Though calcium was the most abundant element in the cement paste and also inherently with many strong emission lines in the region, it has been re-absorbed by the cement

paste that made most of the lines either completely absent or very weak. If this was the case of calcium, one could expect the situation of minor elements like chloride! Chlorine characteristically has many strong to weak atomic emission lines from the neutral chlorine atom and most of these lines were absent due to the re-absorption process. However, two transition lines of neutral chlorine atoms were recorded at 837.5 nm and 594.8 nm.

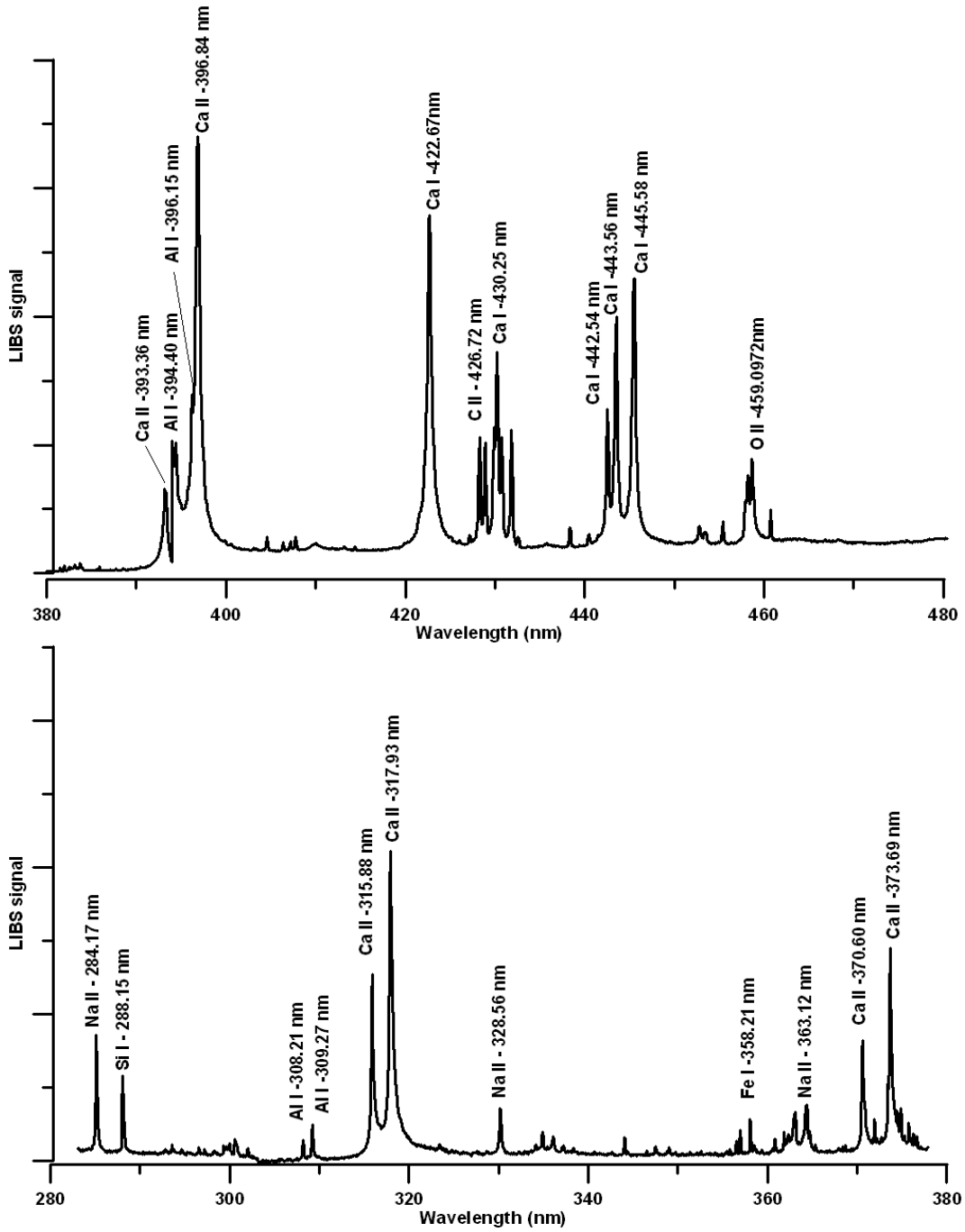

Figure 4.7: LIBS spectrum showing different elements present in Type I cement paste sample with Cl (1.5%) in the 280-380 nm and 380-480 nm regions.

Table 4.2: Identification of the atomic transitions of various elements present in the paste samples according to NIST standard [44]

Wavelength (nm)	Element	Configuration	Wavelength (nm)	Element	Configuration
284.17	**Na II**	$2s^2 2p^5 3s$ - $2s^2 2p^5 3p$	430.25	**Ca I**	$3p^6 4s4p$ - $3p^6 4p^2$
288.15	**Si I**	$3s^2 3p^2$ - $3s^2 3p4s$	442.54	**Ca I**	$3p^6 4s4p$ - $3p^6 4s4d$
308.21	**Al I**	$3s^2 3p$ - $3s^2 3d$	443.56	**Ca I**	$3p^6 4s4p$ - $3p^6 4s4d$
309.27	**Al I**	$3s^2 3p$ - $3s^2 3d$	445.58	**Ca I**	$3p^6 4s4p$ - $3p^6 4s4d$
315.88	**Ca II**	$3p^6 4p$ - $3p^6 4d$	594.85	**Cl I**	$3s^2 3p^4(^3P_1)4p$ - $3s^2 3p^4(^3P)5c$
317.93	**Ca II**	$3p^6 4p$ - $3p^6 4d$	610.27	**Ca I**	$3p^6 4s4p$ - $3p^6 4s5s$
328.56	**Na II**	$2s^2 2p^5 3s$ - $2s^2 2p^5 3p$	612.21	**Ca I**	$3p^6 4s4p$ - $3p^6 4s5s$
358.21	**Fe I**	3d7(2H)4s - 3d6(3D)4s4p(3P°)	649.37	**Ca I**	$3p^6 3d4s$ - $3p^6 3d4p$
363.12	**Na II**	$2s^2 2p^5 3s$ - $2s^2 2p^5 3p$	657.27	**Ca I**	$3p^6 4s2$ - $3p^6 4s4p$
370.60	**Ca II**	$3p^6 4p$ - $3p^6 5s$	671.76	**Ca I**	$3p^6 3d4s$ - $3p^6 4s5p$
373.69	**Ca II**	$3p^6 4p$ - $3p^6 5s$	818.32	**Na I**	$2p^6 3p$ - $2p^6 3d$
393.36	**Ca II**	$3p^6 4s$ - $3p^6 4p$	819.48	**Na I**	$2p^6 3p$ - $2p^6 3d$
394.40	**Al I**	$3s^2 3p$ - $3s^2 4s$	837.59	**Cl I**	$3s^2 3p^4(^3P)4s$ - $3s^2 3p^4(^3P)4p$
396.15	**Al I**	$3s^2 3p$ - $3s^2 4s$	844.67	**O I**	$2s^2 2p^3(^4S^0)3s$ - $2s^2 2p^3(^4S^0)3$
396.84	**Ca II**	$3p^6 4s$ - $3p^6 4p$	849.80	**Ca II**	$3p^6 3d$ - $3p^6 4p$
422.67	**Ca I**	$3p^6 5p$ - $3p^6 8s$	854.20	**Ca II**	$3p^6 3d$ - $3p^6 4p$
426.72	**C II**	$2s^2 3d$ - $2s^2 4f$	866.21	**Ca II**	$3p^6 3d$ - $3p^6 4p$

The intensity of atomic emission line at 594.8 nm was just 0.1% of the intensity of 837.5 nm line and, hence, naturally 837.5 nm line was expected to yield better intensity than the emission line at 594.8 nm. But on the contrary, the signal to noise ratio with 594.8 nm line of neutral Cl I as a marker for the detection of chloride was better than that of the 837.5 nm emission line of neutral Cl I. The excitation – ionization - emission processes in the case of chlorine that take place in the LIBS was demonstrated in the energy level diagram shown in Figure 4.8.

It is to be noted that the first laser created a plasma plume and after a delay, the second laser pulse ionizes the neutral chlorine and detaches the electrons and these electrons were accelerated by the electric field of the laser radiation and further ionize the neutral chlorine and this effect produces LIBS plasma. The recombination process starts when the free electron was captured into atomic energy levels and after that the neutral atom relaxes to the lower energy levels to emit the characteristic atomic emission lines [24]. Generally, in the LIBS process, the transition lines from neutral, singly-ionized and doubly-ionized species were detected and the emission intensity of the singly-ionized atom was much smaller than that of the neutral atom according to the Saha equation [24].

$$n_e \frac{n^{II}}{n_I} = \frac{(2\pi m_e kT)^{3/2}}{h^3} \frac{2U^{II}(T)}{U^{I}(T)} e^{\frac{-E_{ion}}{kT}} \quad \ldots\ldots\ldots\ldots\ldots\ldots\ldots\ldots \quad (4.3)$$

Where ne is the plasma electron density, nI and nII are the number densities of the neutral atomic species and the single ionized species, respectively, Eion is the ionization potential of the neutral species in its ground state, me is the electron mass, and h is Planck's constant. UI and UII are partition functions of the species at temperature T [24].

The atomic emission line at 594.8 nm was due to the transition between 3s2 3p4(3P1)5d 2[1]3/2 (100170.98 cm-1) and 3s2 3p4(3P)4p 2P01/2 (83364.927 cm-1), whereas in the case of the atomic line at 837.594 nm was due to the transition between 3s2 3p4(3P)4p 4D07/2 (83893.037 cm-1) and 3s2 3p4(3P)4s 4P5/2 (71958.363 cm-1), [44], as shown in Figure 4.8.

Dual pulsed LIBS spectra of the cement paste samples around the 594.8 nm atomic transition line of ClI for 1.5% of chloride in the cement paste sample was depicted in Figure 4.9. Besides the marker line (594.8 nm) of ClI, other atomic transition lines of CaI are marked in the spectrum in the same figure. In order to understand the variation of the intensity of the 594.8 nm line, the LIBS spectrum of paste was conducted at five different chloride concentrations by weight in the cement paste samples shown in Figure 4.10: (a) 3.5% (b) 1.5% (c) 1 % and (d) 0.4 % (e) 0.2 %, whereby the increase of signal was nocticed with the chloride concentration.

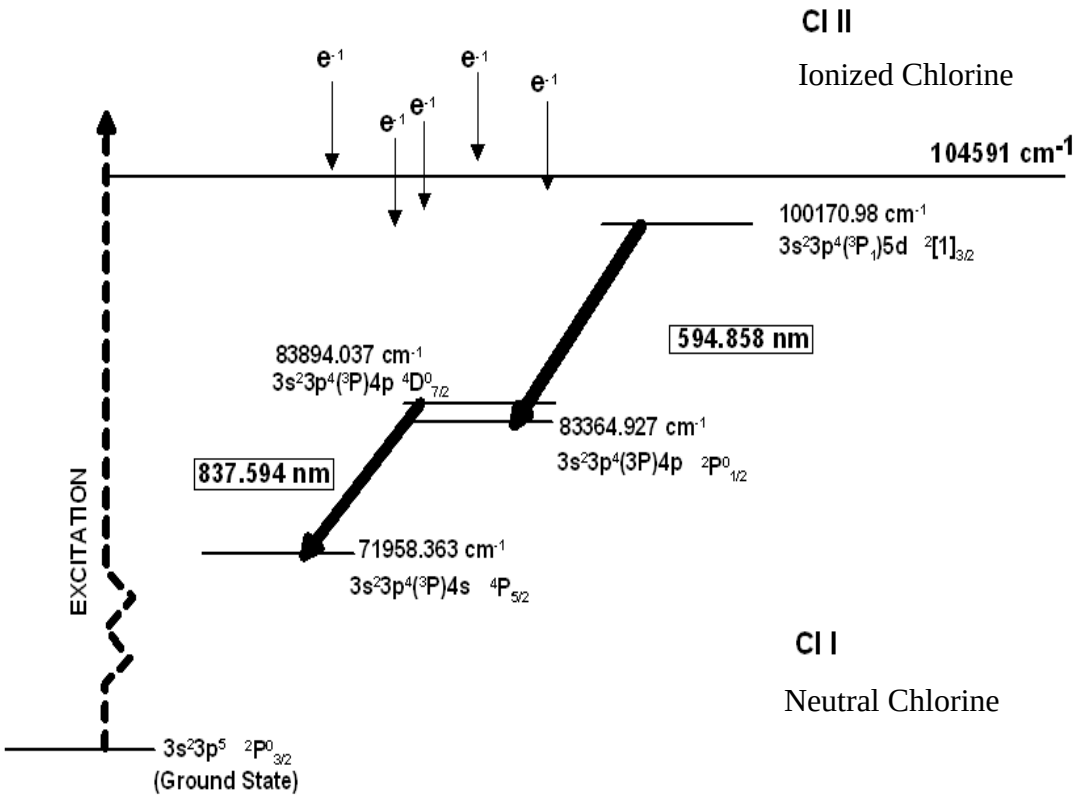

Figure 4.8: Grotrian diagram showing the atomic transitions of ClI at 594.858 nm and 837.594 nm for the two marker atomic lines used for the detection of chloride.

As the chloride concentration increases, the signal level increases which, of course, was the characteristics of the atomic spectrum. In the LIBS studies for the detection of chloride, the atomic emission line at 837.5 nm has been used for various applications including in the cement paste samples as this line was one of the most intense lines of chlorine and also it was in a desirable spectral region of the spectroscopic instrumentation. However, in the case of cement paste samples; the performance of this transition line was not that impressive, considering its characteristic intensity. This was because one of the major constituent of cement paste was calcium and characteristically

calcium has very strong absorption at the near infra-red region, which coincides with the 837.5 nm emission line of ClI.

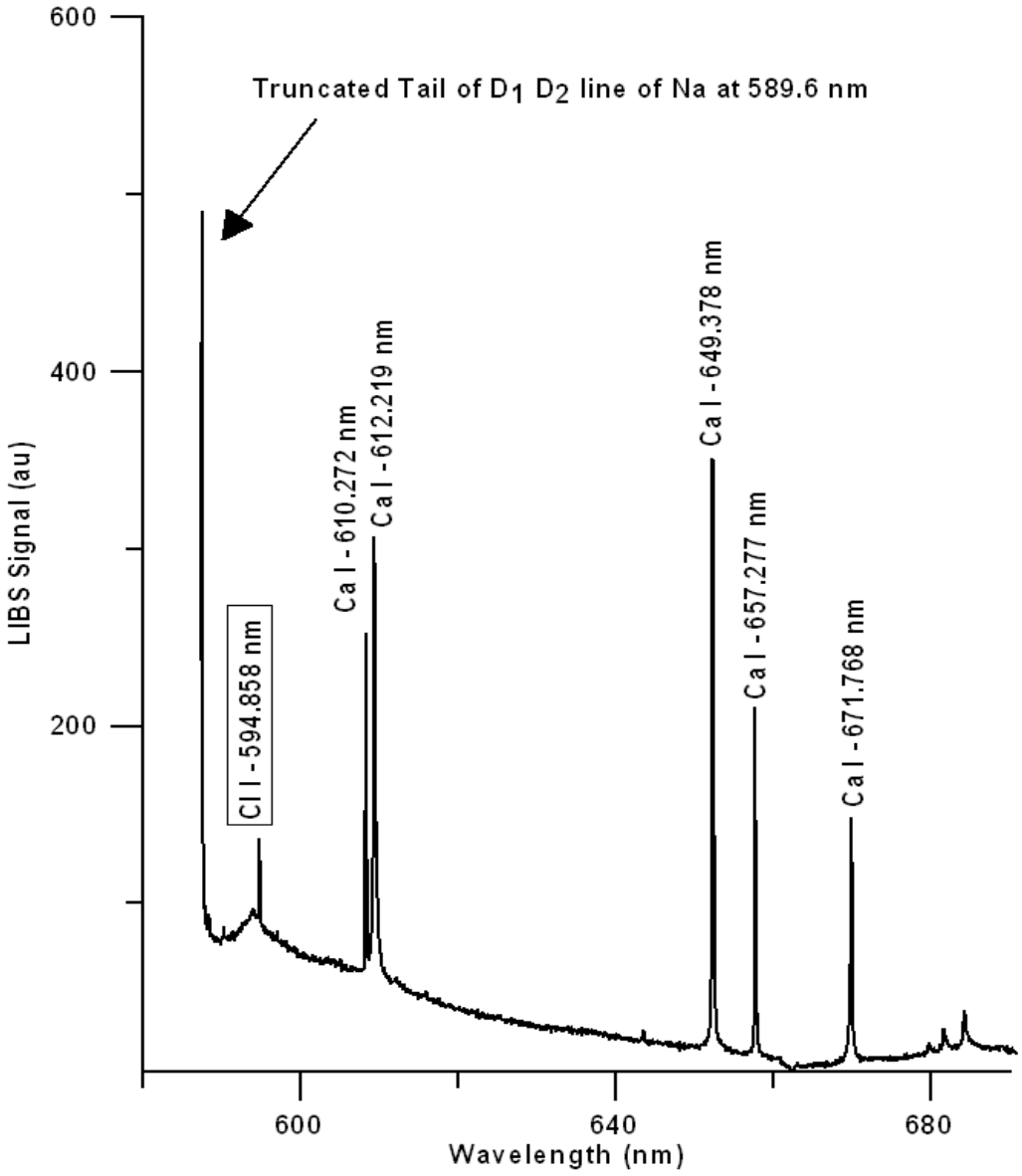

Figure 4.9: Typical LIBS spectrum of the cement paste sample for Type I cement with Cl (1.5%) showing atomic transition line at 594.858 nm and also transitions due to the presence of other elements in this spectral region.

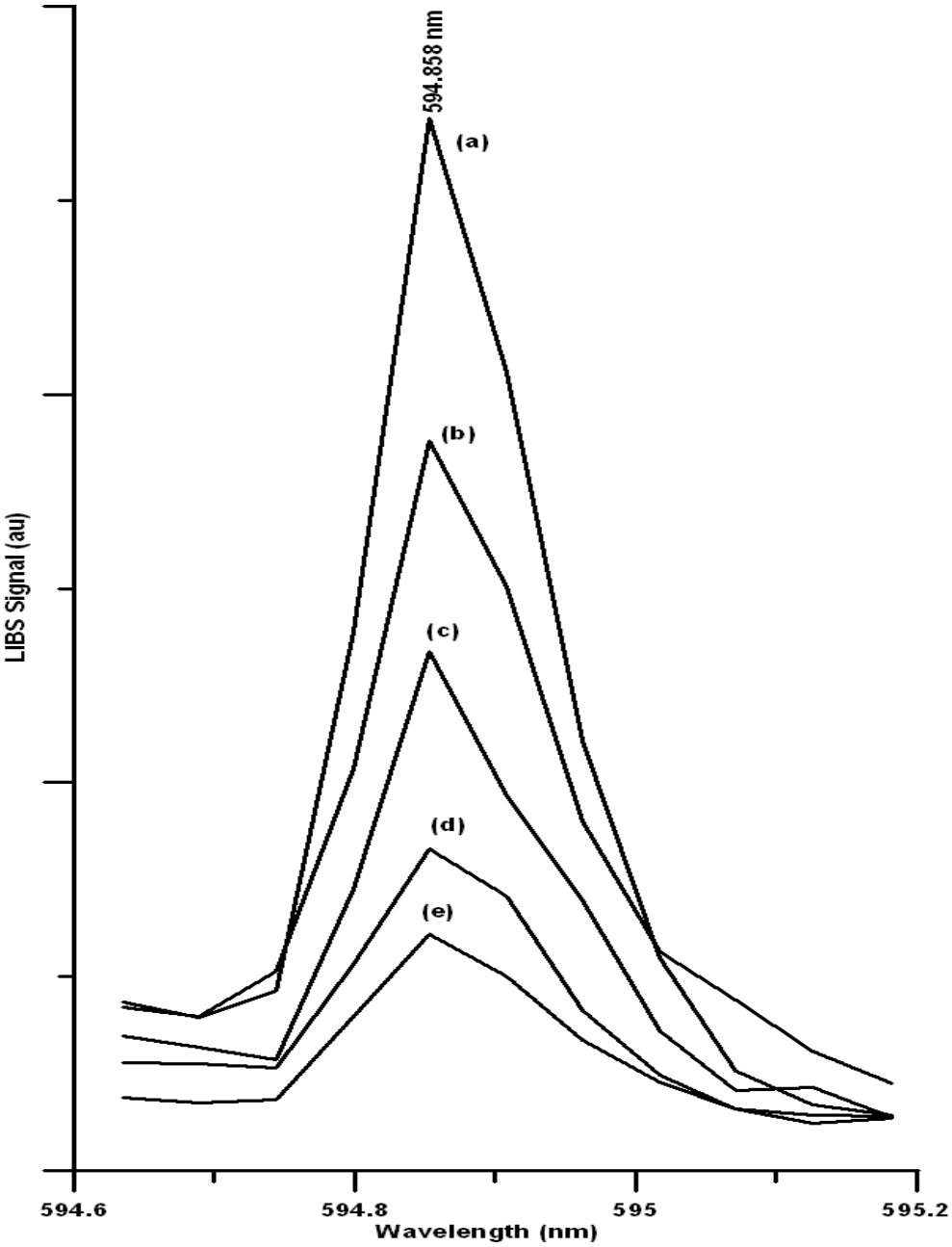

Figure 4.10 : LIBS spectrum of the cement paste sample for Type I cement at five different concentrations of chloride in the paste sample with 594.858 nm atomic transition as a marker: (a) 3.5% (b) 1.5% (c) 1% and (d) 0.4% (e) 0.2% of chloride by weight cementitious materials content.

Figure 4.11 depicts the dual pulsed LIBS spectrum of cement paste sample with 1.5% of chloride in the cement paste sample. In addition to the chlorine line, other atomic lines from NaI; OI and CaII were identified. On comparison, 594.8 nm transition line in Figure 4.9 was more intense than the 837.5 nm transition line. A set of LIBS spectra at 837.5 nm atomic transition line for five different chloride concentrations: (a) 3.5% (b) 1.5% (c) 1% and (d) 0.4% (e) 0.2% are presented in Figure 4.12.

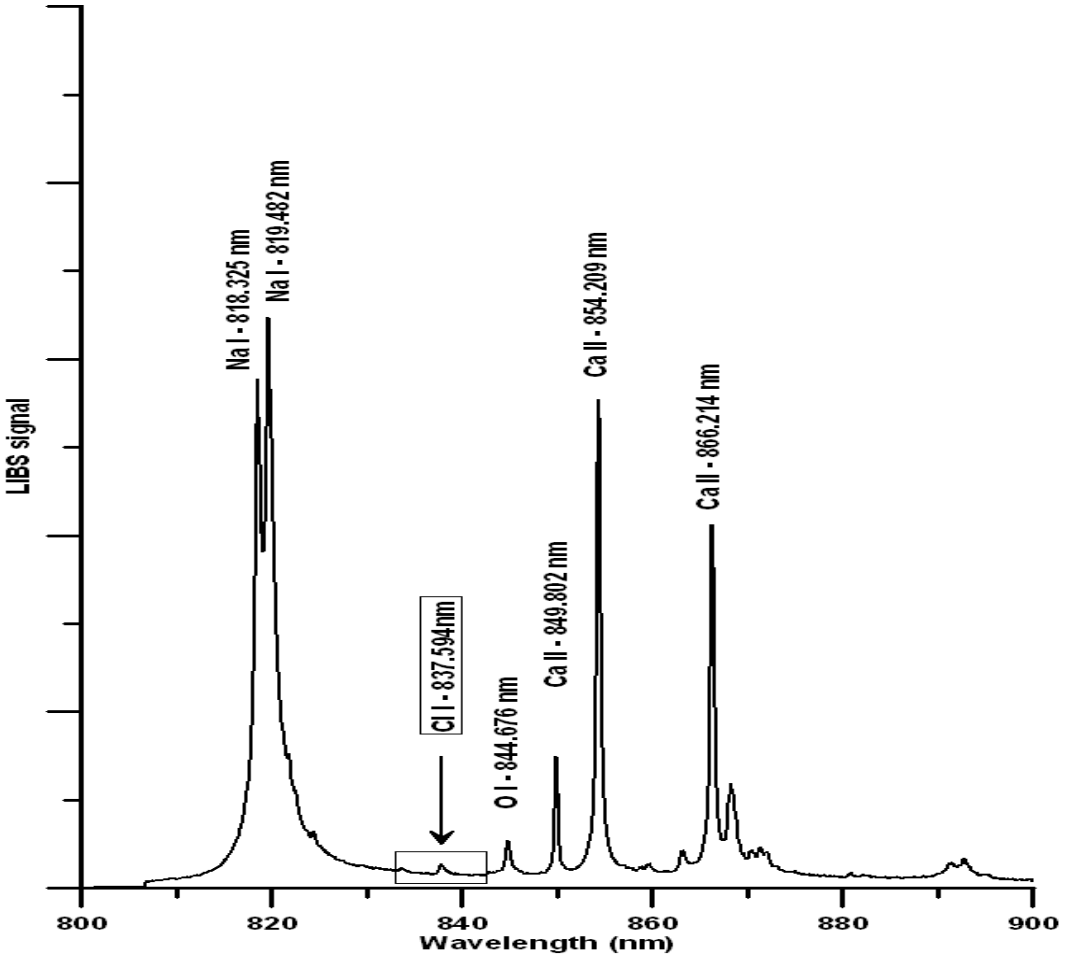

Figure 4.11: Typical LIBS spectrum of the cement paste sample for Type I cement with Cl (1.5%) showing atomic transition line at 837.594 nm and also transitions due to the presence of other elements in this spectral region.

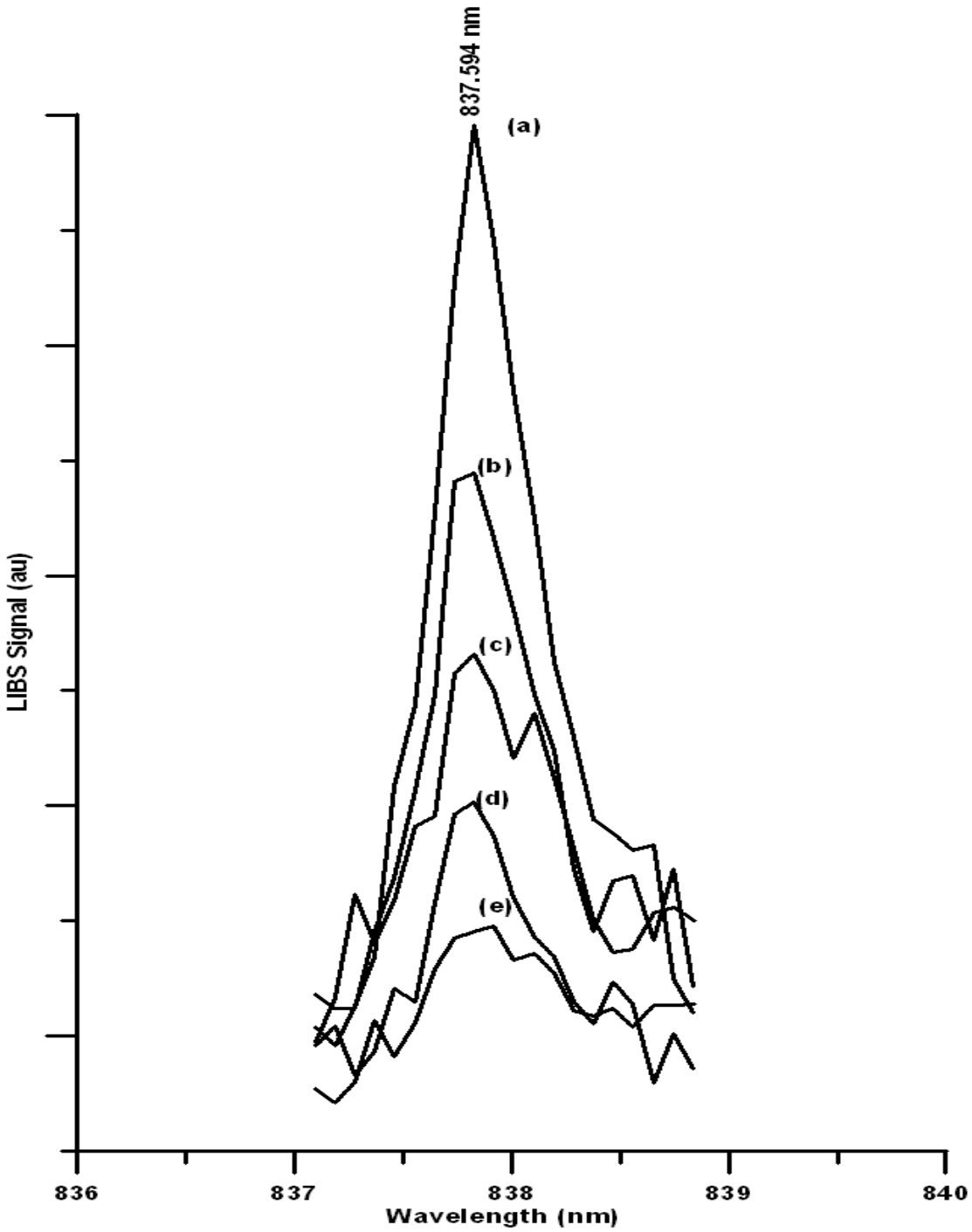

Figure 4.12: LIBS spectrum of the cement paste samples for Type I cement at five different concentrations of chloride with 837.594 nm atomic transition as a marker: (a) 3.5% (b) 1.5% (c) 1% and (d) 0.4% (e) 0.2% of chloride by weight of cementitious materials content.

The calibration curve for the LIBS signal versus chloride concentration in the cement paste for both 837.5 nm and 594.8 nm atomic transition lines is shown in the Figure 4.13. It could be clearly observed that the calibration curve for the 594.89 nm transition line was steeper than that for 837.5 nm line. Characteristically, the atomic emission line at 837.5 nm has the intensity 1000 folds more than that of 594.8 nm line and still this emission line shows a weaker LIBS signal due to the re-absorption of the laser light on the cement paste surface. The stronger atomic transition line having weaker LIBS signal and the weaker atomic transition line showing stronger LIBS signal in the case of cement paste of indicate the limitations of the 837.5 nm atomic transition line in the case of cement paste sample due to the self-absorption process and also the high sensitivity of the dual pulsed LIBS system using 594.8 nm line as a marker.

As mentioned before, one of the major elements present in the cement paste sample was calcium, which coincidently has a very high emission and absorption activity in the 800-900 nm region and, therefore, most of the lines emitted by the cement paste sample were re-absorbed by the calcium atom and, hence, they were absent in the LIBS spectra. In general, in LIBS, atomic emission line at 837.5 nm was used as a good candidate for the detection of chloride in many applications including the cement paste sample owing to its high emission intensity. However, in the case of detection of chloride in the cement paste, 837.5 nm line was not that of attraction due to the presence of calcium. On the other hand, characteristically weaker transition (1000 times weaker) line shows a better candidate for the detection of chloride in the cement paste.

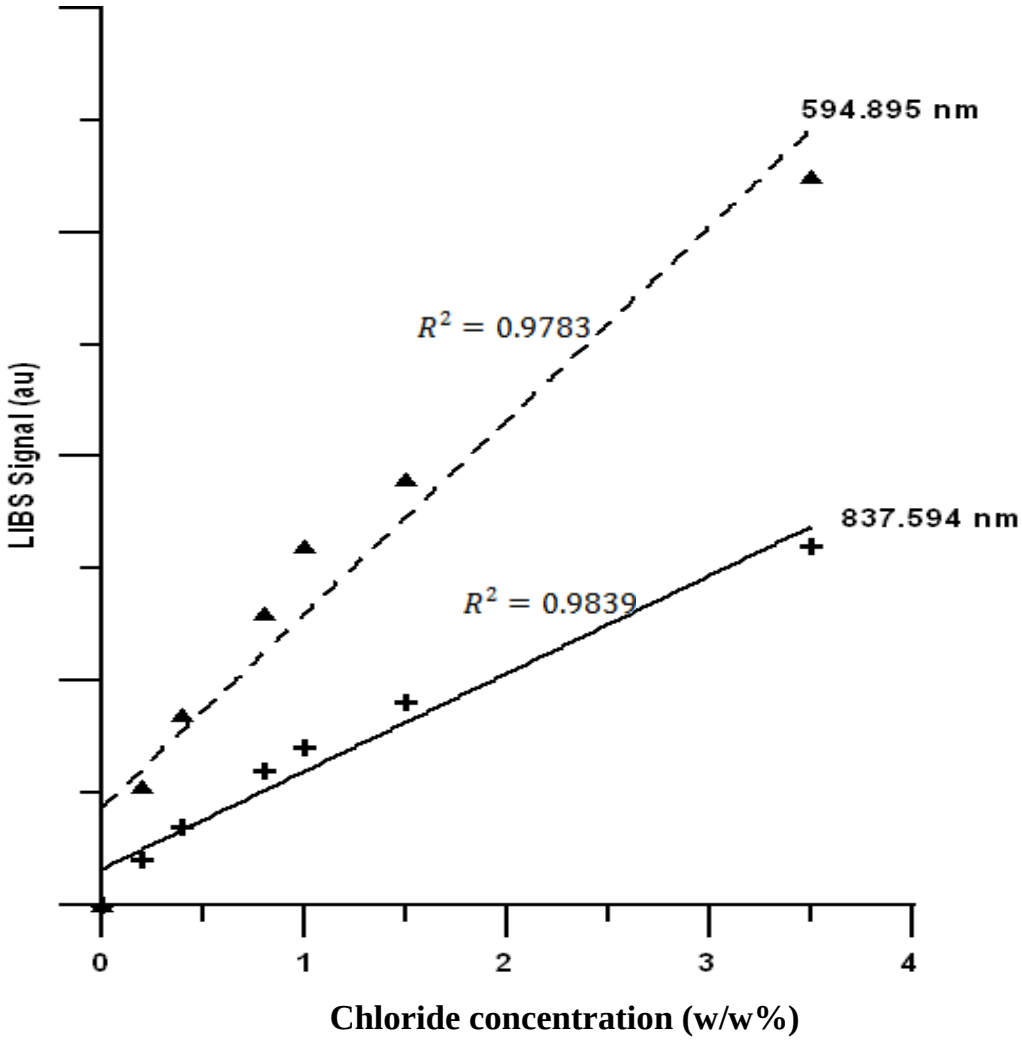

Figure 4.13: Calibration curve for the detection of chloride using 594.858 nm and 837.594 nm transition lines as markers.

4.5 SULFATE DETECTION

As far as the LIBS experiment was concerned, one deals with the elements and their atomic fluorescence and, hence, in the cement paste samples, the main elemental compositions were: calcium, silicon, aluminum and iron in addition to other minor additives and impurities. In this case, sodium sulfate (Na_2SO_4) was mixed in the cement paste mix to make standards for the measurements and, therefore, the presence of sodium and sulfate was expected in the elemental composition of the cement paste. Figure 4.14 depicts the dual pulsed LIBS spectrum recorded in the 280–480 nm region for the cement paste sample mixed with 3% sulfate. In this spectrum, beside the dominating calcium atomic line, aluminum, silicon, iron, carbon, oxygen and sodium (from the additive) were observed.

In the spectral region recorded in Figure 4.14, some emission lines of both neutral calcium (CaI) and singly-ionized calcium (CaII) were present, while some atomic emission lines were absent in this region. In the case of silicon, only one neutral silicon (SiI) emission line at 288.15 nm was observed, which is one of the strongest lines of silicon. For aluminum, all the inherent emission lines of neutral aluminum (AlI) were recorded in Figure 4.14 but the singly-ionized aluminum (AlII) lines were absent. The sodium lines in the spectrum were due to Na_2SO_4 additive and the strong persistent lines were inherently not present in this region [27]. Since cement is a mixture of multi-elements and as different elements have different absorption wavelengths in the region of Figure 4.14, the self-absorption, where the emission of one element was reabsorbed by another element and, consequently, some atomic emission lines that were supposed to be present in the spectra (Figure 4.14) were not recorded. All the lines were assigned by their finger print wavelength and were marked on the spectrum.

The strongest lines of neutral sulfur (SI) were present only either in the infrared or deep UV regions [44]. In the region between 200 and 900 nm, there were very few weak lines present, which could not be easily detectable. For this reason, in this study, the emission line at 545.38 nm was selected with the relative intensity of 40% of the strongest line as a marker. This line was due to the singly-ionized sulfur (SII) and due to the transition

from $3s_2 3p_2$ (3P) p $4D_{7/2}$ (128,599 cm^{-1}) to3s2 $3p_2$(3P)4s4$P_{5/2}$ (110,268 cm^{-1}). The Grotrian diagram of the atomic transitions of SII at 545.38 nm was depicted in Figure 4.15 [44].

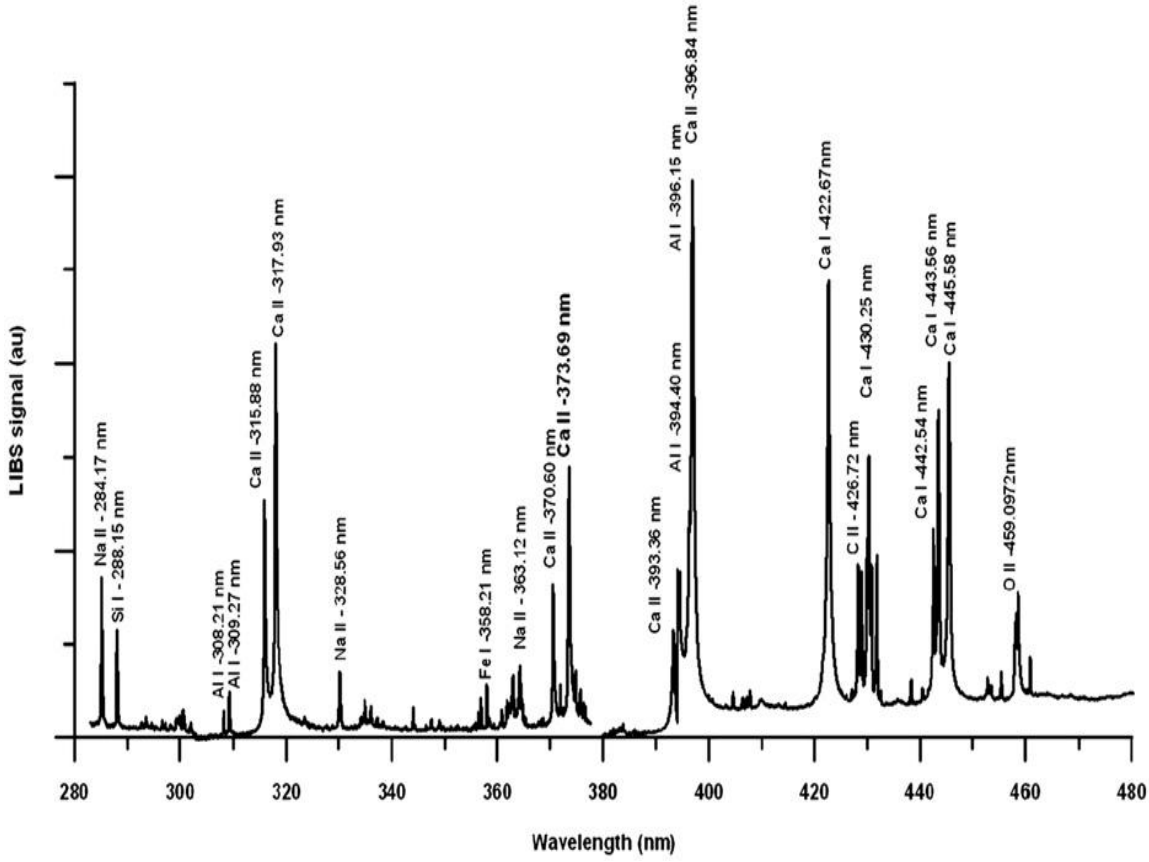

Figure 4.14: LIBS spectrum of the cement paste sample showing different elements present in the paste of Type I cement with S (3.0%) present in the cement paste.

In the normal LIBS studies, the high energy laser pulse was focused on the sample surface where the laser pulse creates local plasma that consists of electrons, ionized species and other neutral atoms. LIBS could record emission spectrum from neutral as well as from the ionized specie [44]. The ionic emission could typically take place from 0.25 μs to 2 μs and after that electron recapture changes all the ionized elements to a neutral one and the emission from the excited neutral atom takes place in the

matter of 0.5–50 μs and finally the molecular recombination takes place between 2 μs to100 μs.

As mentioned earlier, the 545.38 nm marker for the detection of sulfur was due to the emission from singly-ionized sulfur and, hence, the detection gate has to be delayed to less than 1 μs in order to record the emission from the ionized sulfur.

LIBS, as such, is a multi-photon process, where the atoms are promoted to highly ionized levels due to highly energetic laser radiation and electron recombination taking place at various levels. In this case, a second laser was used after an optimum time delay, which considerably enhanced the LIBS signal. This really helped to detect the weak emission lines of sulfur for a concentration less than the permissible level in the cement paste sample.

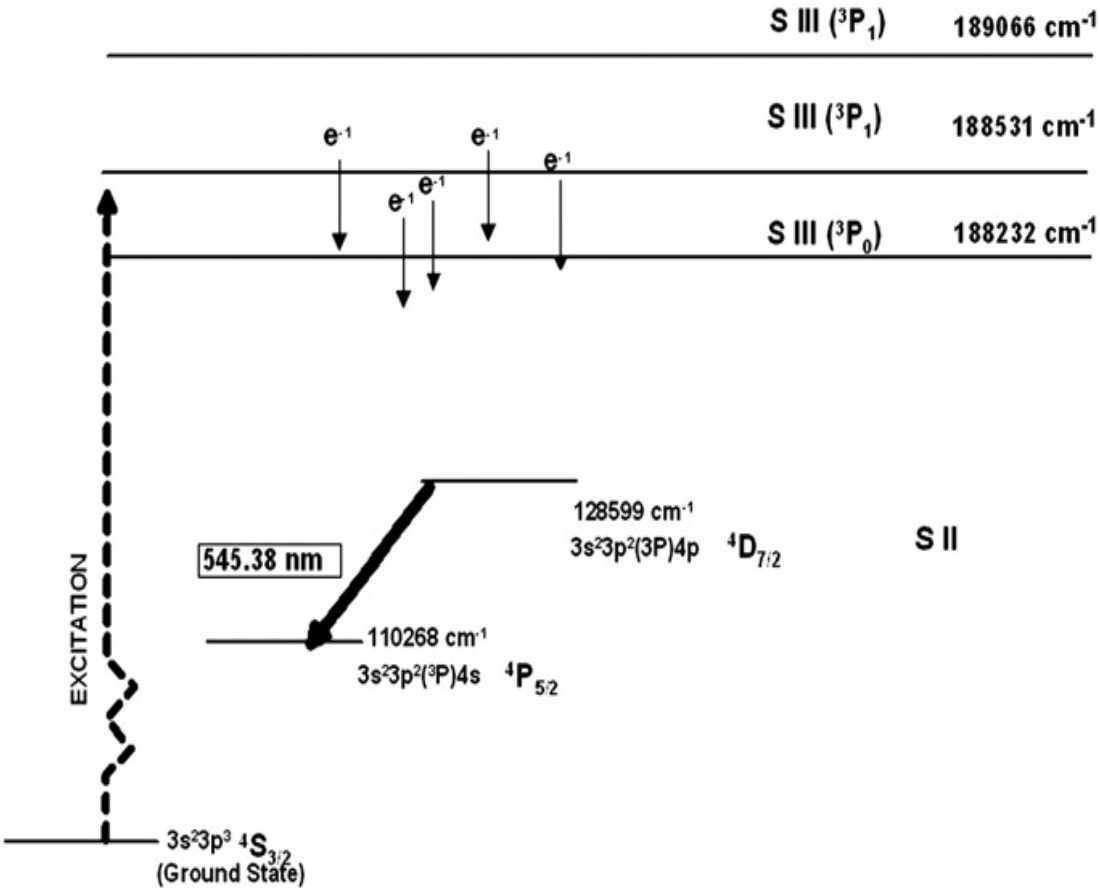

Figure 4.15: Grotrian diagram of the atomic transitions of S II at 545.38 nm

Figure 4.16 shows the dual pulsed LIBS spectrum in the wavelength region, which mainly includes the atomic emission at 545.38 from SII and also the emission at 559.3 nm from Al II. We depict this region separately because the emission from both SII and Al II take place at much earlier time, at a gate delay of 900 ns, whereas in the case of Figure 4.14 the delay was 8 μs, where we noticed neither the trace of emission from SII nor from AlII. Further, for Figure 4.16, the inter pulse delay was around 6 μs. This was quite natural as the typical time delay for the detection of emission from ionized species was from 0.25 to 2 μs, whereas for neutral atom the delay could be as long as 50 μs. In addition to the delay of the detection gate in the LIBS system, in the case of the dual pulsed system, the inter pulse delay plays a crucial role in determining the signal level and all other positive attributes. St-Onge et.al. [26] reported LIBS signals with the dual pulse combination of 1064 and 266 nm laser pulses and observed the larger signal enhancements for ionic lines than for atomic lines, which were also correlated with a higher plume temperature. Further they reported that optimum inter-pulse delay time was around 100 ns for atomic lines and about 3 μs for ionic lines. However, in the case of the detection, the delay was shorter for the ionic species and longer for the atomic species [26].

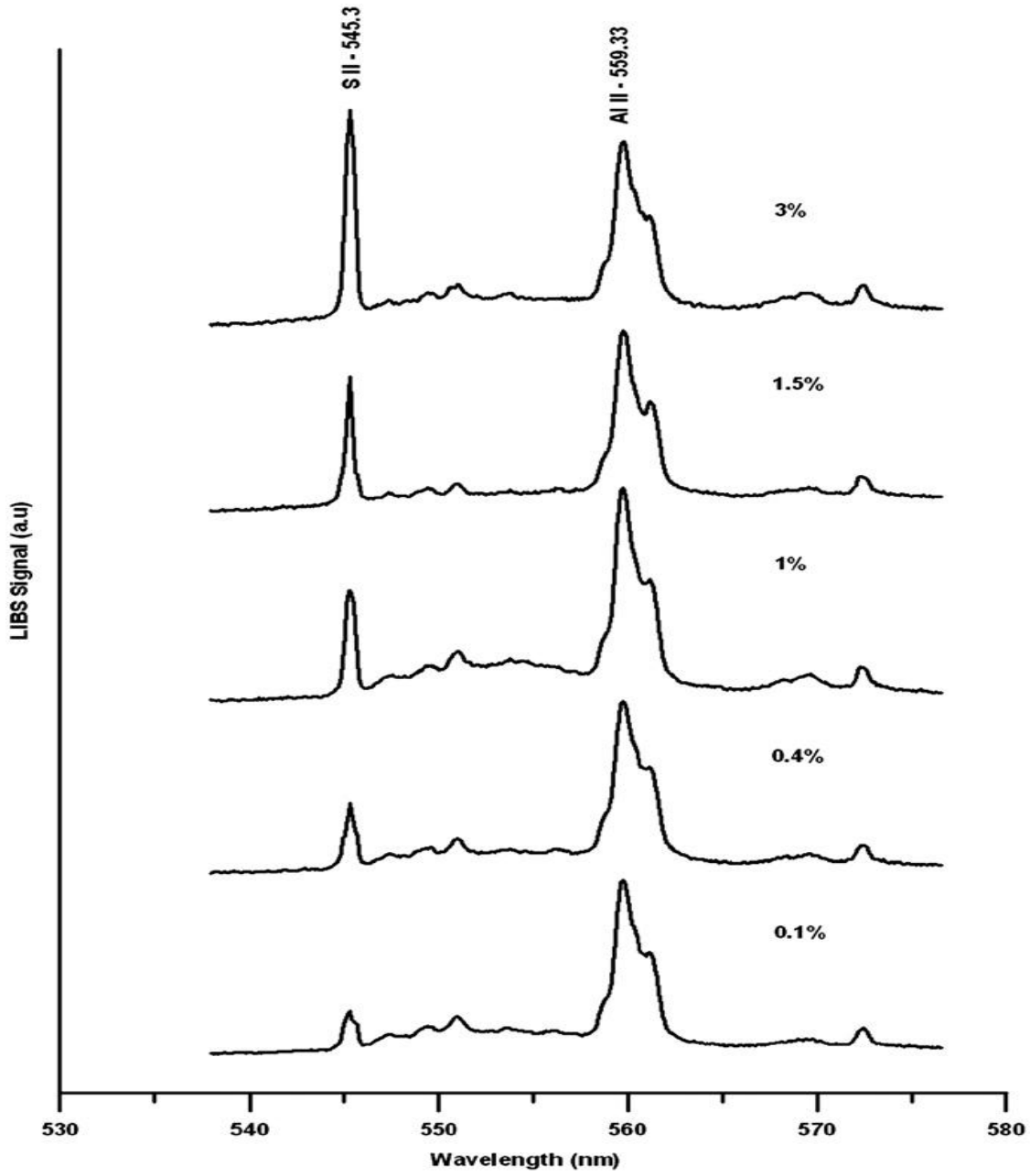

Figure 4.16: LIBS spectrum of the paste samples in 545.3 nm region for five different concentrations of sulfur by weight percentage in the cement paste samples: (a) 3%, (b) 1.5%, (c) 1%, (d) 0.4% and (e) 0.1% by weight of cementitious materials content.

Figure 4.16 shows the LIBS spectrum for five different concentrations of sulfur in the cement paste (by weight percentage). The emission line at 559.3 nm from (AlII) was originally from the cement (as mentioned earlier) and the emission line at 545.38 nm from SII was due to the external addition and, therefore, the AlII line was used as the reference for calibration of the SII. As there was no reason for the line at 559.3 nm (AlII) to change, whatever change observed in the relative intensities of 545.38 (SII) line that would be due to the variation in the different concentrations in the sulfur was deliberately added at the beginning of the experiments.

The data in Figure 4.16 indicate a significant variation in the sulfur peaks. As the concentration of sulfur was increased from 0.1% to 3%, the 545.38 nm peak slowly grows and eventually over shoots the 559.3 nm line when the concentration was 3%. The relative intensities of these two peaks and their relative growth are depicted in Table 4.2. This proves the ability of our LIBS system to detect the variation in sulfur concentration.

In the case of detection of sulfur in cement paste samples, the design of a portable system has been put forward when it comes to detection of sulfur in cement sample. Weritz et al. [45] used a single pulsed LIBS system with SI atomic transition lines at 921.3 nm as marker. The 921.3 nm transition line is in the near infrared (IR) region and it is at the close proximity of the oxygen line at 926.6 nm. In their work, the data for 0.6% of sulfur content by weight is the minimum detection limit. Although 921.3 nm atomic transition line is one of the strongest lines of SI, the limit of detection is not that appreciable. It is to be noted that there are quite a few strong transition lines of SI below 200 nm. As mentioned earlier, the sulfur atom is highly reactive at the excited state and can easily react with the available oxygen and as the cement paste sample has oxygen, using the vacuum ultraviolet (VUV) wavelengths as a marker is not reliable. SI also has many atomic transition lines in the near IR region, one of these lines (921.3 nm) was used by Weritz et al. [45] as a marker.

In the case of cement paste sample, sulfur is abundant with the calcium element and the singly-ionized calcium atom (CaII) has a strong atomic transition line at exactly 921.3

nm [44], which coincides with 921.3 nm marker and also it is possible that this 921.3 nm emission line is self-absorbed by the sample itself, resulting in a weak LIBS signal. Moreover, at the neighborhood of 921.3 nm, the atomic transition line of oxygen is at 926.6 nm and this oxygen line cannot be used as a reference line to study the relative growth of 921.3 nm marker line because, in addition to the sample, oxygen is present in the environment that will alter the strength of 926.6 nm line of oxygen.

In this study, a dual pulsed LIBS system was developed for the detection of sulfur in the cement paste sample, and doing so, the signal strength of the dual pulsed system described above is improved. The two lasers radiations used in this work are 1064 nm and 266 nm from two different lasers and an emission line of SII at 545.38 nm is used as a marker wavelength. This transition line of SII in the visible region was closer in spite of the fact that the line intensity is much smaller than its counter parts in vacuum ultraviolet (VUV) and near infrared NIR regions due to the following reasons: the problem with the transition lines in the VUV region is ascribed to the fact that sulfur is highly reactive and the signal level of sulfur is not that appreciable. In the NIR region, the calcium, which is a predominant element present in the cement paste sample, has strong emission lines. Further, in the 545.38 nm region, there is no overlap of the atomic lines of elements present in the cement paste sample.

Aluminum is one of the major elements present in the cement paste sample, whose concentration remains constant and, hence, the transition line of AlII at 559.33 nm can be used as a reference peak to study the variation of sulfur atomic transition peak. With the right choice of inter-pulse delay, detection gate delay and gate width, it was possible to detect sulfur as low as 0.1% in the cement paste sample and calibration curve is presented. In dual pulsed LIBS system, the original LIBS signal is considerably enhanced by the combined effect of two high power incident collinear laser pulse with proper time delays between the two laser pulses and also the delay between the initial laser pulse and the detection system.

The relative intensities of SII peak at 545.38 nm and AlII peak at 559.33 nm, respectively, are given in Table 4.3. The relative growth of the 545.38 (SII) line was quite emphatic and could give reliable data for calibration of sulfate concentration

versus LIBS signal in arbitrary units, which was depicted in Figure 4.17 and the calibration curve demonstrates that the LIBS signal intensity at 545.38 nm line increases linearly with the concentration of sulfur. The R^2 of the linear fit for the data in Figure 4.17 was 0.9860.

Table 4.3: Relative intensities of S II peak at 545.38 nm and Al II peak at 559.33 nm.

Concentration	Intensity of S II peak at 545.38 nm (arbitrary counts)	Intensity of Al II peak at 559.33 nm (arbitrary counts)	Percentage of relative intensities (%)
0.1	5021	37,860	13,2
0.4	12,210	38,046	32
1	22,610	38,283	59
1.5	31,030	38,540	80.5
3	49,650	38,490	128.9

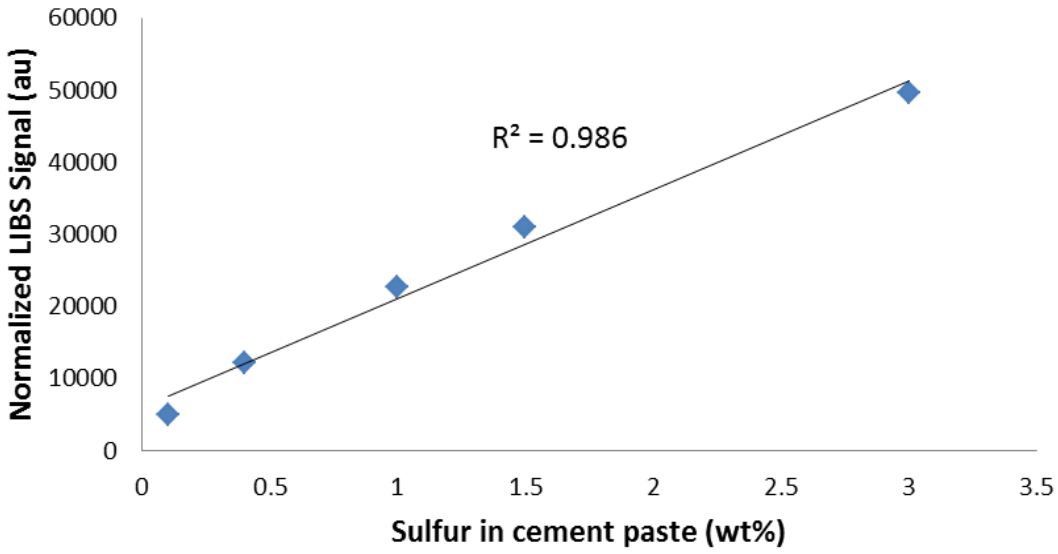

Figure 4.17: Calibration curve for the sulfur concentration in the cement paste sample versus LIBS signal.

Each data point in Figure 4.17 is the statistical average of six scans and the standard error (standard deviation divided by square root of 6) is depicted with the error bar. Since the error was quite small, a multiplier of 8 was used in the error bar of Figure 4.17. In order to find the limit of detection, 12 blank samples were used at different locations and using the standard deviation of this data and the slope of the calibration curve, the limit of detection (LOD) was found to be 0.00385% or in other words the LOD was approximately 38 µg/g, as shown in Figure 4.18.

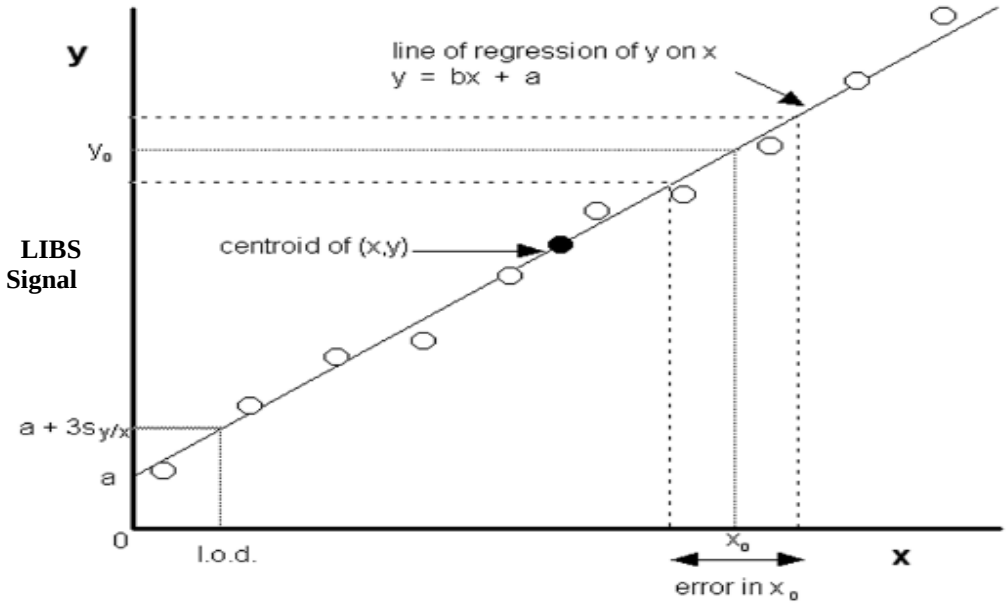

Figure 4.18: Graphical representation of calculating the limit of detection from the regression line.

4.6 CHLORIDE AND SULFATE DETECTION

As shown in Figure 4.19 through 4.22, sulfate and chloride have both only few spectral lines, which are suitable for detection. Almost every publication concerning Cl detection reports about the Cl spectral line at 837.6 nm [19,26] and most applications concern sulfate measurements reports about S spectral lines at 921.3 (and at 922.8 nm and 923.8 nm) can be used for S detection in building materials [45]. These two spectral lines for Cl (837.6 nm) and SI (921.3 nm) are used to detect the chloride and sulfate in cement paste samples. Table 4.4 shows the configuration and energy levels for the Cl and S spectral lines.

Table 4.4: Configuration and energy levels of the strongest Cl and S spectral lines.

Element	Wavelength (nm)	Initial configuration	Final configuration
Cl I	837.6	$3p_4 4s$	$3p_4(3P)4p$
S I	921.3	$3s_2 3p_3(4S°)4s$	$3s_2 3p_3(4S°)4p$

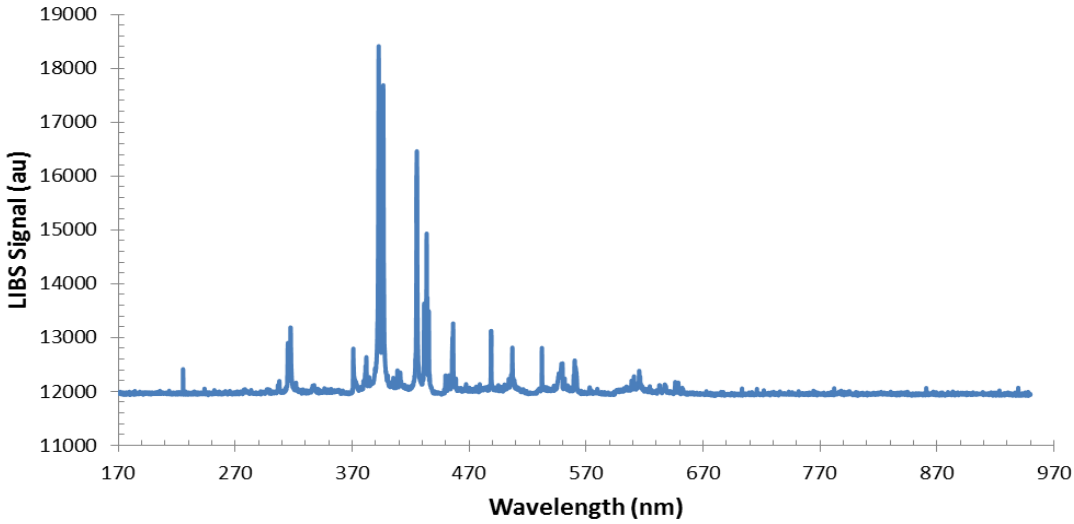

Figure 4.19: Typical LIBS spectra of Type I cement sample in the region of 170 to 950 nm for concentrations of 0.4% chloride and 0.2% sulfate by weight of the cementitiuos materials content.

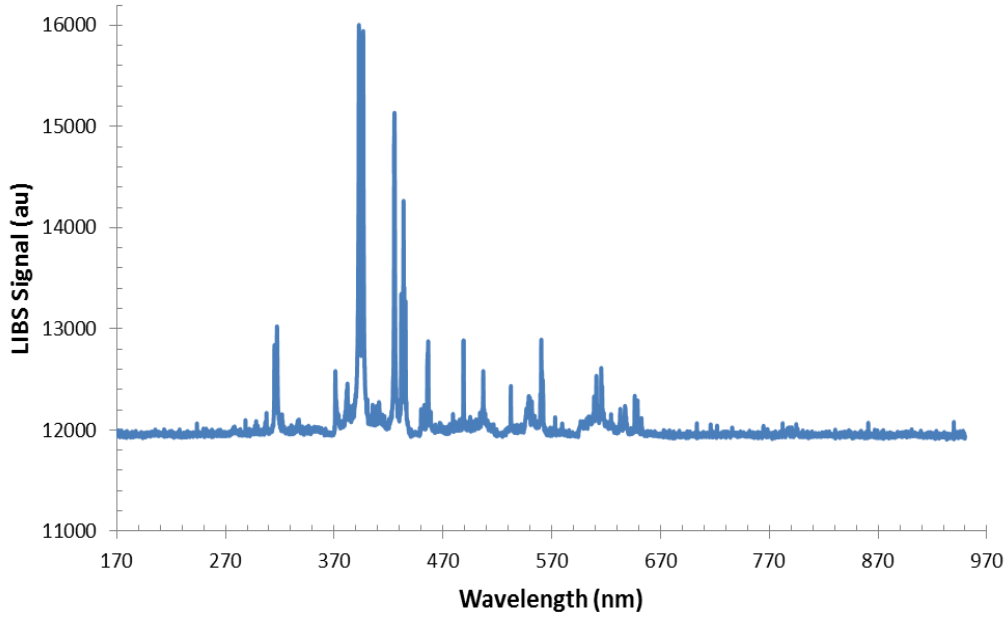

Figure 4.20: Typical LIBS spectra of Type V cement sample in the region of 170 to 950 nm for concentrations of 0.4% chloride and 0.2% sulfate by weight of the cementitiuos materials content.

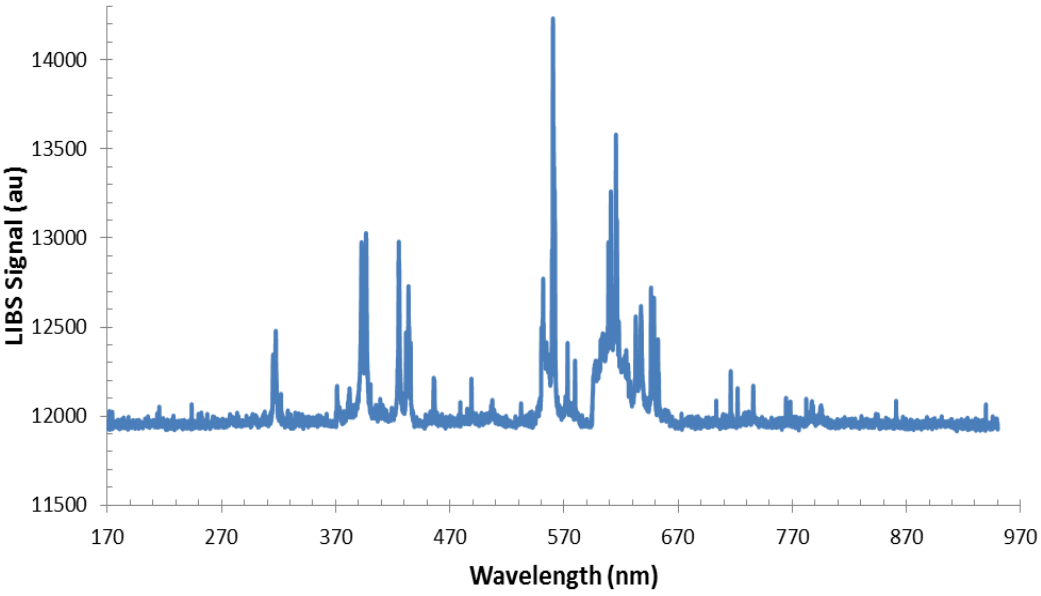

Figure 4.21: Typical LIBS spectra of Type I + fly ash cement sample in the region of 170 to 950 nm for concentrations of 0.4% chloride and 0.2% sulfate by weight of the cementitiuos materials content.

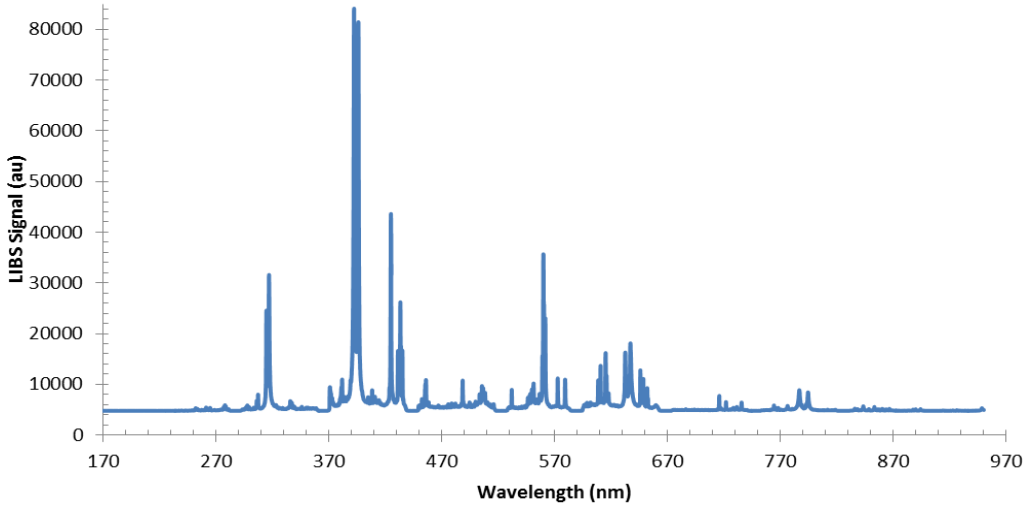

Figure 4.22: Typical LIBS spectra of Type I + silica fume cement sample in the region of 170 to 950 nm for concentrations of 0.4% chloride and 0.2% sulfate by weight of the cementitiuos materials content.

Figure 4.23 shows the spectral using region of the cement paste made Type I cement with 0.8% chloride and 0.2% sulfate with 921.3 nm atomic transition as a marker. The spectral line for SI (921.2 nm) is used to detect the sulfate in the cement paste sample.

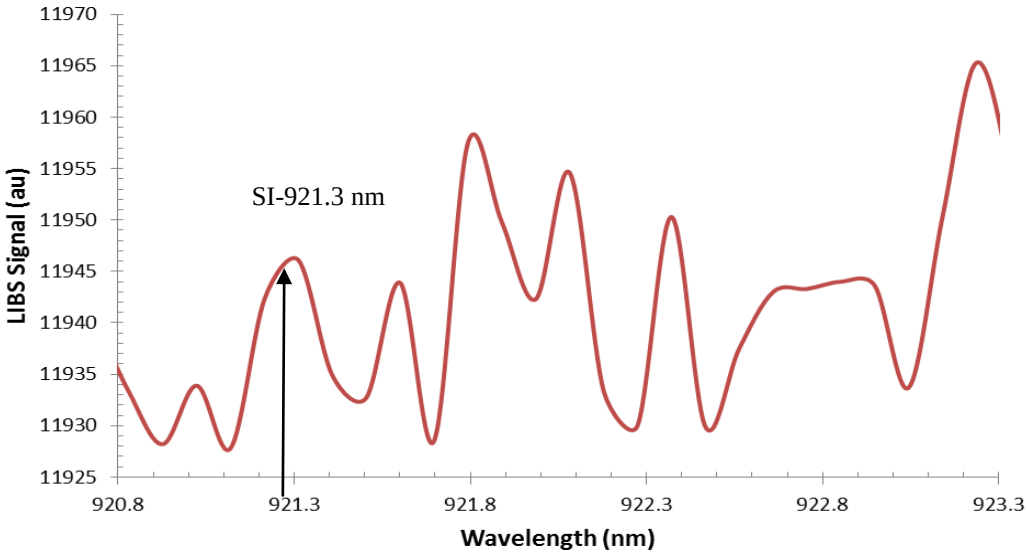

Figure 4.23: Typical LIBS spectrum of the cement paste samples using Type I cement with 0.8% chloride and 0.2% sulfate with 921.3 nm atomic transition as a marker.

Similarly, Figure 4.24 shows the spectral using region of the cement paste made Type I cement at 0.8% chloride and 0.2% sulfate with 837.6 nm atomic transition as a marker. The spectral line for ClII (837.6 nm) is used to detect the chloride in the cement paste sample.

The LIBS spectra for all the other cement paste specimens investigated in this study are shown in Appendix "A".

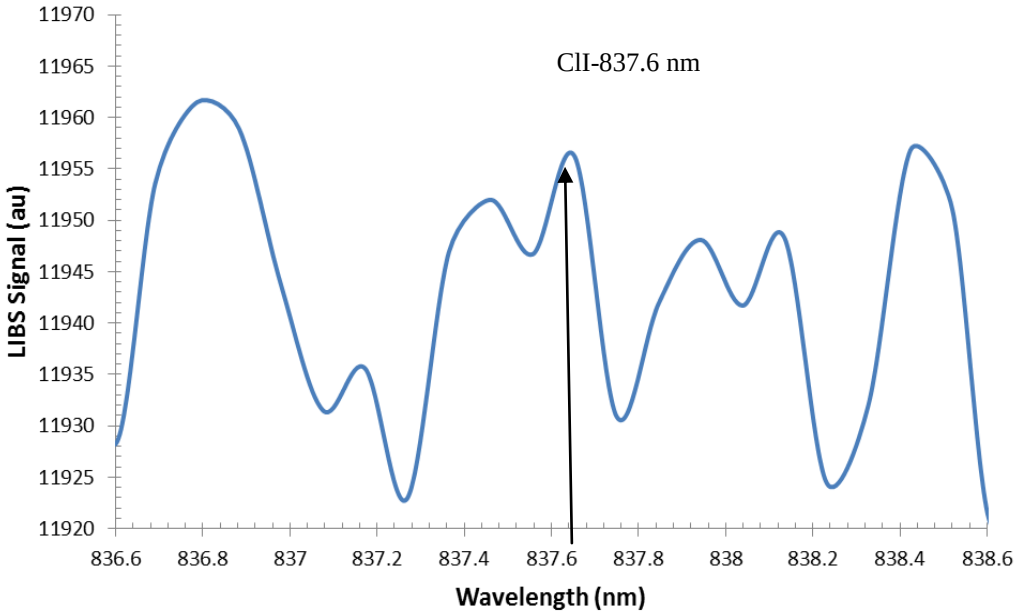

Figure 4.24: LIBS spectrum of the cement paste samples with Type I cement with 0.8% chloride and 0.2% sulfate with 837.6 nm atomic transition as a marker.

CHAPTER 5

CONCLUSIONS AND FUTURE WORK

5.1 CONCLUSIONS

In this study, a dual pulsed laser induced breakdown spectrometer was employed to detect chloride content in the cement paste specimens. The dual pulsed LIBS spectra for various chloride concentrations in cement paste samples were carried out using two emission lines of chlorine at 594.8 and 837.5 nm as a marker. Following conclusions can be made based on the data developed in this study.

Characteristically, the relative intensity of 594.8 nm line is 1000 times less than that of 837.5 nm emission line and, hence, the 837.5 nm emission line is widely used as a marker for the detection of chloride ion in LIBS. However, due to the abundance of calcium ion in concrete and its predominantly high emission absorption activity in the 800-900 nm region, emission line of chloride at 837.5 nm turns out to be a weaker marker in the case of cement paste than the line at 594.8 nm despite the fact that this emission line is characteristically much weaker than the 837.5 nm line.

A dual pulsed LIBS system with a high sensitive gated ICCD camera was developed in this investigation to detect sulfate ions in the cement paste. The atomic emission line of singly-ionized sulfur (SII) at 545.38 nm was used. A systematic growth of the LIBS signal at 545.38 nm peak of (SII) with respect to the neighboring 559.3 nm peak of AlII ion was noticed as the concentration of sulfate increased. The limit of detection of the system is 0.00385% equivalent to 38 mg/g.

The LIBS results were successfully validated by comparison with the results of ICP. It was shown that the LIBS technique is a suitable tool for the determination of chloride and sulfate content in cement paste A linear relationship between the LIBS

measurements and actual values was obtained. Further, a good correlation between LIBS and ICP measurements was obtained.

5.2 FUTURE WORK

The leading multi-disciplinary research program conducted in this investigation is new in the area of civil engineering. To complement the findings of this investigation, it is proposed to extend the research program in the following areas:

- The possibility of utilizing LIBS on mortar and concrete specimens should be investigated.
- LIBS set-up should be used to determine free- and bound-chloride contents.
- LIBS system, as a portable tool, should be developed.

REFERENCES

1. Al-Amoudi, O.S.B. Protection of reinforced concrete structures in sulfate-chloride exposures. *NACE Corrosion 2007 Conference and EXPO*, Paper 07279, 2007, pp. 16.

2. Al-Amoudi, O.S.B., Rasheeduzzafar, Maslehuddin, M. and Abduljawwad, S.N. Influence of chloride ions on sulfate attack in plain and blended cements. *Magazine of Concrete Research*, 1994a, Vol. 46, No. 167, pp 113-123.

3. Al-Amoudi, O.S.B., Rasheeduzzafar, Maslehuddin, M. and Abduljawwad, S.N. Influence of sulfate ions on chloride-induced reinforcement corrosion in plain and blended cements. *Journal of Cement, Concrete, and Aggregates*, 1994b, Vol. 16, No. 1, pp. 3-11.

4. Breit, W. *Investigations about the critical corrosion causing chloride content*. PhD thesis. 1997, RWTH Aachen, Germany.

5. Maslehuddin, M., Saricimen, H., Al-Mana, A.I., and Shamim, M., Performance of concrete in a high chloride-sulfate environment, *American Concrete Institute, Special Publication SP*-122, 1990, pp. 469-494.

6. Gondal, M. A. and Hussain, T. Determination of poisonous metals in waste water collected from paint manufacturing plant using laser-induced breakdown spectroscopy, *Talanta*, 2007, Vol. 71, pp. 73-80.

7. Gondal, M.A.; Hussain, T.; Yamani, Z.H. and Baig, M.A. Detection of heavy metals in Arabian crude oil residue using laser-induced breakdown spectroscopy. *Talanta*, 2006, Vol. 69, pp. 1072-1078.

8. Gondal, M. A; Hussain, T.; Yamani, Z. H. and Baig, M. A. The role of various binding materials for trace elemental analysis of powder samples using laser induced breakdown spectroscopy. *Talanta*, 2007, Vol. 72, pp. 642-649.

9. Gondal, M. A. Laser photo acoustic spectrometer for remote monitoring of atmospheric pollutants. *Appl. Opts*, 1997, Vol. 36, pp. 3195-3201.

10. Gondal, M. A. and Mastromarino, Pulsed laser photoacoustic detection of SO_2 near 225.7 nm. J. *Applied Optics*, 2001, Vol. 40, pp. 2010 -2017.

11. Gondal, M. A. and Mastromarino, J. Lidar system for remote environmental studies, *Talanta*, 2000, Vol. 53, pp.147-154.

12. Gondal, M. A, T. Hussain, Z. H. Yamani and A.H. Bakry, Determination of elemental composition in iron slag waste using laser induced breakdown spectroscopy, *J. Environment Science and Health*, 2007, Vol. 42, No. 6, pp. 767-775.

13. Gondal, M. A. M. N. Siddiqui. Identification of different kinds of plastics using laser induced breakdown spectroscopy for waste management, *J. Environment Science and Health, Part A*, 2007, Vol. 42, No. 13.

14. Gondal, M. A T. Hussain, Z. Ahmad, A. Bakry. Detection of contaminants in ore samples using laser induced break down spectroscopy. *J. Environment Science and Health, Part A*, 2007, Vol. 42, No. 7, pp. 879-887.

15. Hussain, T. M. A. Gondal. Detection of toxic metals in waste water from dairy product plant using laser-induced breakdown spectroscopy. *Bulletin of Environmental Contamination & Toxicology,* Vol. 80, Number 6, June 2008, pp. 561-565.

16. Hussain, T. M. A. Gondal. Monitoring and assessment of toxic metals in gulf war oil spill contaminated soil using laser-induced breakdown spectroscopy. *Environmental Monitoring and Assessment*, Vol. 136, No. 1-3. , 2008, pp. 391-399.

17. Knopp, R., Scherbaum, F.J and Kim, J.I. Laser-induced breakdown spectroscopy (LIBS) as an analytical tool for the detection of metal ions in aqueous solutions. *J. Anal. Chem*., 1996, Vol. 355, pp. 16–20.

18. Noll, R., Bette, H., Brysch, A., Kraushaar, M.; Mönch, I.; Peter, L.; Sturm, V. Laser-induced breakdown spectrometry-Applications for production control and quality assurance in the steel industry. *Spectrochim. Acta Part B,* 2001, Vol. 56, pp. 637- 649.

19. Sallé, B.; Cremers, D.A.; Maurice, S. and Wiens, R.C. Laser-induced breakdown spectroscopy for space exploration applications: Influence of the ambient pressure on the calibration curves prepared from soil and clay samples. *Spectrochim, Acta Part B,* 2005, Vol. 60, pp. 479–490.

20. Ciucci, M. Corsi, V. Palleschi, S. Rastelli, A. Salvetti and E. Tognoni. New procedure for quantitative elemental analysis by laser-induced plasma spectroscopy. *Appl. Spectrosc*, Vol. 53, 1999, pp. 960–964.

21. Andersson and K.O. Nilsson, Enrichment of trace elements from sewage sludge fertilizer in soils and plants, *AMBIO*, Vol. 1, 1972, pp. 176–179.

22. Kagawa, K. M. Ohtani, S. Yokoi and S. Nakajima. Characteristics of the plasma induced by the bombardment of N_2 laser pulse at low pressures. Spectrochim. *Acta Part B*, Vol. 39, 1984, pp. 525–536

23. Adamson, M. A. Padmanabhan, G.J. Godfrey and S.J. Rehse. Laser-induced breakdown spectroscopy at a water/gas interface: A study of bath gas-dependent molecular species. *Spectrochim. Acta Part B,* Vol. 62, 2007, pp. 1348–1360.

24. Miziolek, A.W., V. Palleschi and I. Schechter, Editors, *Laser-Induced Breakdown Spectroscopy (LIBS): Fundamentals and Applications,* Cambridge University Press, 2006.

25. Ismail, M.A. G. Cristoforetti, S. Legnaioli, L. Pardini, V. Palleschi, A. Salvetti, E. Tognoni and M.A. Harith. Comparison of detection limits, for two metallic matrices, of laser-induced breakdown spectroscopy in the single and double-pulse configuration. *Chem*, Vol. 385, 2006, pp. 316-325.

26. St-Onge, L., M. Sabsabi and P. Cielo. Quantitative analysis of additives in solid zinc alloys by laser-induced plasma spectrometry, *J. Anal. At. Spectrom*, Vol. 12, 1997, pp. 997–1004.

27. Samek, O. D., C.S. Beddows, J. Kaiser, S.V. Kukhlevsky, M. Liška, H.H. Telle and J. Young. Application of laser-induced breakdown spectroscopy to in situ analysis of liquid samples, *Opt. Eng*, Vol. 39, 2000, pp. 2248–2262.

28. Mateo, M.P., Ctvrtnickova, T., Fernandez, E., Ramos, J.A., Yáñez, A., Nicolas, G. Laser ablation of powdered samples and analysis by means of laser-induced breakdown spectroscopy. *Applied Surface Science*, Vol. 255, No. 10, 2009, pp. 5579-5583.

29. Ctvrtnickova, T., Cabalin, L., Laserna, J., Kanicky, V., Nicolas, G. Laser ablation of powdered samples and analysis by means of laser-induced breakdown spectroscopy, *Applied Surface Science*, Vol. 255, No. 10, 2009, pp. 5329-5333.

30. Čtvrtníčková, T., Fortes, F.J., Cabalín, L.M., Laserna, J.J. Optical restriction of plasma emission light for nanometric sampling depth and depth profiling of multilayered metal samples, *Applied Spectroscopy*, Vol. 61, No. 7, 2008, pp. 719-724.

31. Panne, U., R.E. Neuhauser, C. Haisch, H. Fink, and R. Niessner. Remote analysis of a mineral melt by laser-induced plasma spectroscopy, *Applied Spectroscopy*, Vol. 56, No. 3, 2002, pp. 375-380

32. Fink, H., U. Panne, and R. Niessner Analysis of recycled thermoplasts from consumer electronics by laser-induced plasma spectroscopy. *Analytica Chimica Acta*, Vol. 440, No. 1, 2001, pp. 17-25

33. Akshaya Kumar, Fang-Yu Yueh, Jagdish P. Singh, Shane Burgess. Characterization of malignant tissue cells by laser-induced breakdown spectroscopy, *Applied Optics*, Vol. 43, Issue 28, 2004, Page 5399

34. Radivojevic, I., C. Haisch, R. Niessner, S. Florek, H. Becker-Ross, and U Panne, microanalysis by laser-iInduced plasma spectroscopy in the vacuum ultraviolet, *Anal. Chem*., Vol. 76, No. 6, 2004, pp. 1648–1656

35. Panne; U., C. Haisch, M. Clara, R. Niessner. Analysis of glass and glass melts during the vitrification process of fly and bottom ashes by laser-induced plasma spectroscopy. *Part I*: Normalization and plasma diagnostics. *Spectrochimica Acta Part B: Atomic Spectroscopy*, Vol. 53, No. 14, 1998, pp. 1957-1968.

36. Gondal, M.A., Dastageer, A., Maslehuddin, M., Alnehmi, A.J., Al-Amoudi, O.S. Sensitivity enhancement at 594.8 nm atomic transition of Cl I for chloride detection in the reinforced concrete using LIBS. *Journal of Environmental Science and Health. Part A*, Toxic/hazardous substances & environmental engineering, Vol. 46, Issue 2, January 2011, pp. 198-203.

37. Gondal, M.A., Dastageer, A., Maslehuddin, M., Alnehmi, A.J., Al-Amoudi, O.S. Detection of chloride in the reinforced concrete using dual pulsed LIBS system . A comparative study of atomic transition lines of Cl I at 594.85nm and 837.59 nm. *Applied Optics*, Vol. 50, Issue 20, 2011, pp. 3488-3496.

38. Gondal, M.A., Dastageer, A., Maslehuddin, M., Alnehmi, A.J., Al-Amoudi, O.S. Detection of sulfur in the reinforced concrete structures using a dual pulsed LIBS system. *Optics & Laser Technology*, Vol. 44, Issue 3, 2011, pp. 566-571.

39. Capitelli, M.A., Casavola, G., Colonna, A., De Giacomo, "Laser-induced plasma expansion: theoretical and experimental aspects" *Spectrochim Acta, Part B*, Vol. 59, 2004, pp. 271–289.

40. Cremers, D. A., Radziemski, L. J. *Handbook of Laser-induced breakdown Spectroscopy*. Wiley Publisher, England, 2006.

41. Orer, S. *Characterization of ion implanted surface by laser induced breakdown spectroscopy*. MS Thesis, İzmir Institute of Technology, 2008, Izmir, Turkey.

42. Andor technology, digital camera fundamentals rank top 2 http://www.andor.com/learning/digital_cameras/.

43. Aurelio, I. A. *Laser-induced breakdown spectroscopy as a diagnostic tool for coal fines*. MS Thesis, 2005, West Virginia University Morgantown, West Virginia, USA.

44. NIST Atomic spectra database; http://www.nist.gov/pml/data/asd.cfm.

45. Weritz, F., Ryahi, S., Schaurich, D., Taffe, A., Wilsch, G. Quantitative determination of sulfur content in concrete with laser-induced breakdown spectroscopy. *Spectrochimica Acta Part B,* Vol. 60, 2005, pp. 1121–1131.

APPENDIX “A”

LIBS SPECTRA

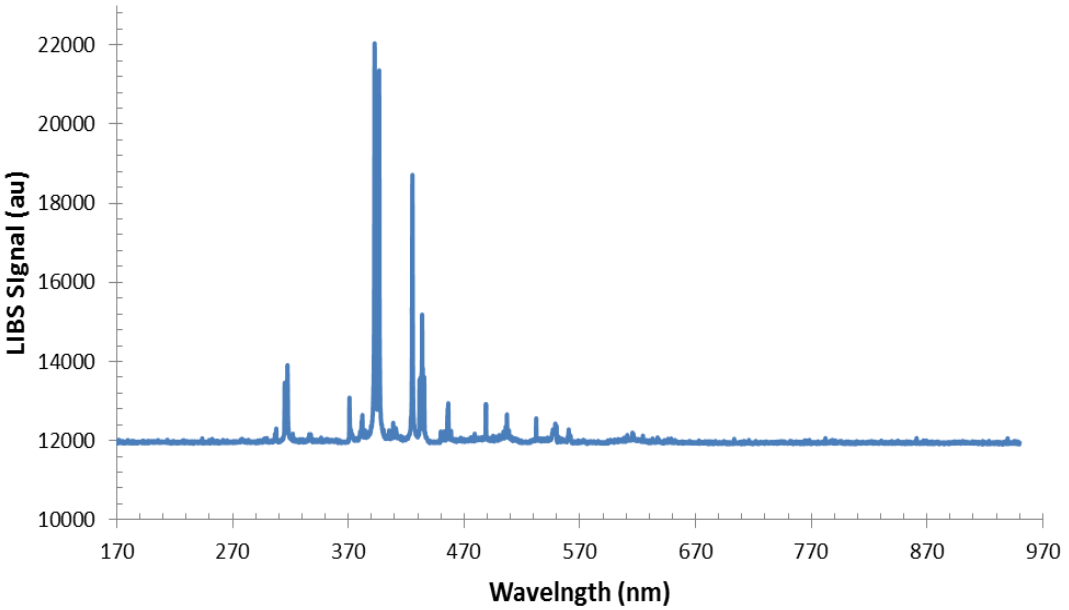

Figure A.1: Typical LIBS spectra of Type I cement sample in the region of 170 to 950 nm for concentrations of 0.4% chloride and 0.4% sulfate by weight of the cementitiuos materials content.

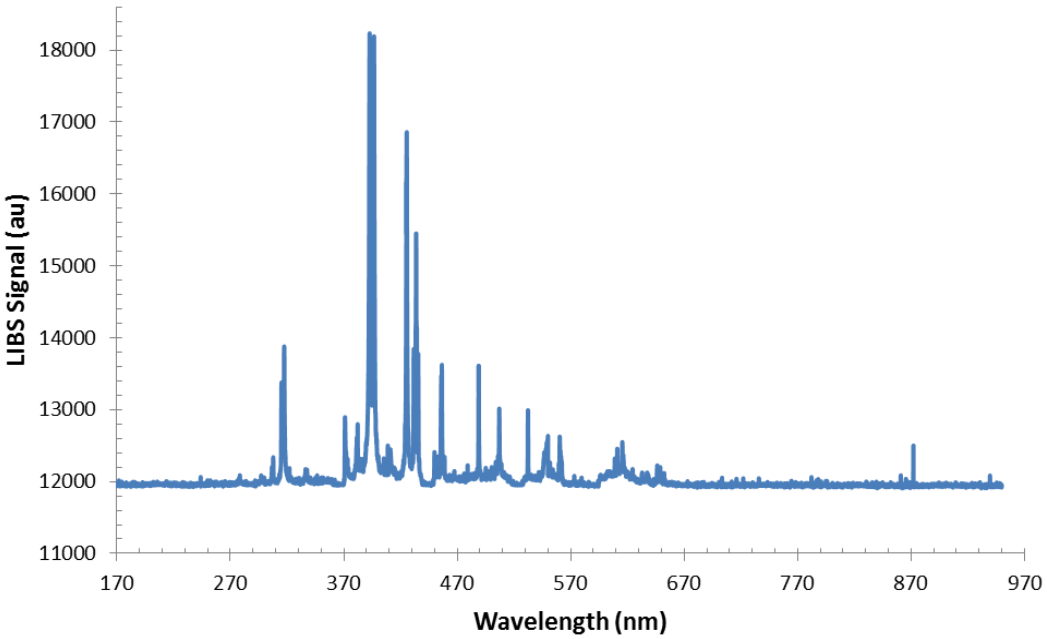

Figure A.2: Typical LIBS spectra of Type I cement sample in the region of 170 to 950 nm for concentrations of 0.8% chloride and 0.2% sulfate by weight of the cementitiuos materials content.

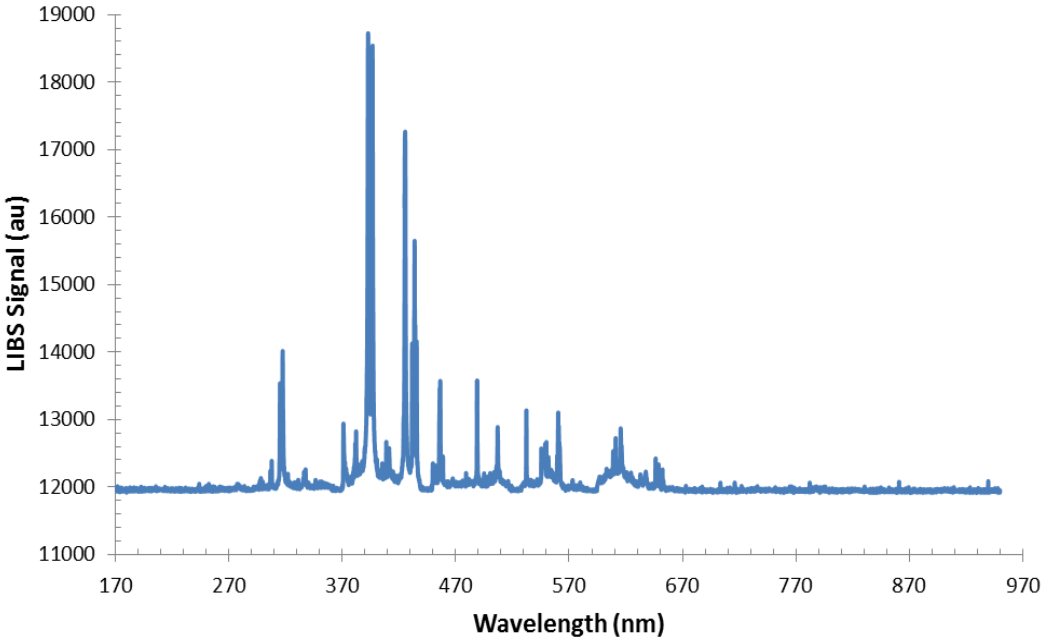

Figure A.3: Typical LIBS spectra of Type I cement sample in the region of 170 to 950 nm for concentrations of 0.8% chloride and 0.4% sulfate by weight of the cementitiuos materials content.

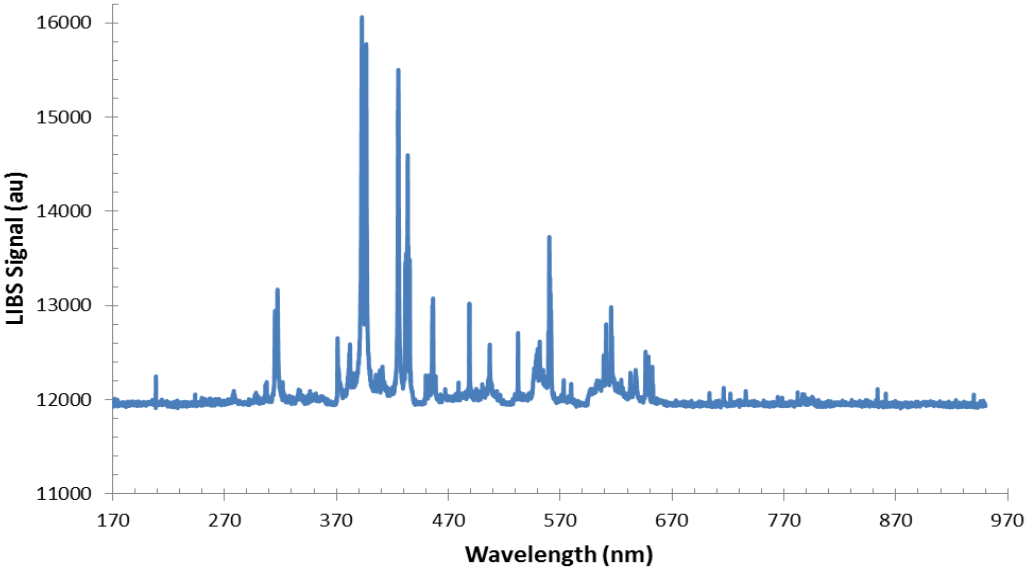

Figure A.4: Typical LIBS spectra of Type V cement sample in the region of 170 to 950 nm for concentrations of 0.4% chloride and 0.4% sulfate by weight of the cementitiuos materials content.

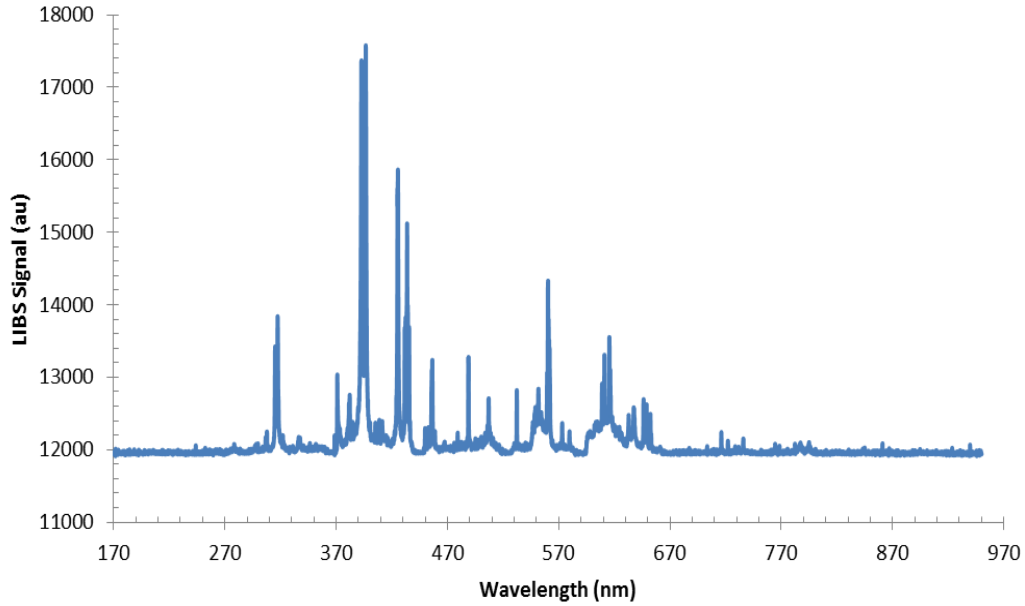

Figure A.5: Typical LIBS spectra of Type V cement sample in the region of 170 to 950 nm for concentrations of 0.8% chloride and 0.2% sulfate by weight of the cementitiuos materials content.

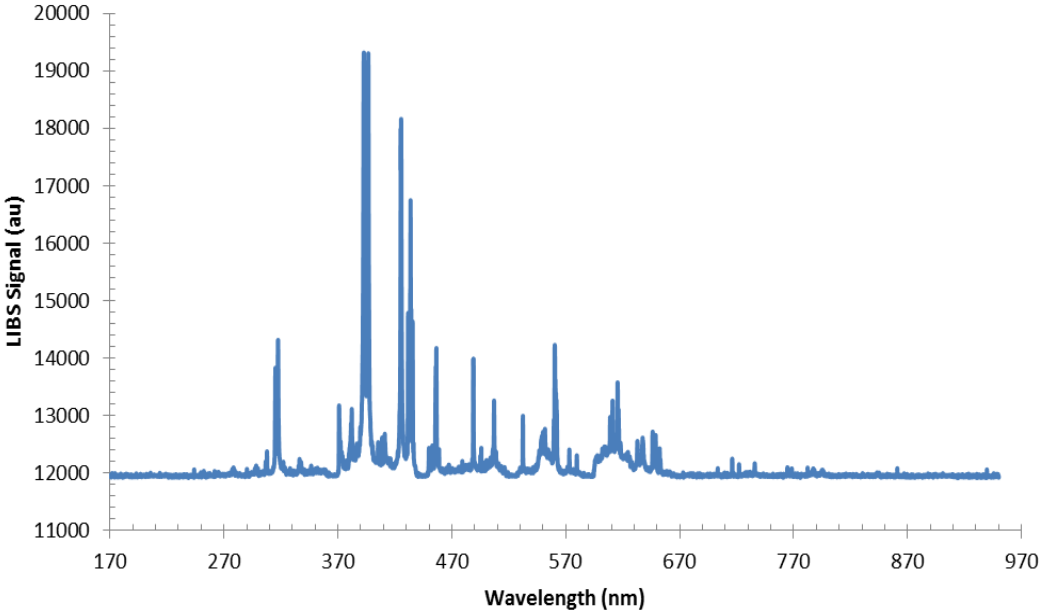

Figure A.6: Typical LIBS Spectra of Type V cement sample in the region of 170 to 950 nm for concentrations of 0.8% chloride and 0.4% sulfate by weight of the cementitiuos materials content.

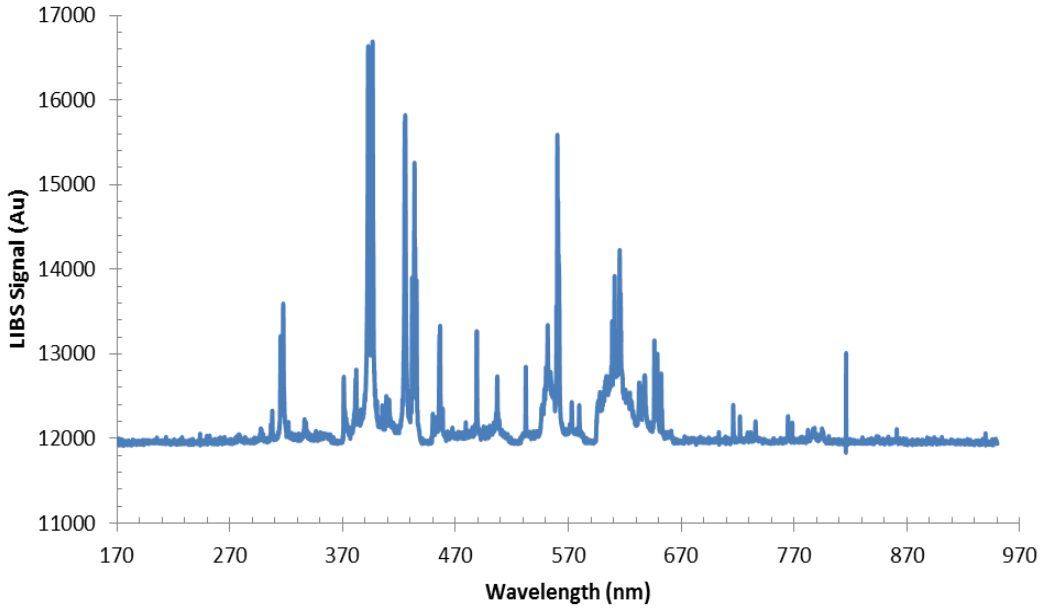

Figure A.7: Typical LIBS spectra of Type I + fly ash cement sample in the region of 170 to 950 nm for concentrations of 0.4% chloride and 0.4% sulfate by weight of the cementitiuos materials content.

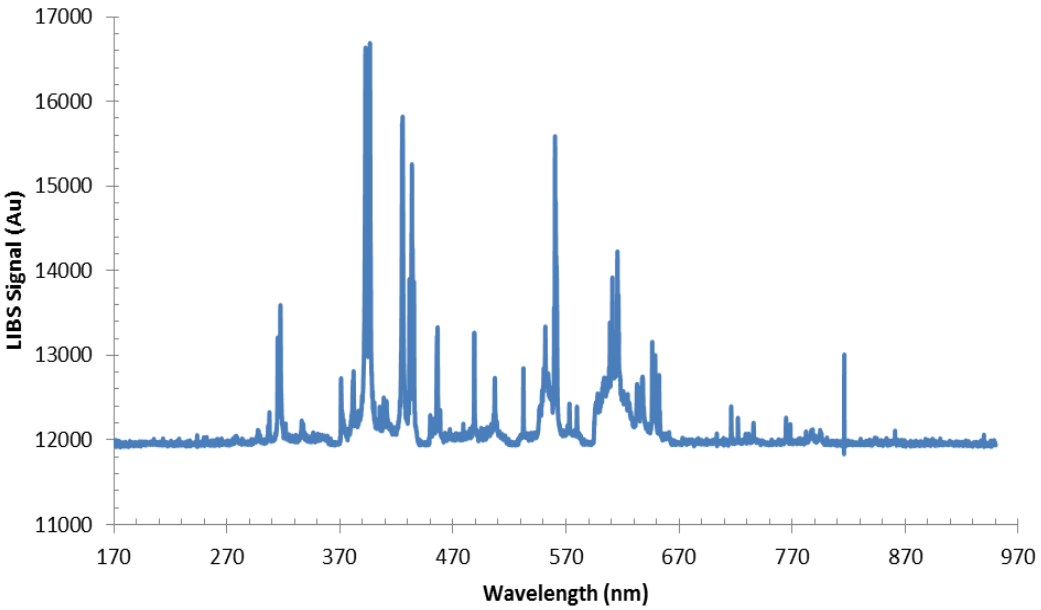

Figure A.8: Typical LIBS spectra of cement Type I + fly ash sample in the region of 170 to 950 nm for concentrations of 0.8% chloride and 0.2% sulfate by weight of the cementitiuos materials content.

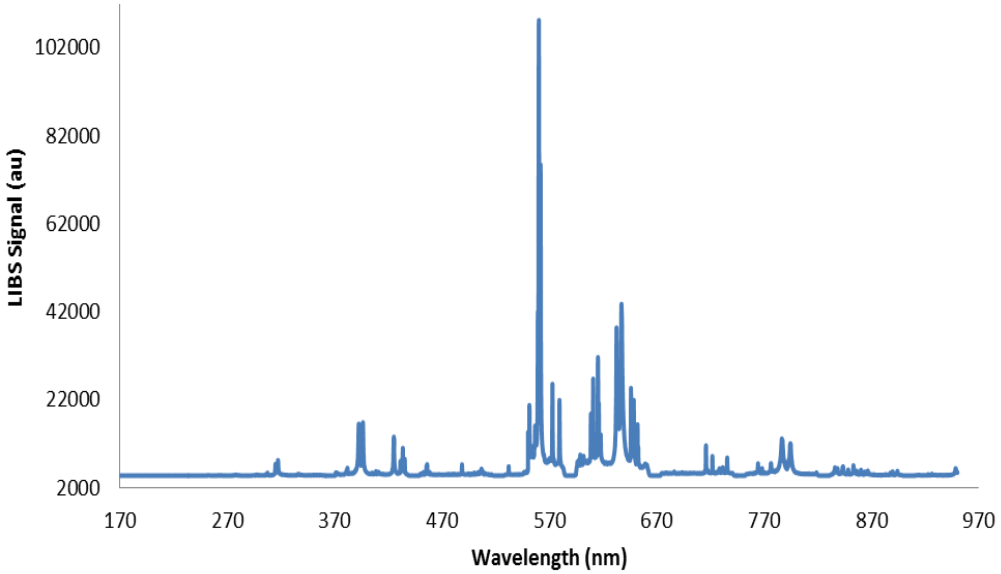

Figure A.9: Typical LIBS spectra of Type I + fly ash cement sample in the region of 170 to 950 nm for concentrations of 0.8% chloride and 0.4% sulfate by weight of the cementitiuos materials content.

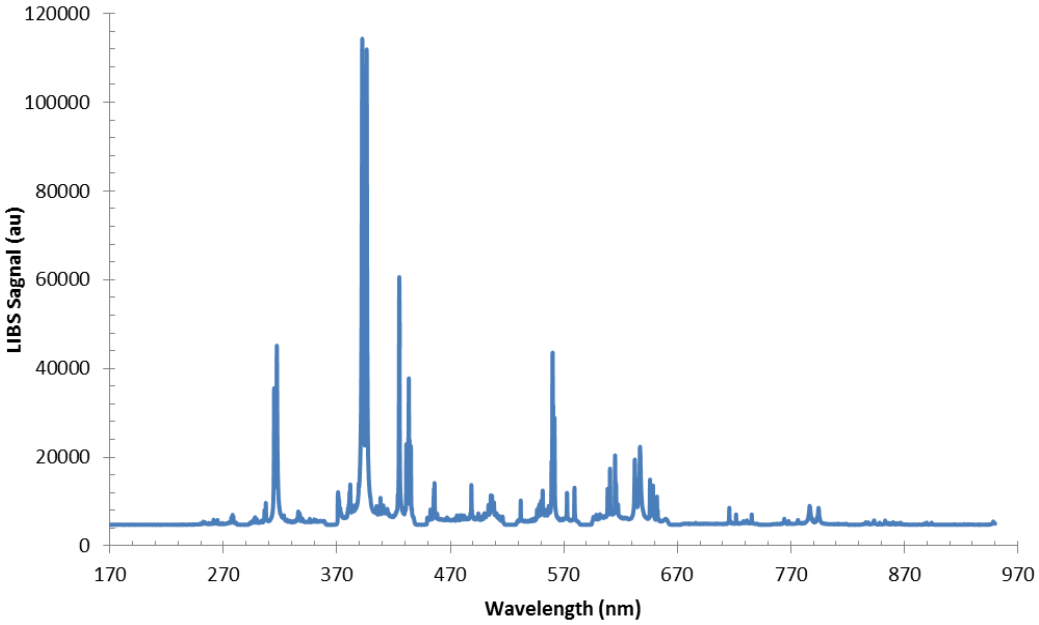

Figure A.10: Typical LIBS spectra of Type I + silica fume cement sample in the region of 170 to 950 nm for concentrations of 0.4% chloride and 0.4% sulfate by weight of the cementitiuos materials content.

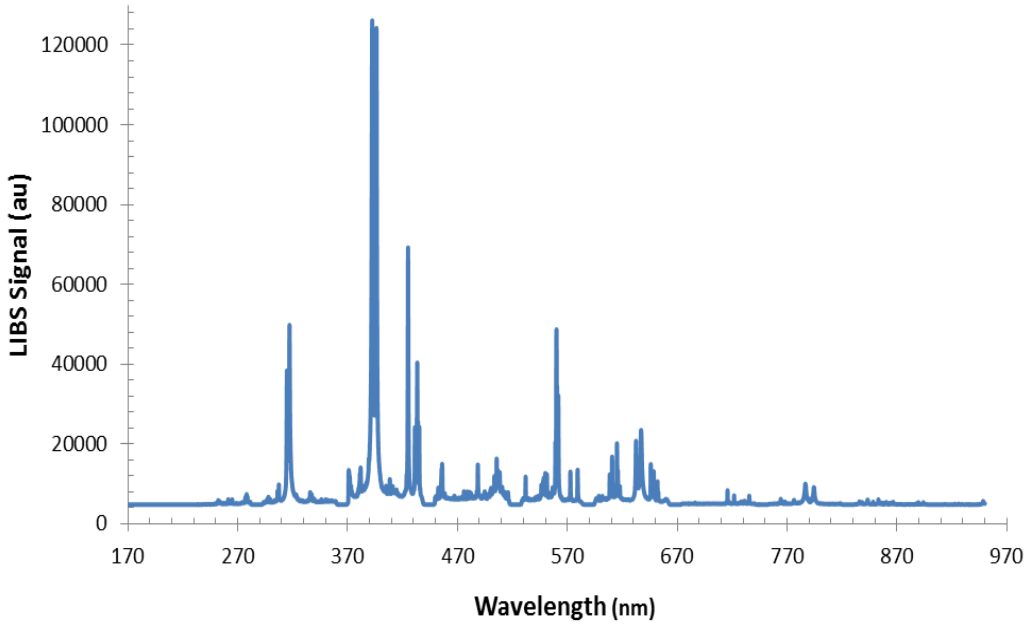

Figure A.11: Typical LIBS spectra of Type I + silica fume cement sample in the region of 170 to 950 nm for concentrations of 0.8% chloride and 0.2% sulfate by weight of the cementitiuos materials content.

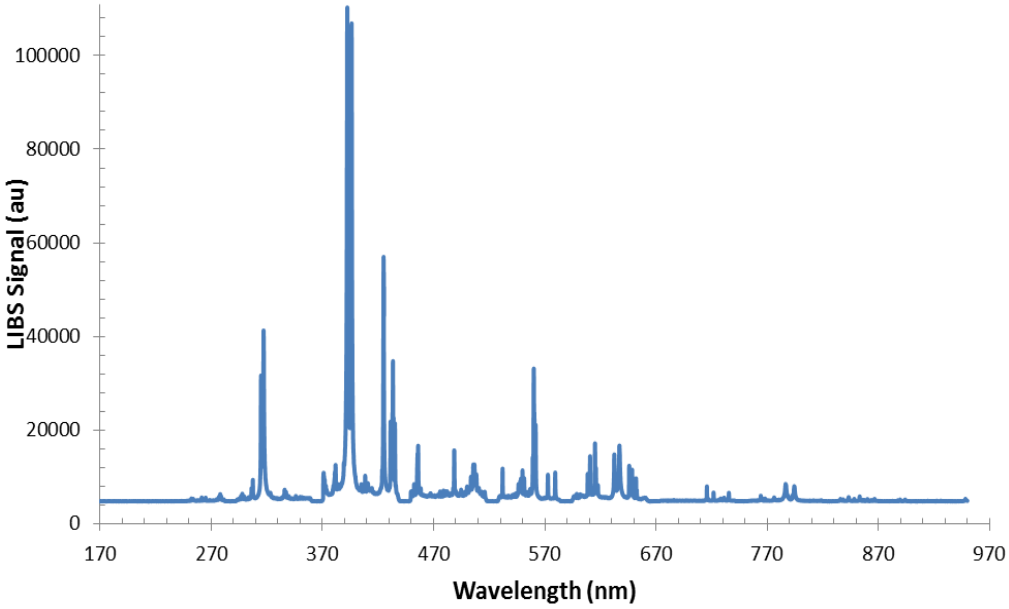

Figure A.12: Typical LIBS spectra of Type I + silica fume cement sample in the region of 170 to 950 nm for concentrations of 0.8% chloride and 0.4% sulfate by weight of the cementitiuos materials content.

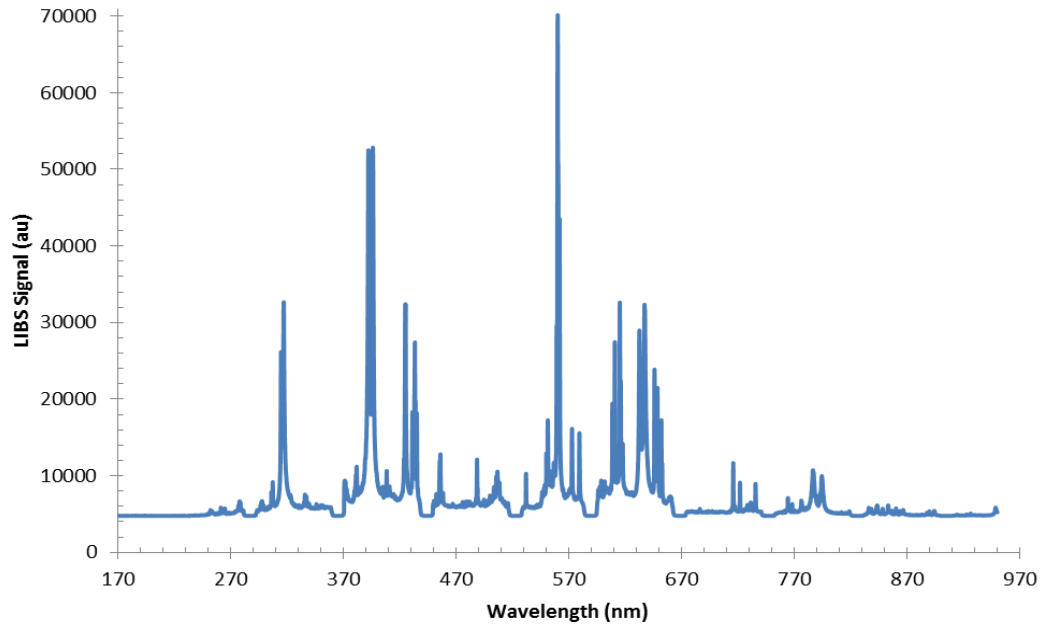

Figure A.13: Typical LIBS spectra of Type I cement sample in the region of 170 to 950 nm for concentrations of 2% chloride and 0.5% sulfate by weight of the cementitiuos materials content.

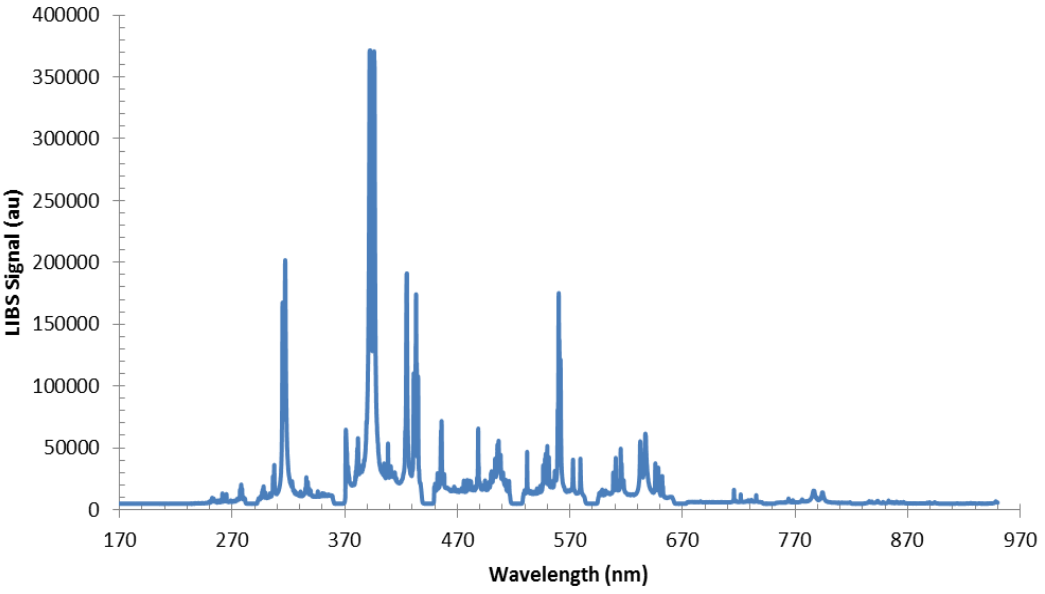

Figure A.14: Typical LIBS spectra of Type I cement sample in the region of 170 to 950 nm for concentrations of 2% chloride and 1% sulfate by weight of the cementitiuos materials content.

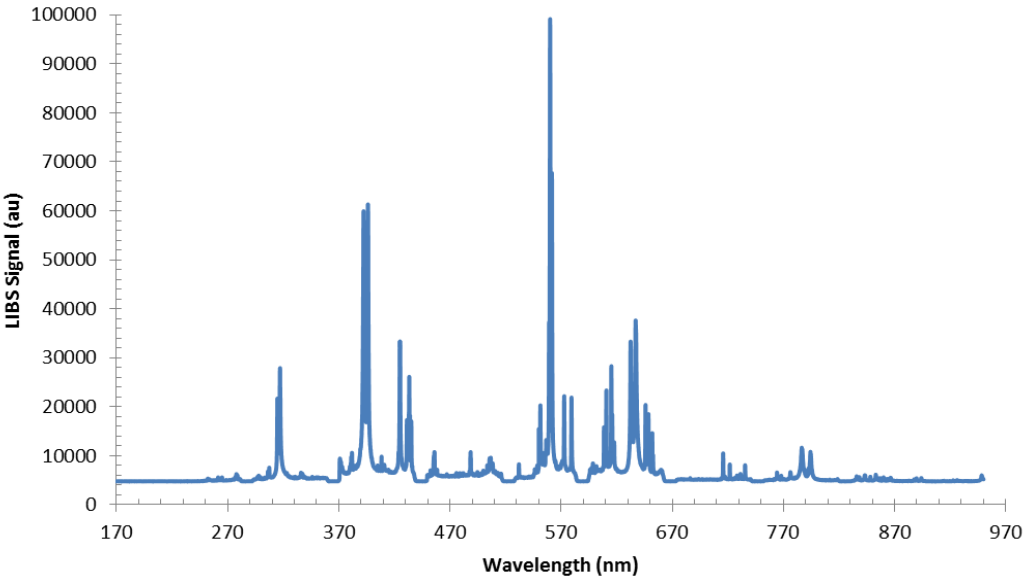

Figure A.15: Typical LIBS spectra of Type I cement sample in the region of 170 to 950 nm for concentrations of 3% chloride and 2% sulfate by weight of the cementitiuos materials content.

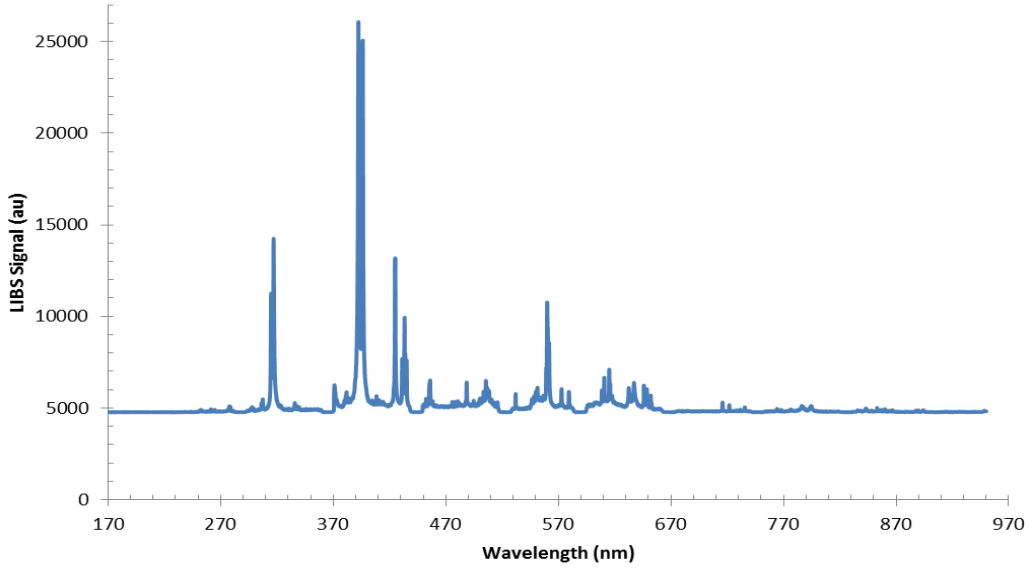

Figure A.16: Typical LIBS spectra of Type I cement sample in the region of 170 to 950 nm for concentrations of 3% chloride and 3% sulfate by weight of the cementitiuos materials content.

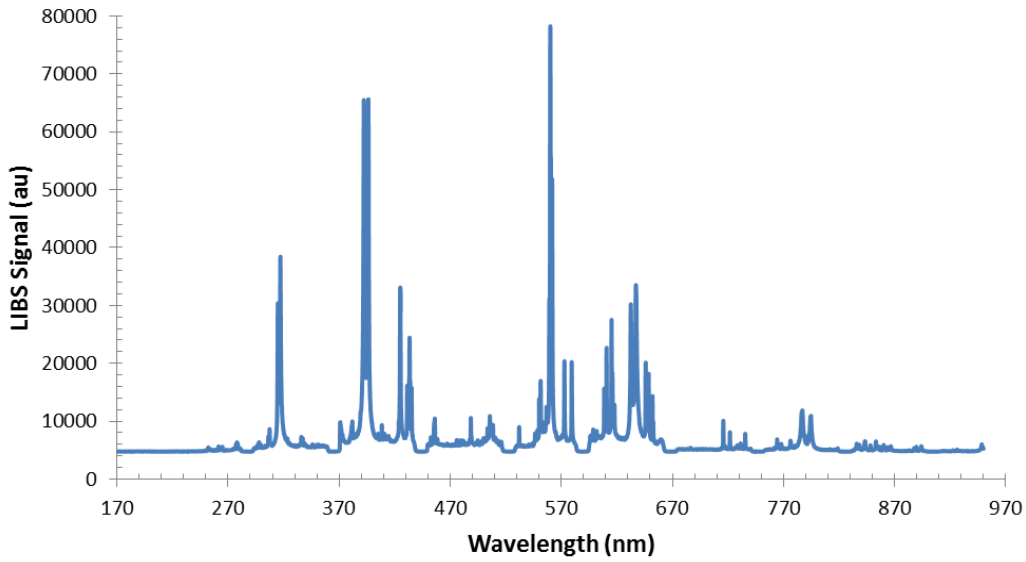

Figure A.17: Typical LIBS spectra of Type I + silica fume cement sample in the region of 170 to 950 nm for concentrations of 2% chloride and 0.5% sulfate by weight of the cementitiuos materials content.

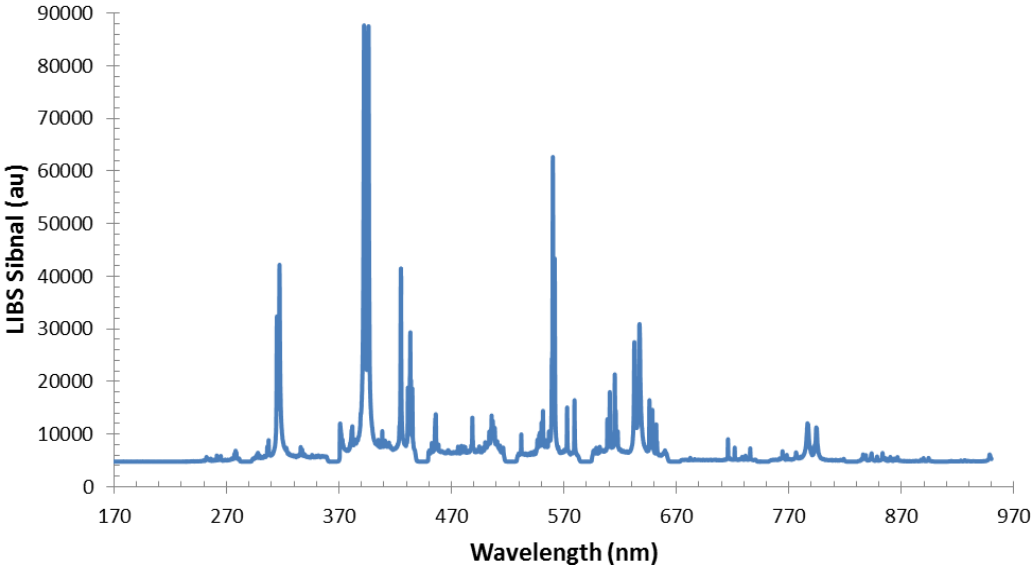

Figure A.18: Typical LIBS spectra of Type I + silica fume cement sample in the region of 170 to 950 nm for concentrations of 2% chloride and 1% sulfate by weight of the cementitiuos materials content.

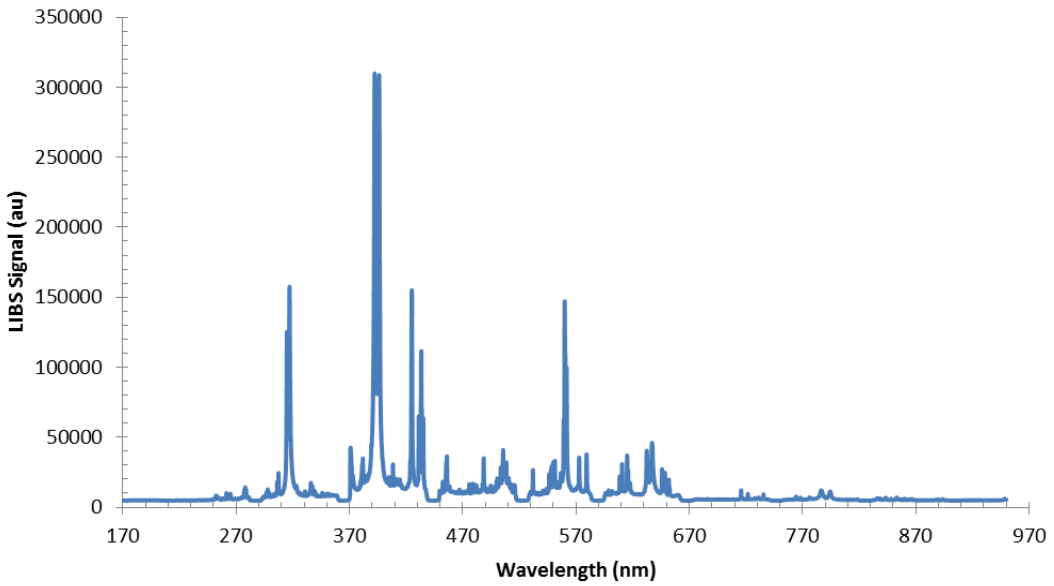

Figure A.19: Typical LIBS spectra of Type I + silica fume cement sample in the region of 170 to 950 nm for concentrations of 3% chloride and 2% sulfate by weight of the cementitiuos materials content.

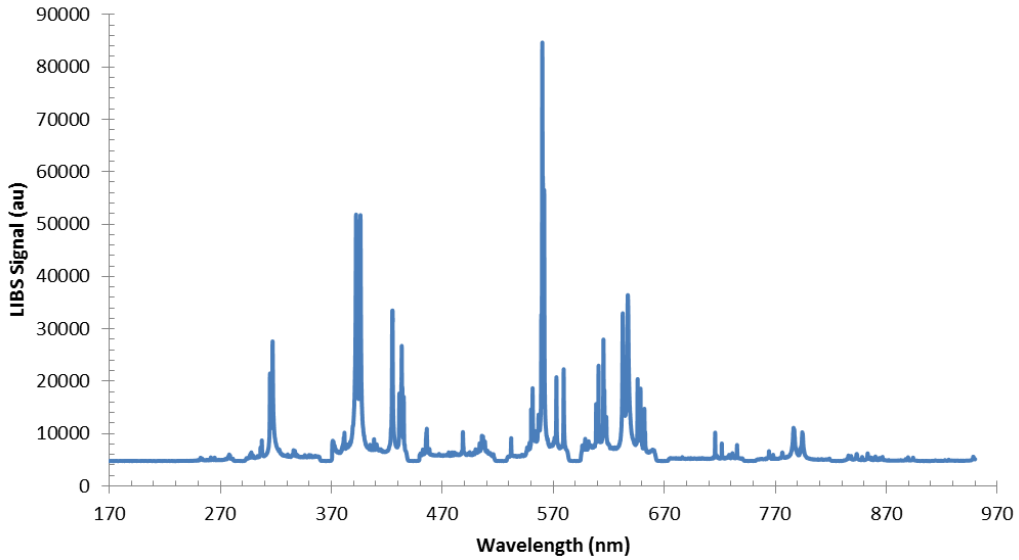

Figure A.20: Typical LIBS spectra of Type I + silica fume cement sample in the region of 170 to 950 nm for concentrations of 3% chloride and 3% sulfate by weight of the cementitiuos materials content.

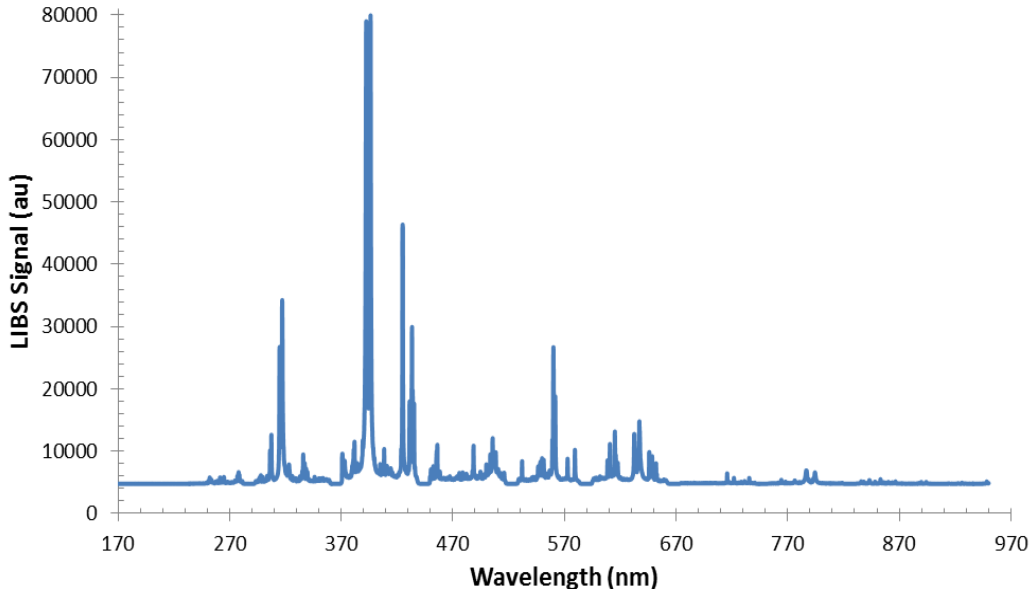

Figure A.21: Typical LIBS spectra of Type I + fly ash cement sample in the region of 170 to 950 nm for concentrations of 2% chloride and 0.5% sulfate by weight of the cementitiuos materials content.

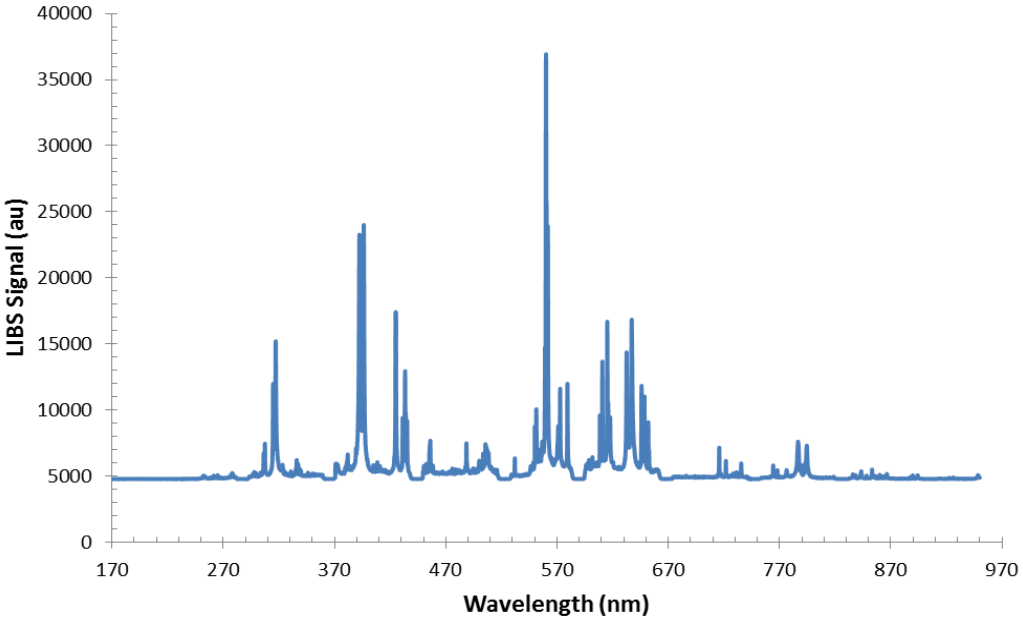

Figure A.22: Typical LIBS spectra of Type I + fly ash cement sample in the region of 170 to 950 nm for concentrations of 2% chloride and 1% sulfate by weight of the cementitiuos materials content.

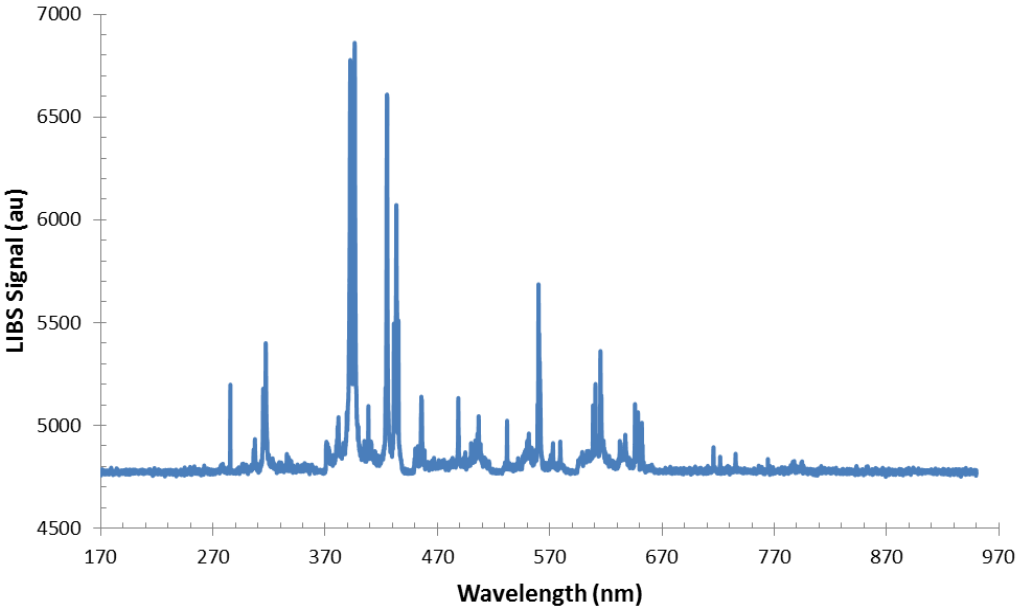

Figure A.23: Typical LIBS spectra of Type I + fly ash cement sample in the region of 170 to 950 nm for concentrations of 3% chloride and 2% sulfate by weight of the cementitiuos materials content.

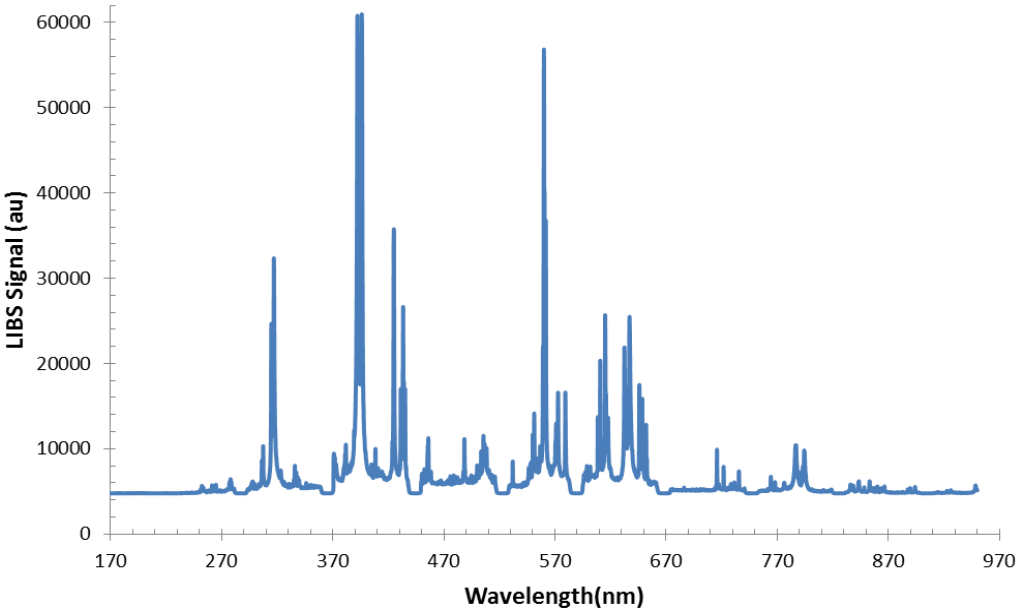

Figure A.24: Typical LIBS spectra of Type I + fly ash cement sample in the region of 170 to 950 nm for concentrations of 3% chloride and 3% sulfate by weight of the cementitiuos materials content.

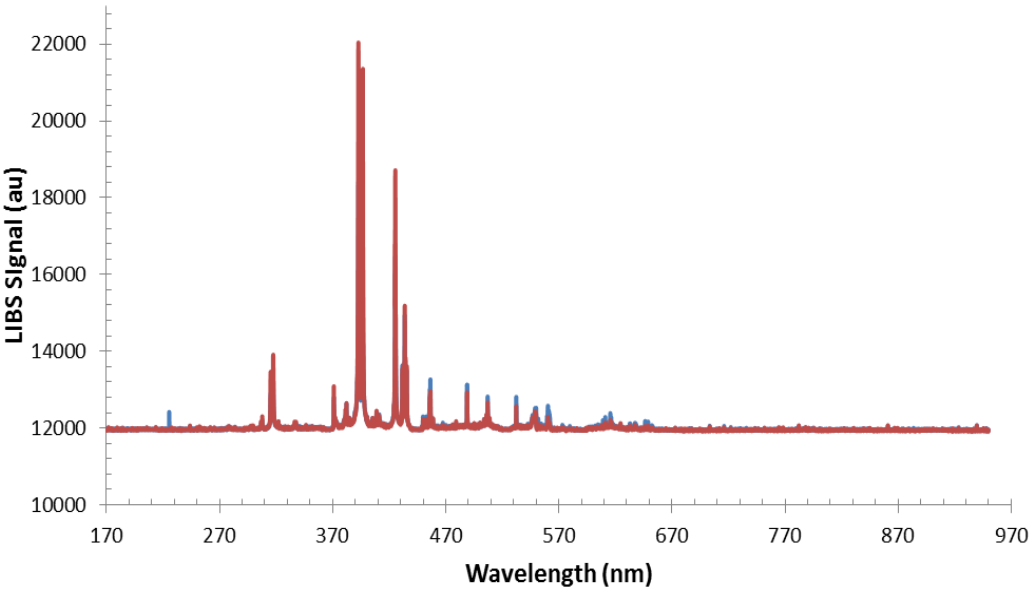

Figure A.25: Typical LIBS spectra of Type I cement sample in the region of 170 to 950 nm for concentrations of 0.4% chloride and [0.2% - 0.4%] sulfate by weight of the cementitiuos materials content.

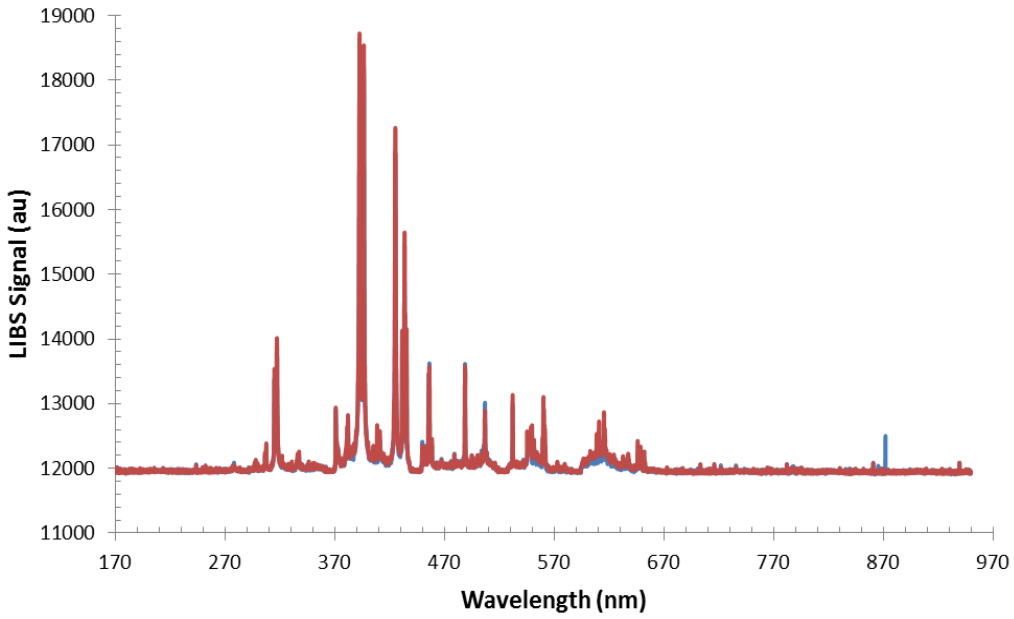

Figure A.26: Typical LIBS spectra of Type I cement sample in the region of 170 to 950 nm for concentrations of 0.8% chloride and [0.2% - 0.4%] sulfate by weight of the cementitiuos materials content.

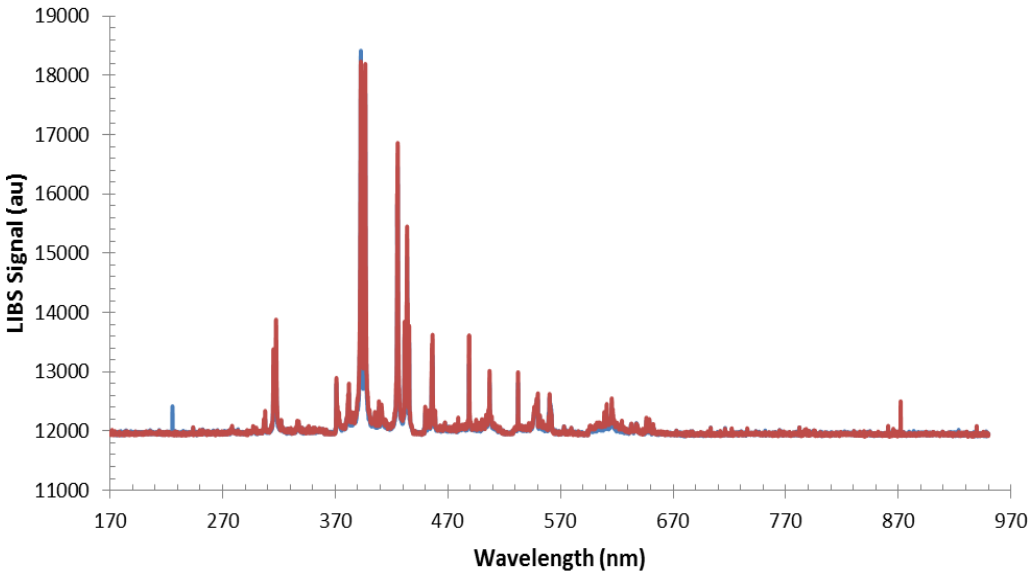

Figure A.27: Typical LIBS spectra of Type I cement sample in the region of 170 to 950 nm for concentrations of [0.4% - 0.8%] chloride and 0.2% sulfate by weight of the cementitiuos materials content.

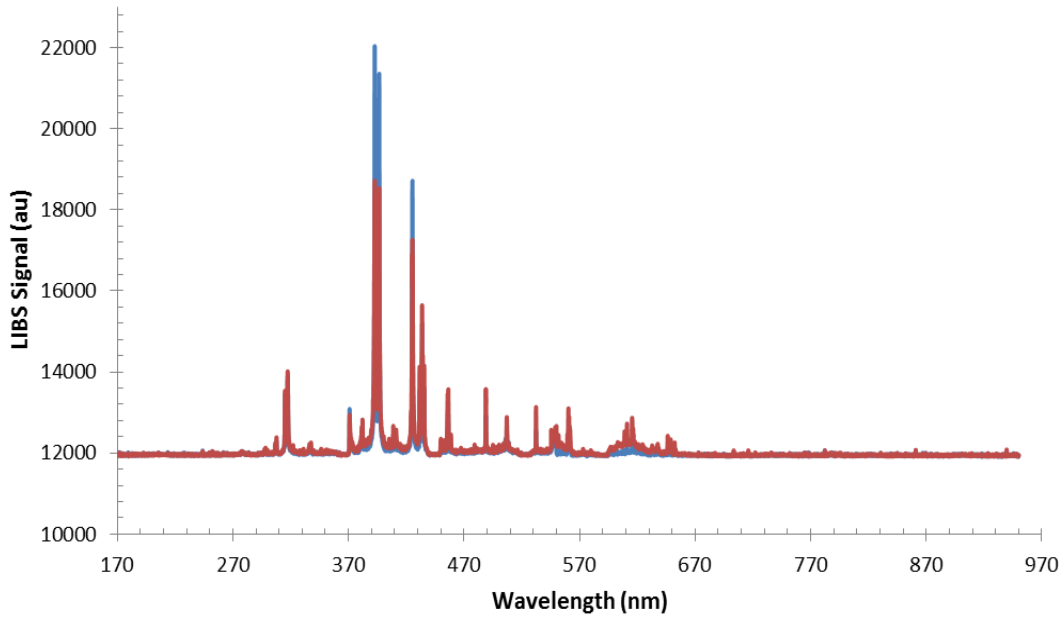

Figure A.28: Typical LIBS spectra of Type I cement sample in the region of 170 to 950 nm for concentrations of [0.4% - 0.8%] chloride and 0.4% sulfate by weight of the cementitiuos materials content.

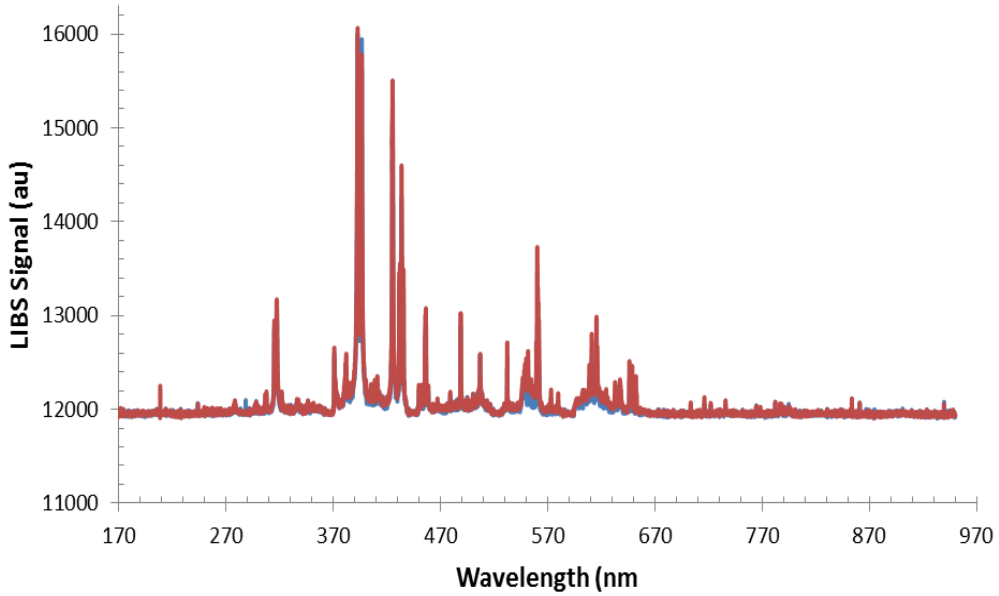

Figure A.29: Typical LIBS spectra of Type V cement sample in the region of 170 to 950 nm for concentrations of 0.4% chloride and [0.2% - 0.4%] sulfate by weight of the cementitiuos materials content.

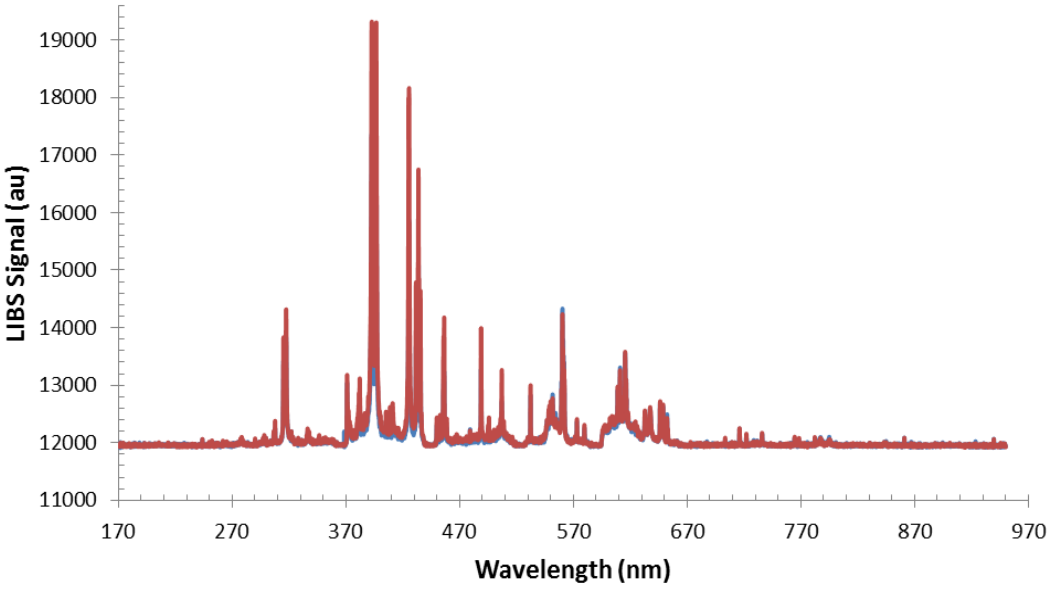

Figure A.30: Typical LIBS spectra of Type I cement sample in the region of 170 to 950 nm for concentrations of 0.8% chloride and [0.2% - 0.4%] sulfate by weight of the cementitiuos materials content.

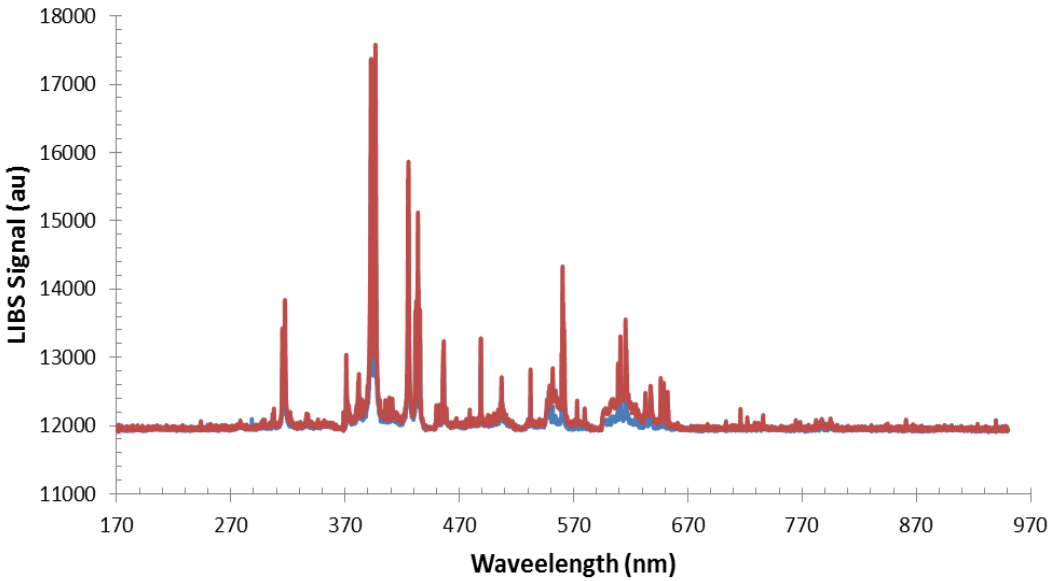

Figure A.31: Typical LIBS spectra of Type V cement sample in the region of 170 to 950 nm for concentrations of [0.4% - 0.8%] chloride and 0.2% sulfate by weight of the cementitiuos materials content.

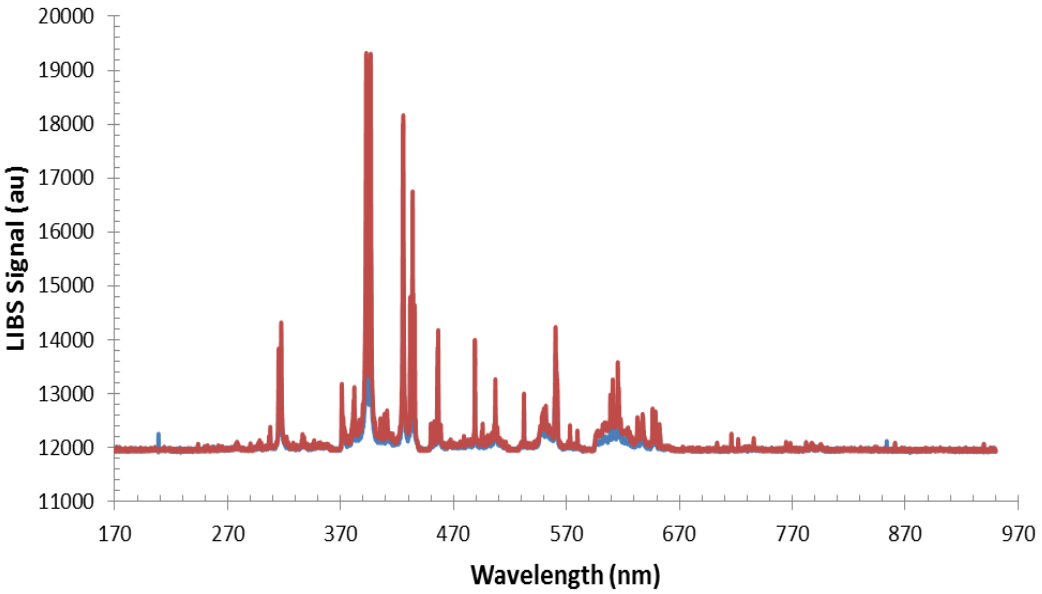

Figure A.32: Typical LIBS spectra of Type V cement sample in the region of 170 to 950 nm for concentrations of [0.4% - 0.8%] chloride and 0.4% sulfate by weight of the cementitiuos materials content.

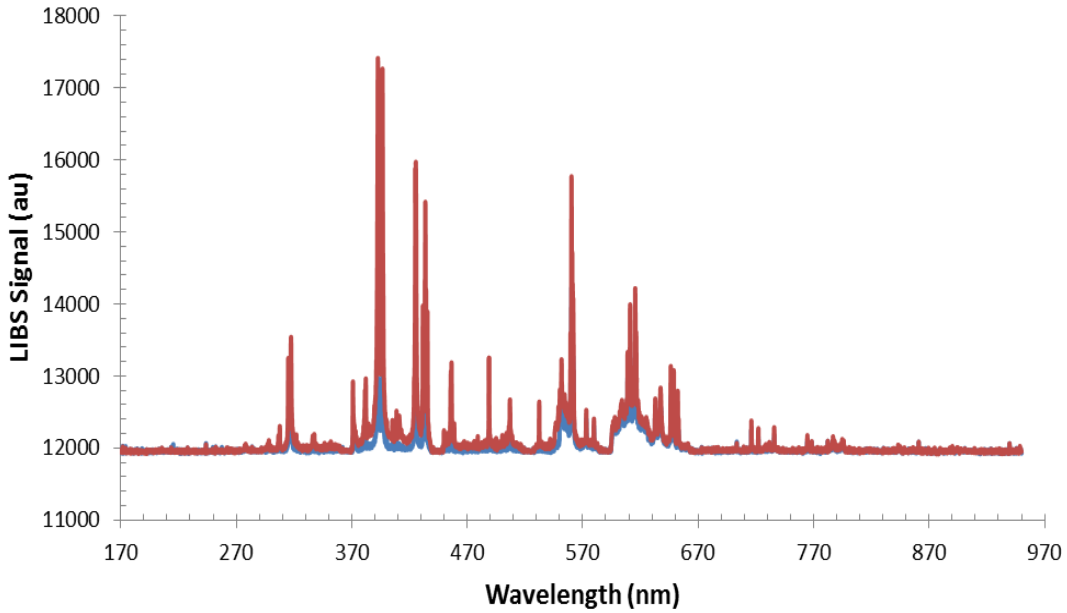

Figure A.33: Typical LIBS spectra of Type I + fly ash cement sample in the region of 170 to 950 nm for concentrations of [0.4% - 0.8%] chloride and 0.2% sulfate by weight of the cementitiuos materials content.

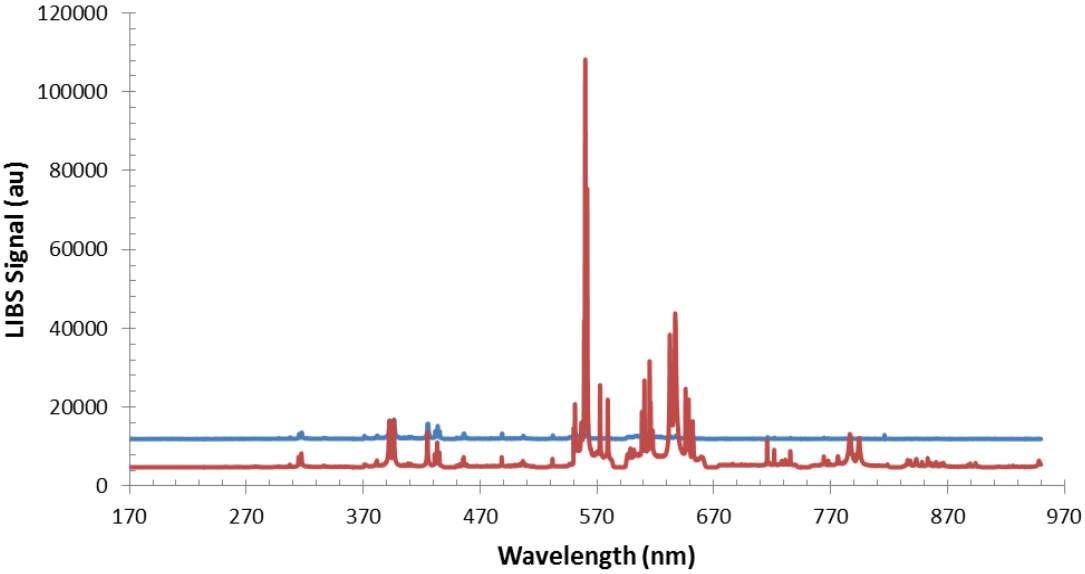

Figure A.34: Typical LIBS spectra of Type I + fly ash cement sample in the region of 170 to 950 nm for concentrations of 0.8% chloride and [0.2% - 0.4%] sulfate by weight of the cementitiuos materials content.

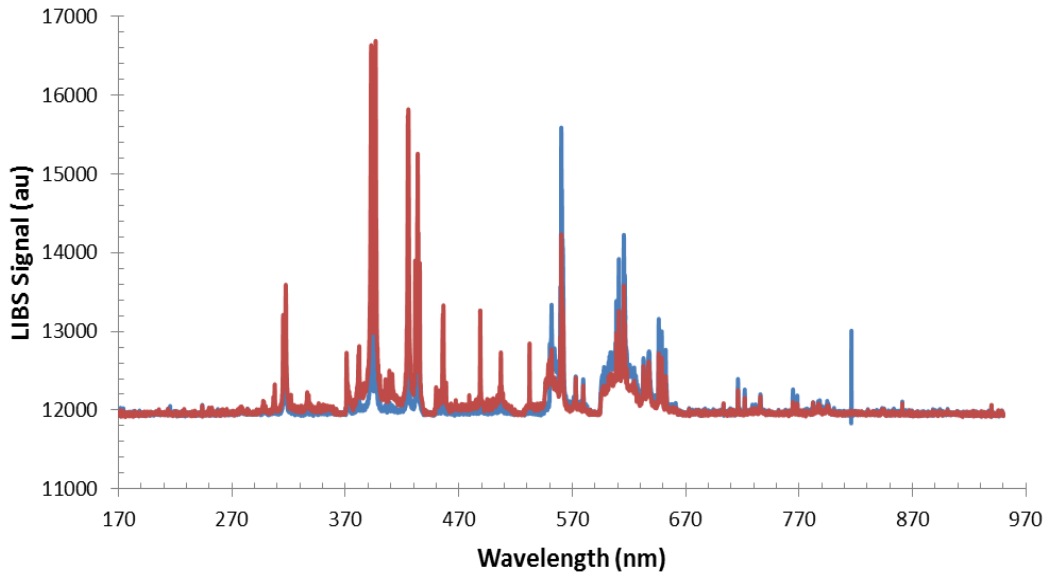

Figure A.35: Typical LIBS Spectra of cement Type I + silica fume sample in the region of 170 to 950 nm for concentrations of 0.4% chloride and [0.2% - 0.4%] sulfate by weight percentage in the cementitiuos materials content.

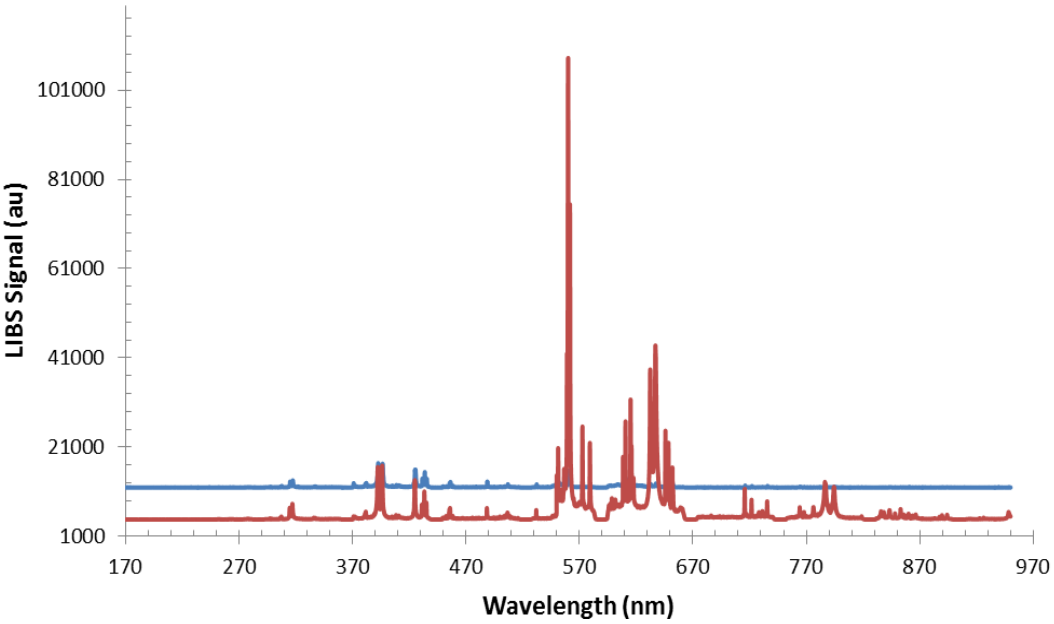

Figure A.36: Typical LIBS spectra of Type I + silica fume cement sample in the region of 170 to 950 nm for concentrations of 0.8% chloride and [0.2% - 0.4%] sulfate by weight of the cementitiuos materials content.

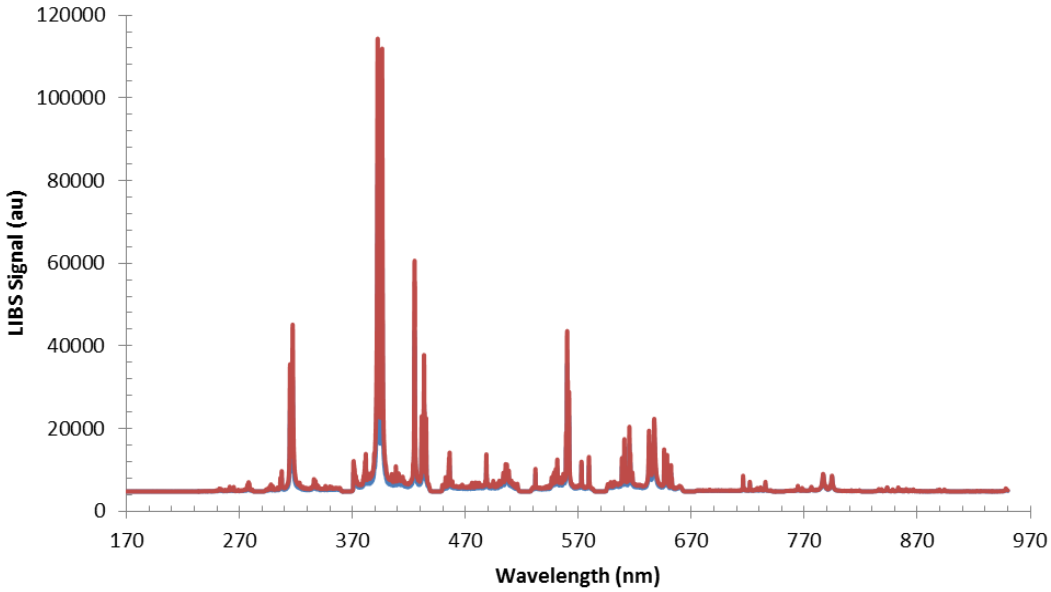

Figure A.37: Typical LIBS spectra of Type I + silica fume cement sample in the region of 170 to 950 nm for concentrations of [0.4% - 0.8%] chloride and 0.2% sulfate by weight of the cementitiuos materials content.

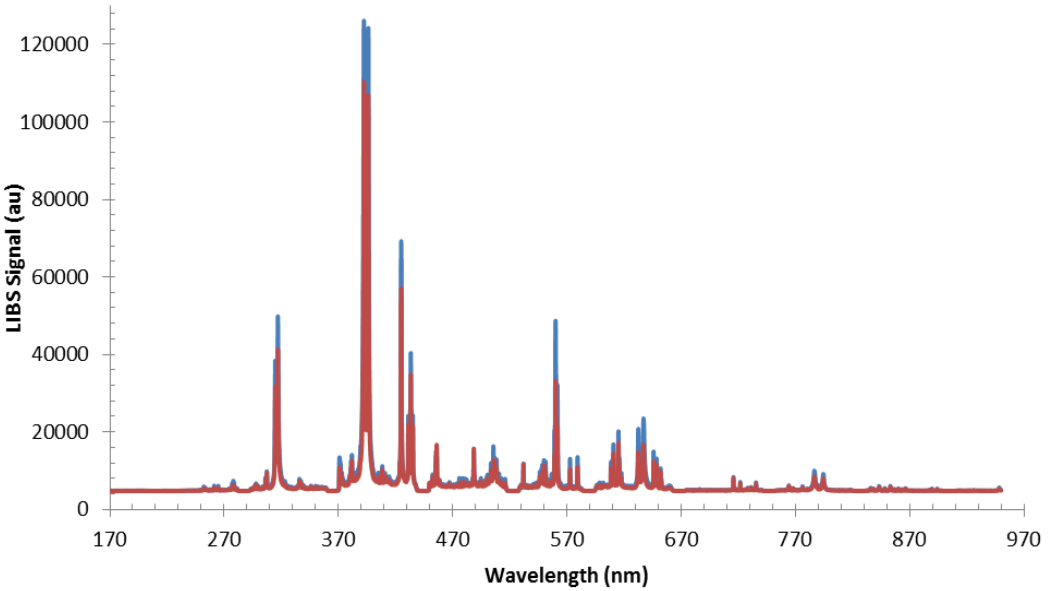

Figure A.38: Typical LIBS spectra of Type I + silica fume cement sample in the region of 170 to 950 nm for concentrations of [0.4% - 0.8%] chloride and 0.4% sulfate by weight of the cementitiuos materials content.

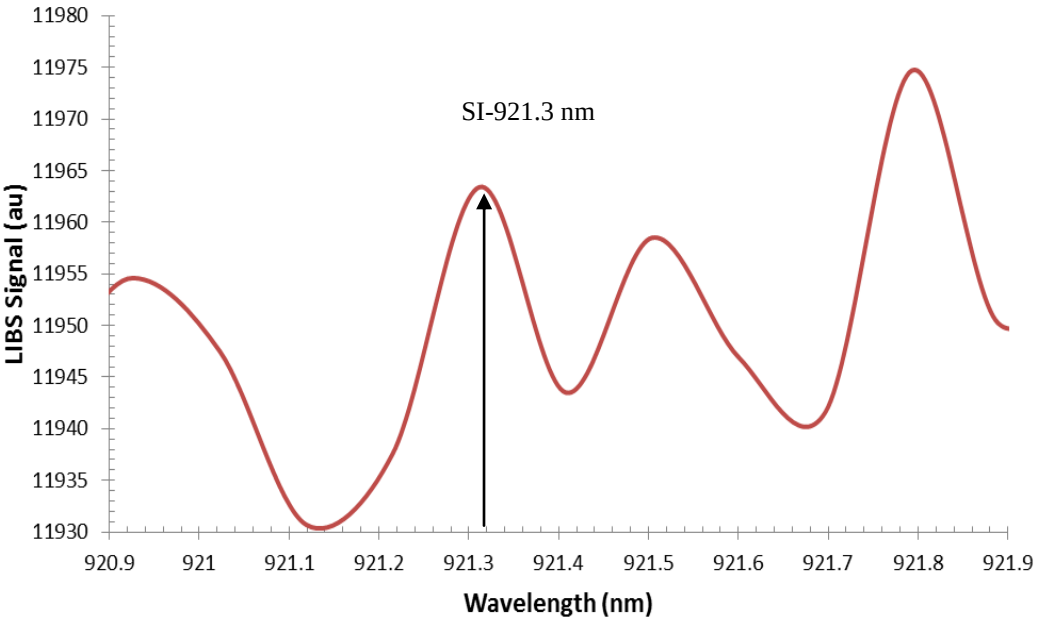

Figure A.39: LIBS spectrum of the cement paste samples using Type (I) cement with fly ash with 0.8% chloride and 0.2 % sulfate with 921.3 nm atomic transition as a marker.

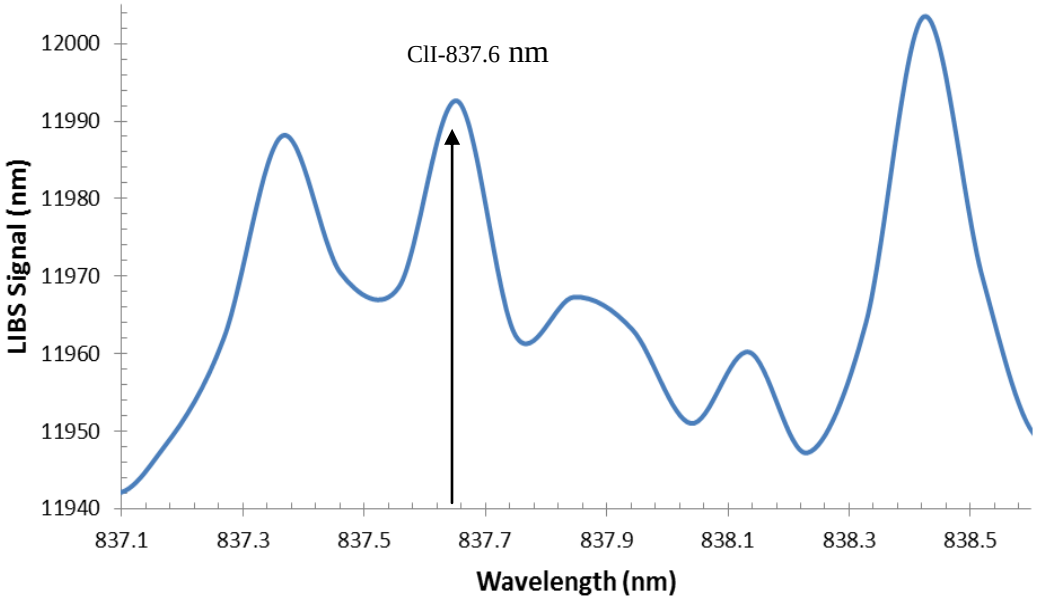

Figure A.40: LIBS spectrum of the cement paste samples using Type (I) cement with fly ash with 0.8% chloride and 0.2% sulfate with 837.6 nm atomic transition as a marker.

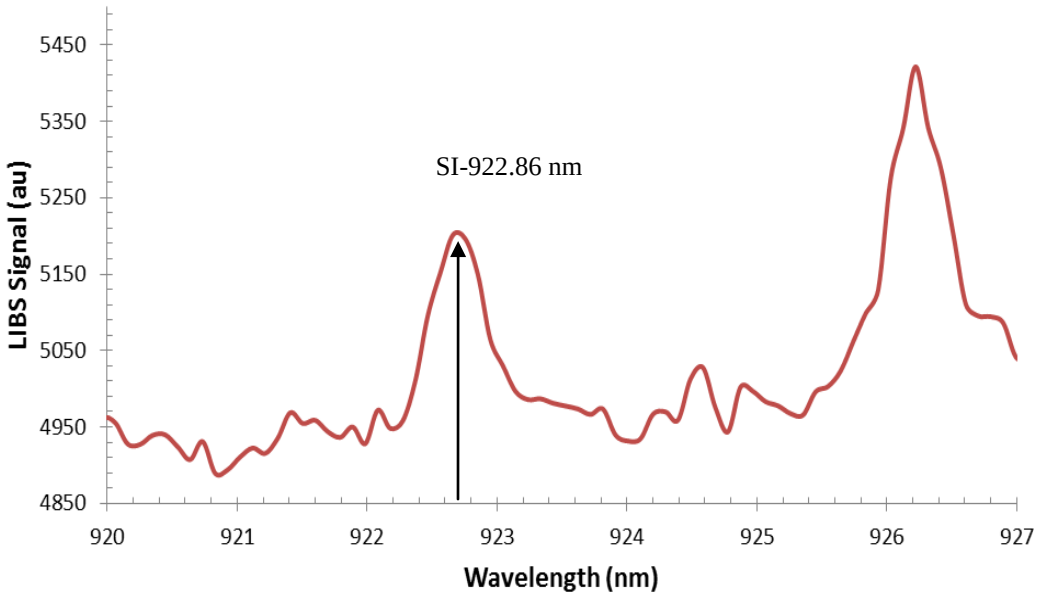

Figure A.41: LIBS spectrum of the cement paste samples using Type (I) cement with 2% chloride and 1% sulfate with 922.86 nm atomic transition as a marker.

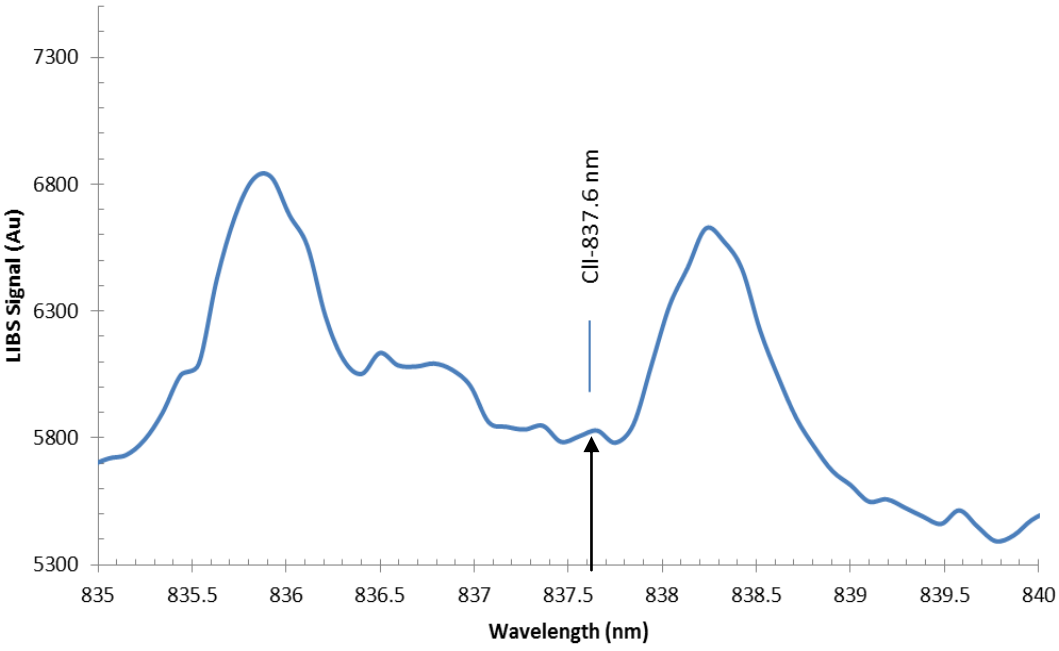

Figure A.42: LIBS spectrum of the cement paste samples using Type (I) cement with 2% chloride and 1% sulfate with 837.6 nm atomic transition as a marker.

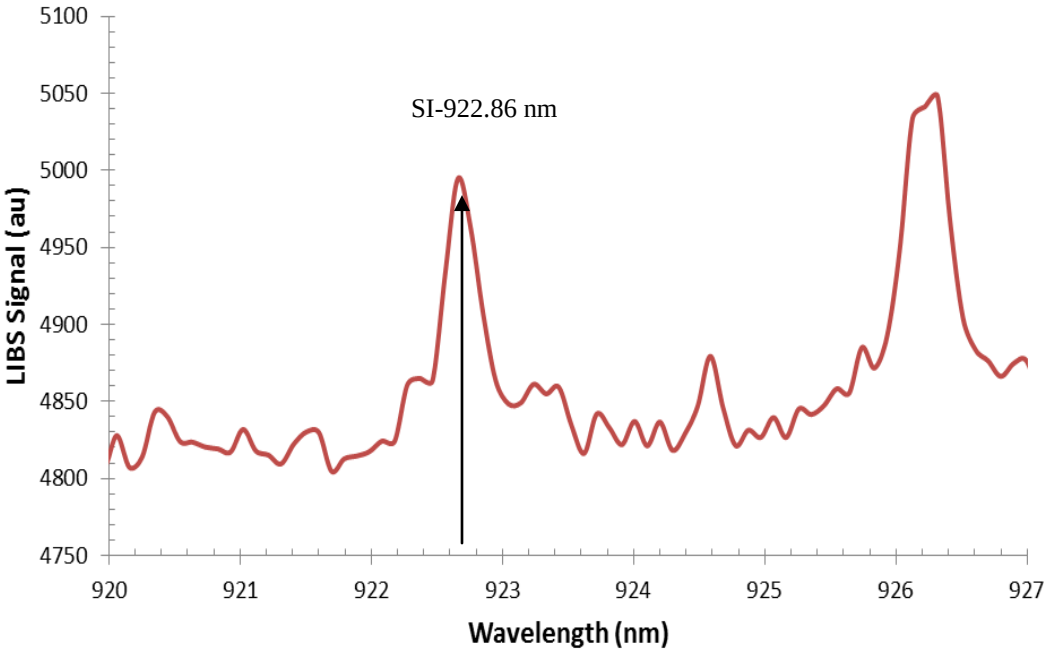

Figure A.43: LIBS spectrum of the cement paste samples using Type (I) cement with 3% chloride and 2% sulfate with 922.8 nm atomic transition as a marker.

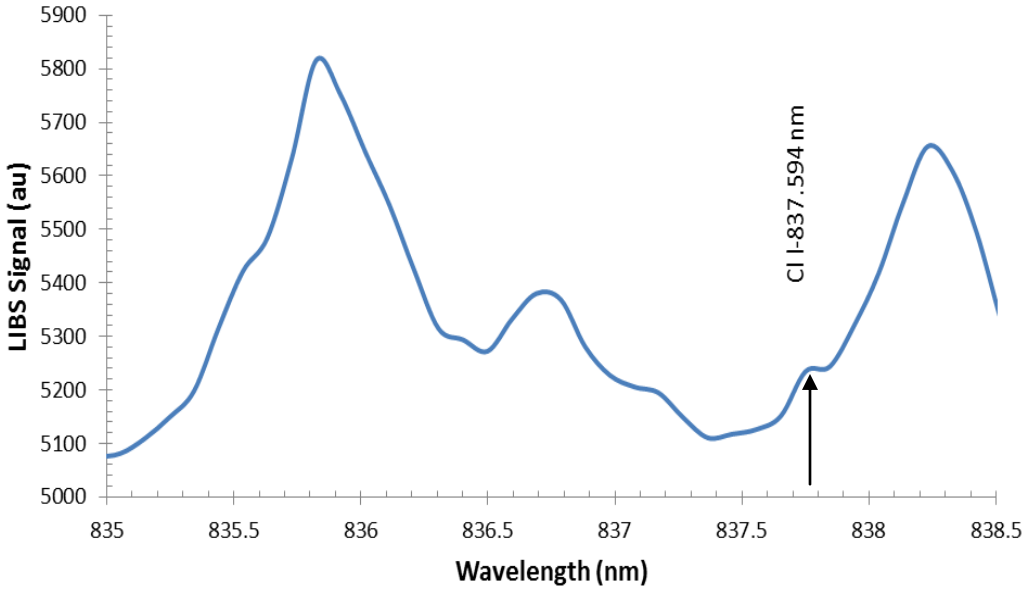

Figure A.44: LIBS spectrum of the cement paste samples using Type (I) cement with 3% chloride and 2% sulfate with 837.6 nm atomic transition as a marker.

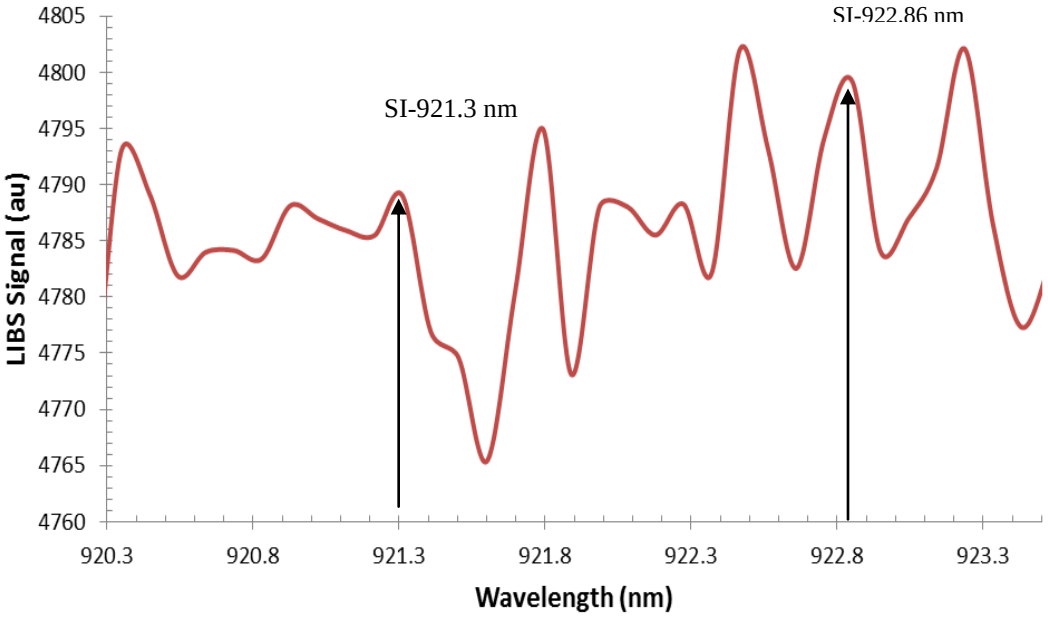

Figure A.45: LIBS spectrum of the cement paste samples using Type (I) cement with 3% chloride and 3% sulfate with 921.3 nm and 922.86 nm atomic transitions as a marker.

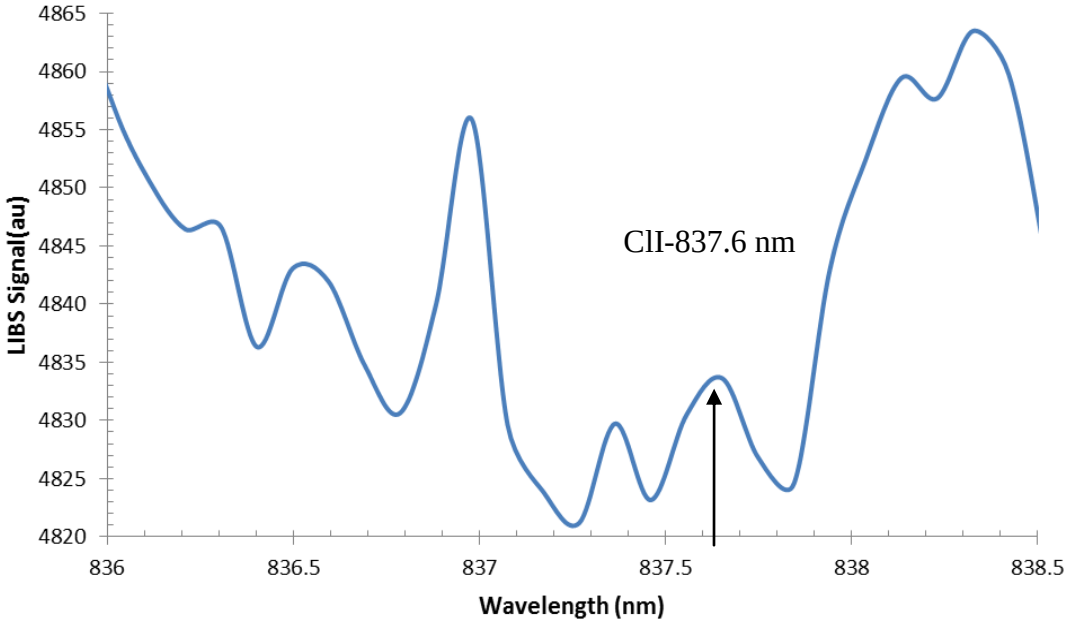

Figure A.46: LIBS spectrum of the cement paste samples using Type (I) cement with 3% chloride and 3% sulfate with 837.6 nm atomic transition as a marker.

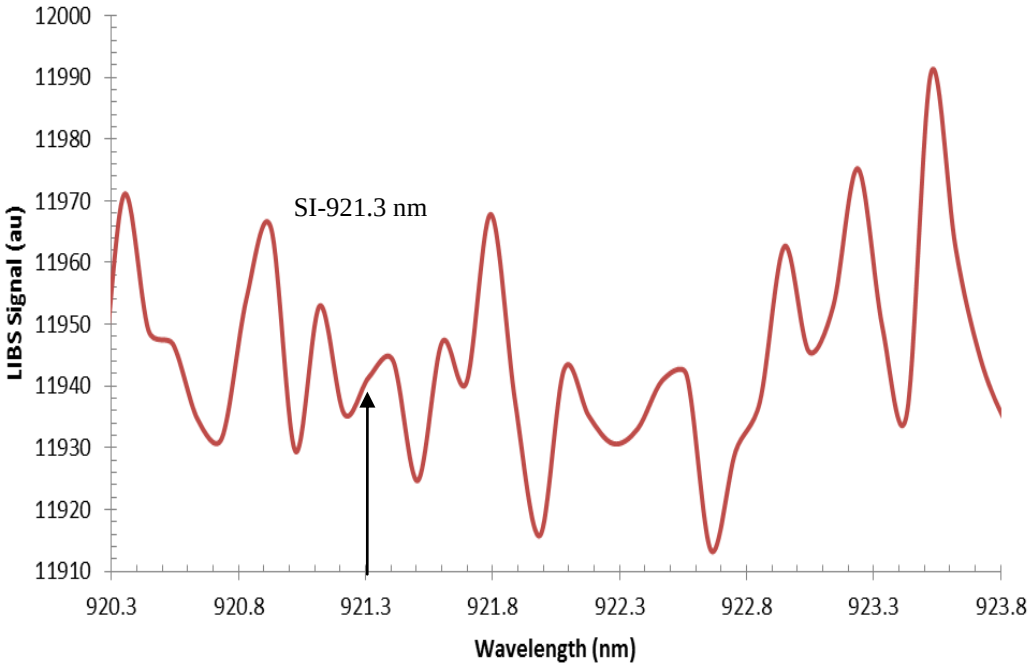

Figure A.47: LIBS spectrum of the cement paste samples using Type (V) cement with 0.4% chloride and 0.2% sulfate with 921.3 nm atomic transition as a marker.

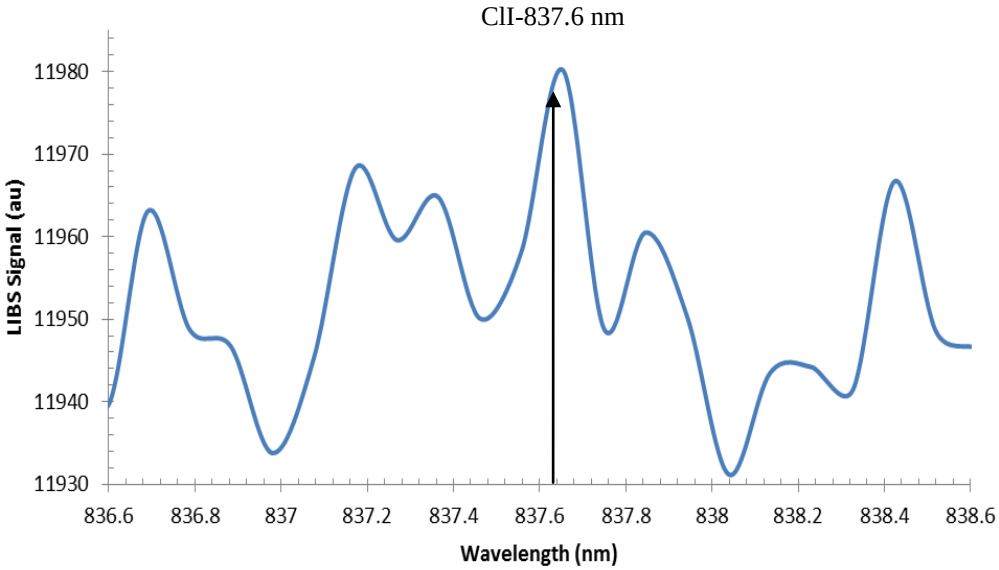

Figure A.48: LIBS spectrum of the cement paste samples using Type (V) cement with 0.4% chloride and 0.2% sulfate with 837.6 nm atomic transition as a marker.

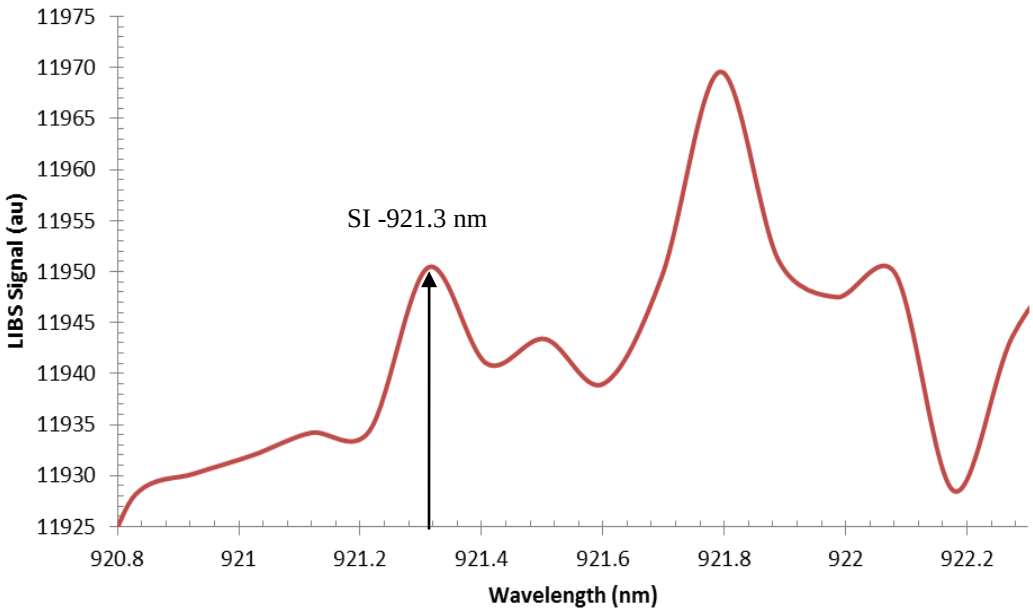

Figure A.49: LIBS spectrum of the cement paste samples using Type (V) cement with 0.4% chloride and 0.4% sulfate with 921.3 nm atomic transition as a marker.

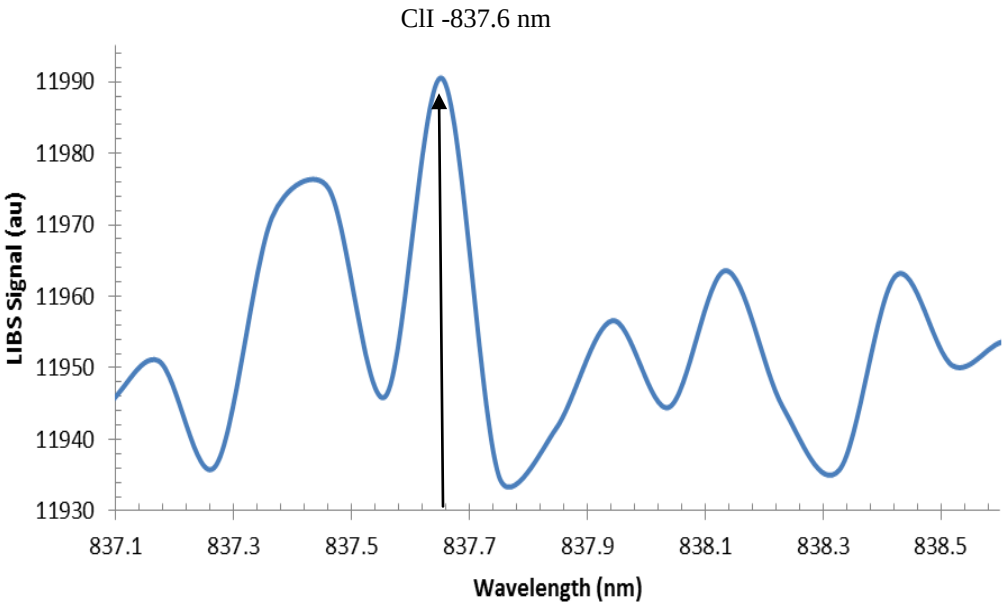

Figure A.50: LIBS spectrum of the cement paste samples using Type (V) cement with 0.4% chloride and 0.4% sulfate with 837.6 nm atomic transition as a marker.

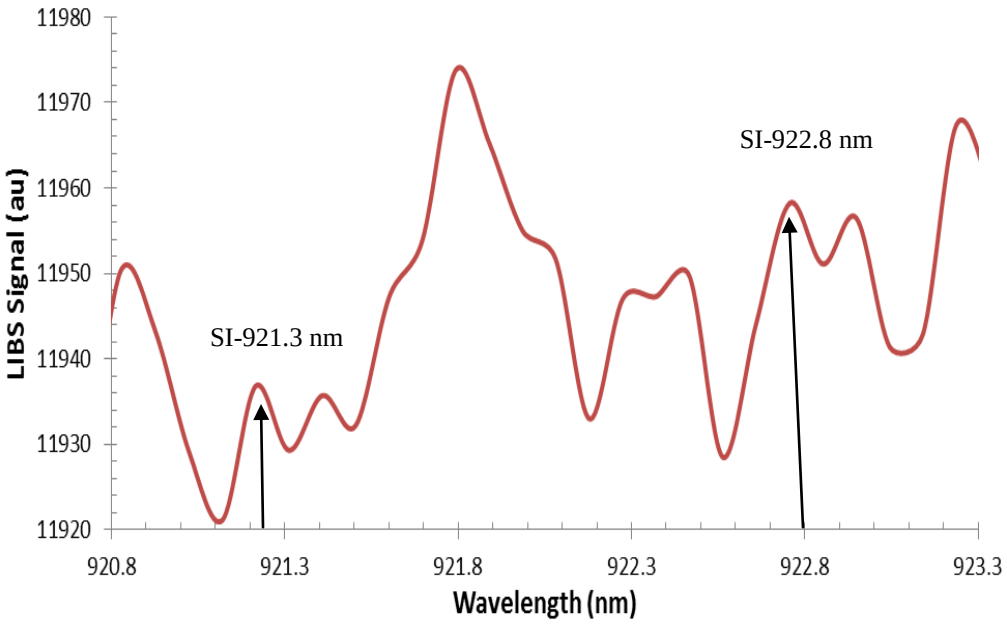

Figure A.51: LIBS spectrum of the cement paste samples using Type (V) cement with 0.8% chloride and 0.2% sulfate with 921.3 nm and 922.8 nm atomic transitions as markers.

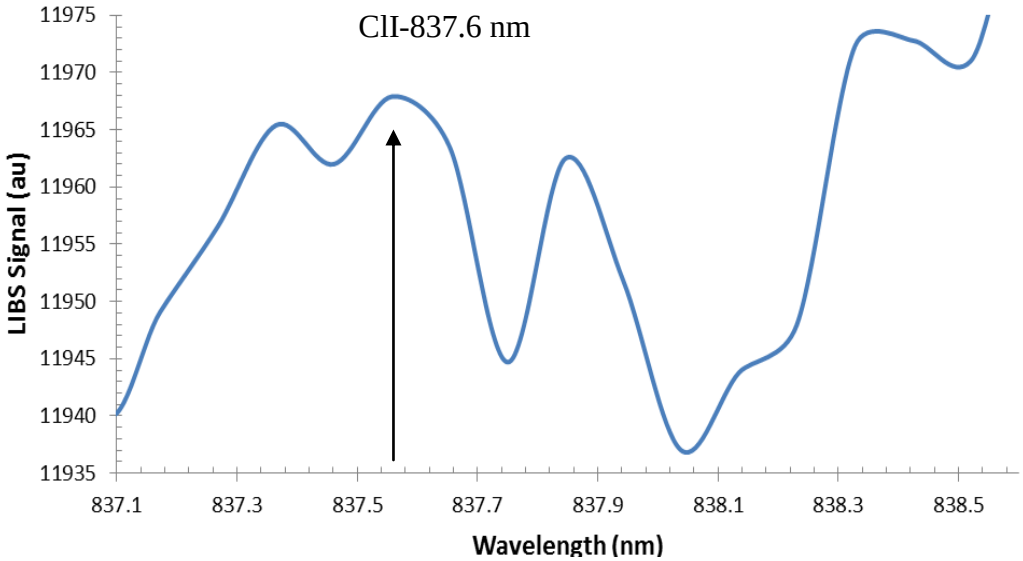

Figure A.52: LIBS spectrum of the cement paste samples using Type (V) cement with 0.8% chloride and 0.2% sulfate with 837.6 nm atomic transition as a marker.

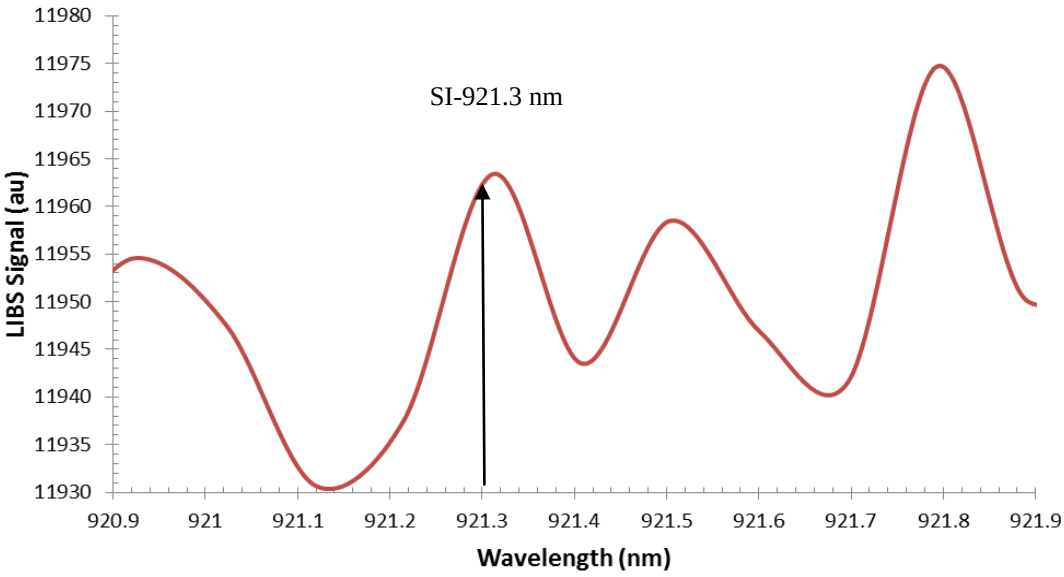

Figure A.53: LIBS spectrum of the cement paste samples using Type (I) cement with fly ash with 0.8% chloride and 0.2% sulfate with 921.3 nm atomic transition as a marker.

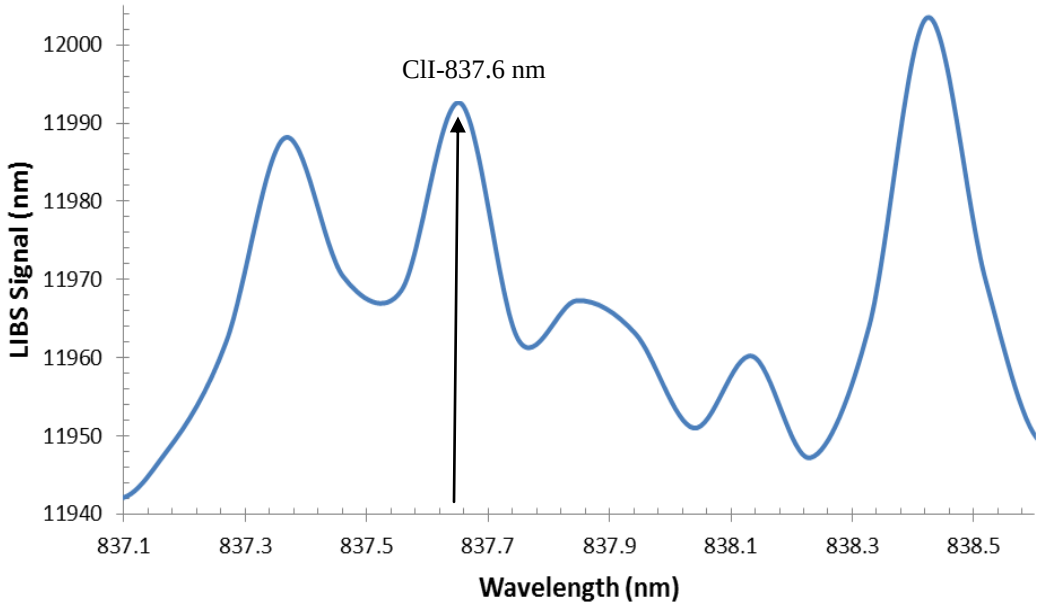

Figure A.54: LIBS spectrum of the cement paste samples using Type (I) cement with fly ash with 0.8% chloride and 0.2% sulfate with 837.6 nm atomic transition as a marker.

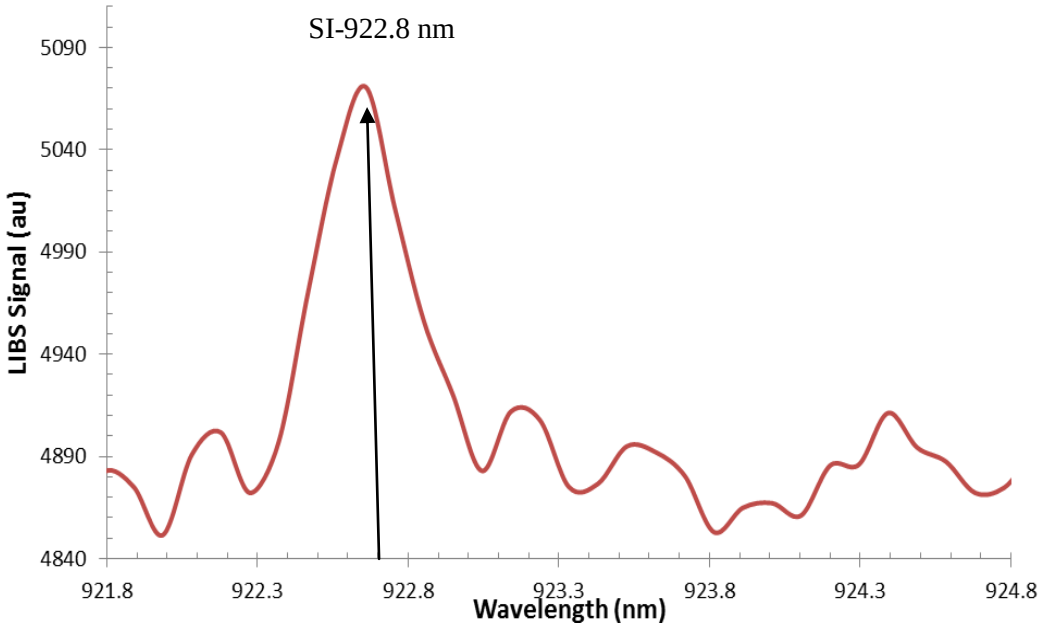

Figure A.55: LIBS spectrum of the cement paste samples using Type (I) cement with fly ash with 0.8% chloride and 0.4% sulfate with 922.8 nm atomic transition as a marker.

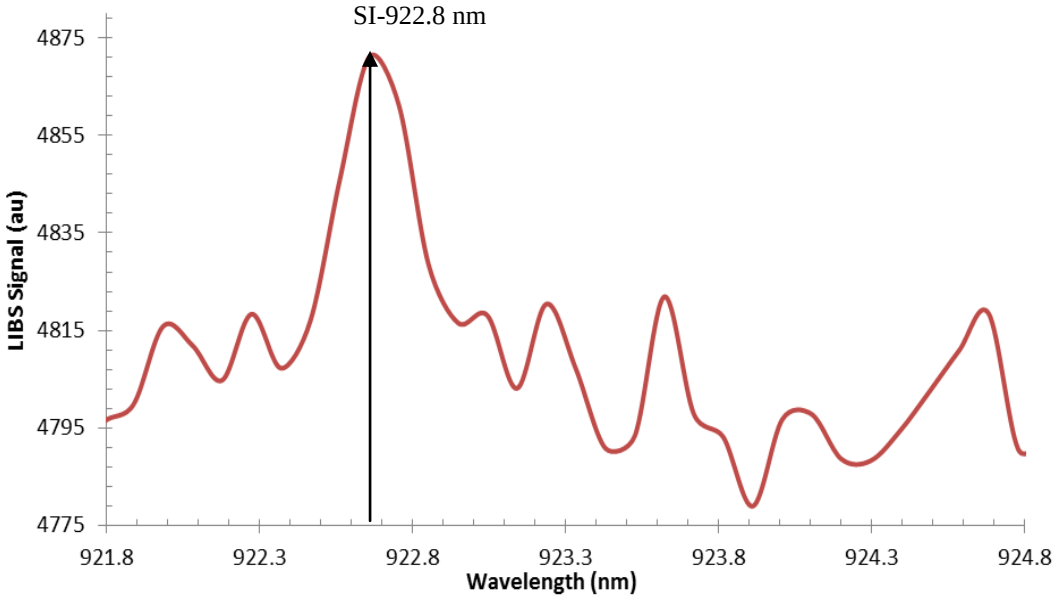

Figure A.56: LIBS spectrum of the cement paste samples using Type (I) cement with fly ash with 2% chloride and 0.5% sulfate with 922.8 nm atomic transition as a marker.

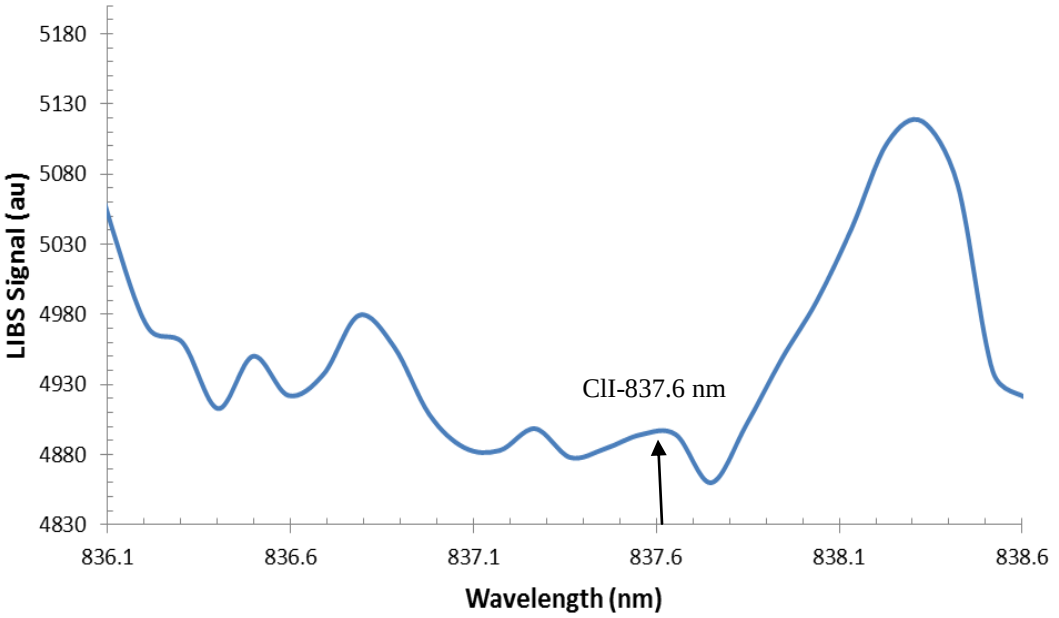

Figure A.57: LIBS spectrum of the cement paste samples using Type (I) cement with fly ash with 2% chloride and 0.5% sulfate with 837.6 nm atomic transition as a marker.

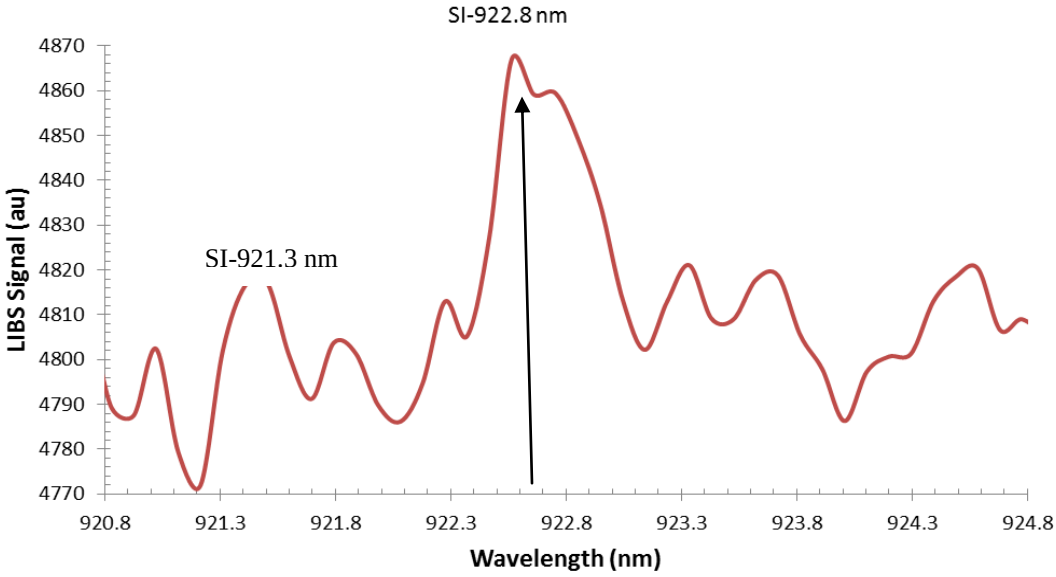

Figure A.58: LIBS spectrum of the cement paste samples using Type (I) cement with fly ash with 2% chloride and 1% sulfate with 921.3 nm and 922.8 nm atomic transitions as a markers.

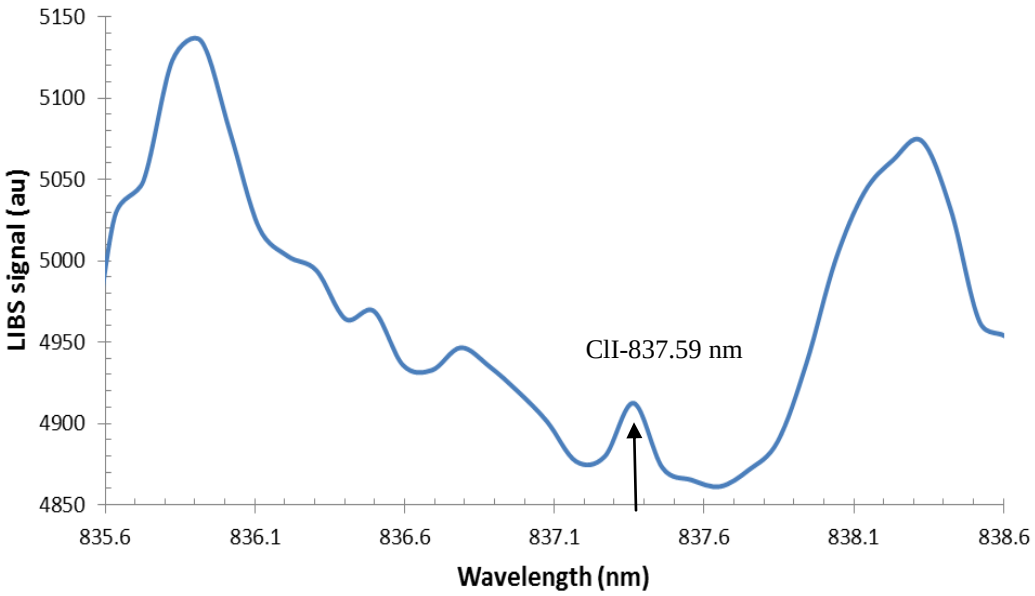

Figure A.59: LIBS spectrum of the cement paste samples using Type (I) cement with fly ash with 2% chloride and 1% sulfate with 837.59 nm atomic transition as a marker.

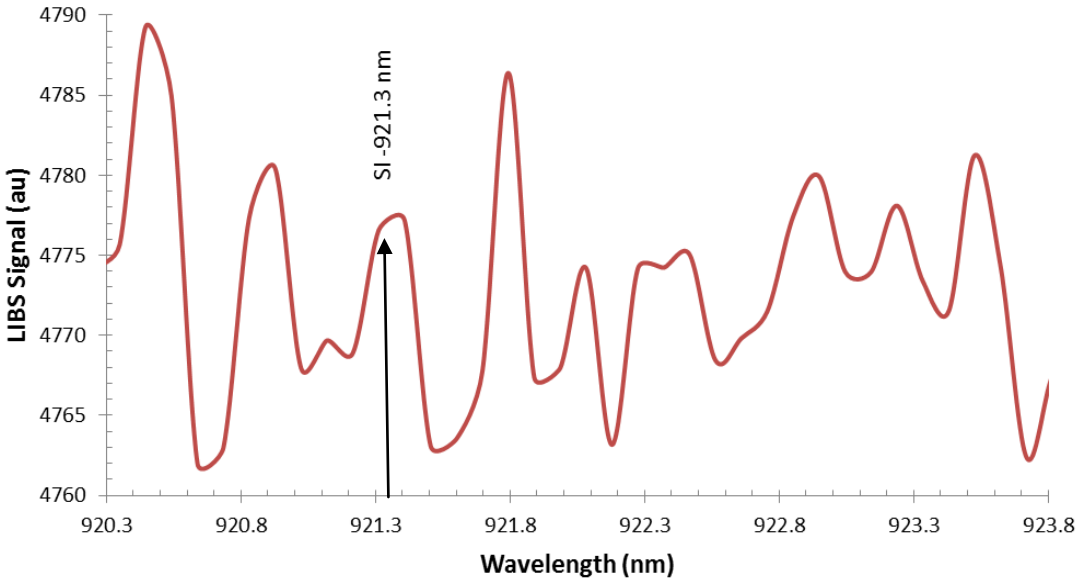

Figure A.60: LIBS spectrum of the cement paste samples using Type (I) cement with fly ash with 3% chloride and 2% sulfate with 921.3 nm atomic transition as a marker.

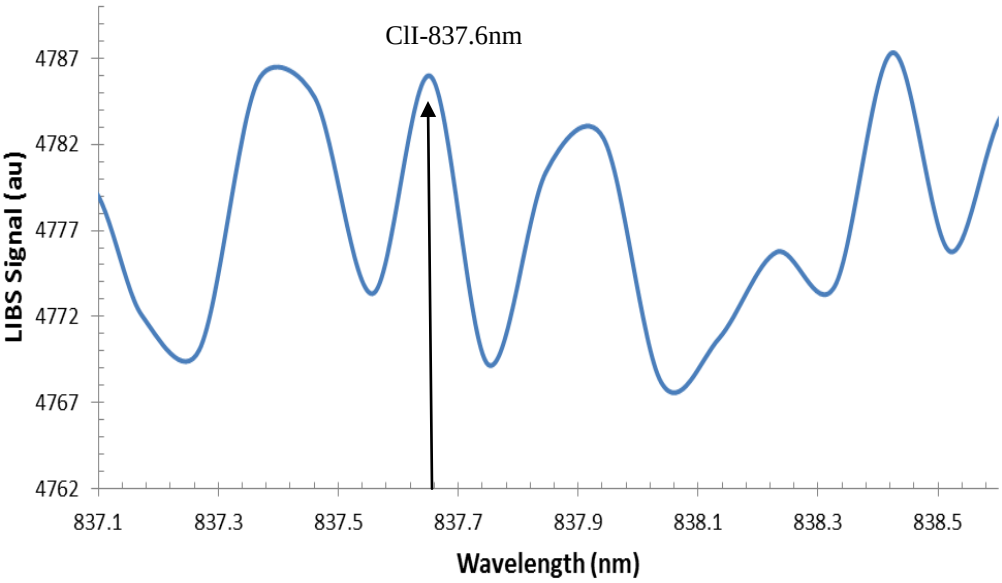

Figure A.61: LIBS spectrum of the cement paste samples using Type (I) cement with fly ash with 3% chloride and 2% sulfate with 837.6 nm atomic transition as a marker.

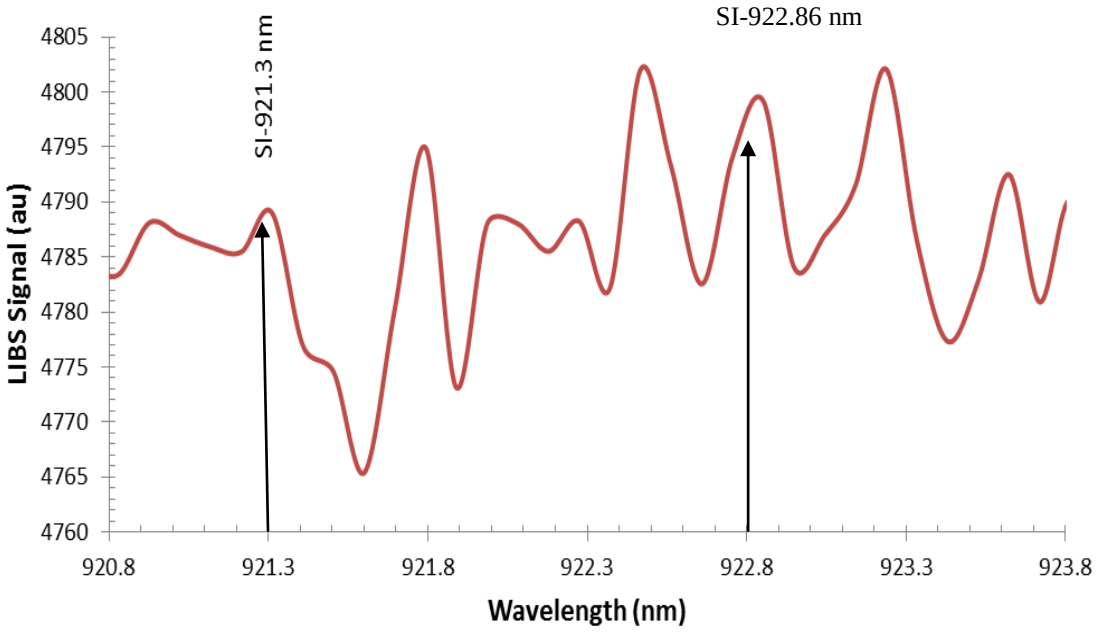

Figure A.62: LIBS spectrum of the cement paste samples using Type (I) cement with silica fume with 2% chloride and 0.5% sulfate with 921.3 nm and 922.86 nm atomic transitions as markers.

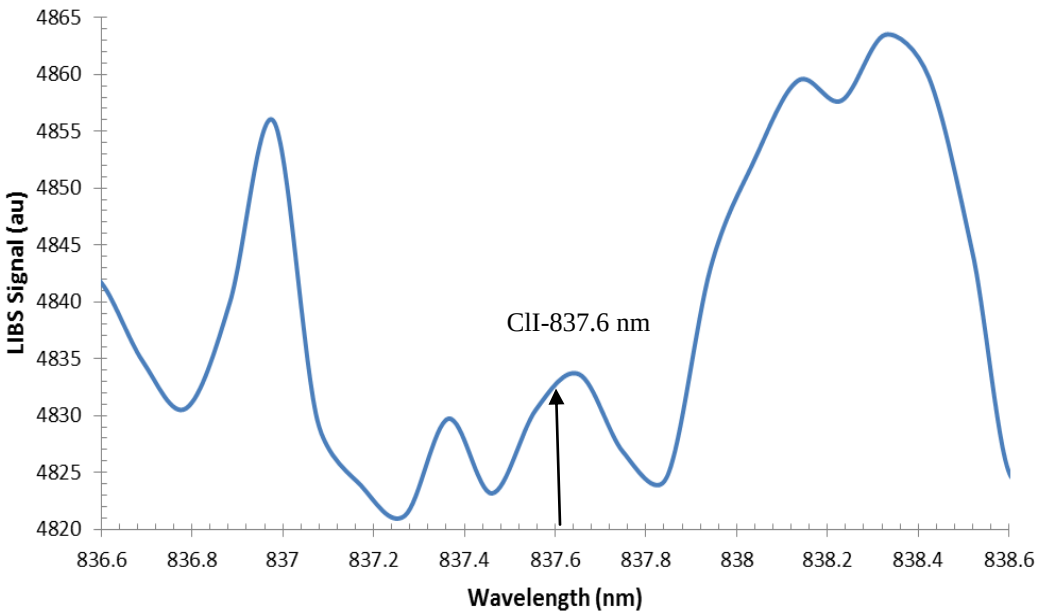

Figure A.63: LIBS spectrum of the cement paste samples using Type (I) cement with silica fume with 2% chloride and 0.5% sulfate with 837.6 nm atomic transition as a marker.

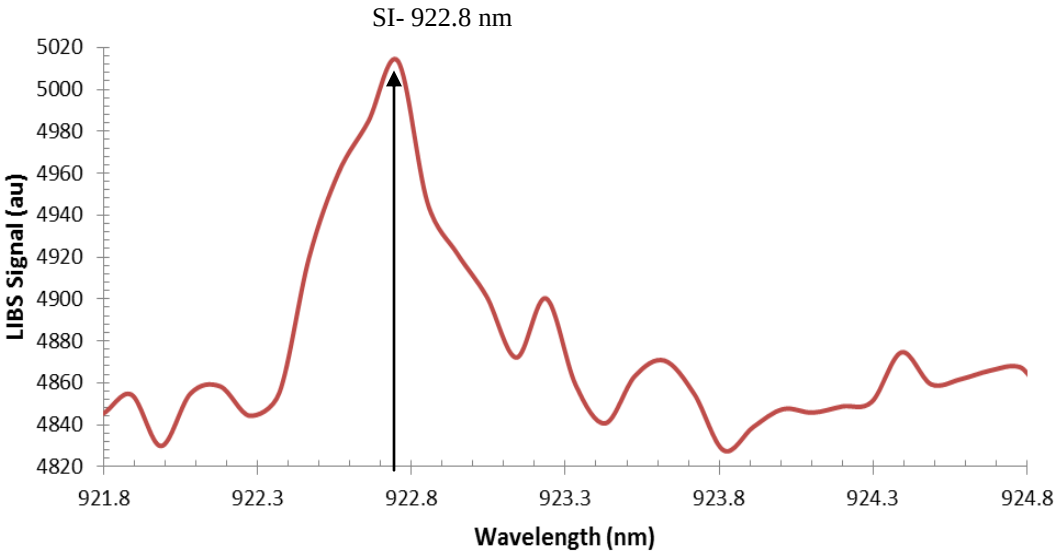

Figure A.64: LIBS spectrum of the cement paste samples using Type (I) cement with silica fume with 2% chloride and 1% sulfate with 922.8 nm atomic transition as a marker.

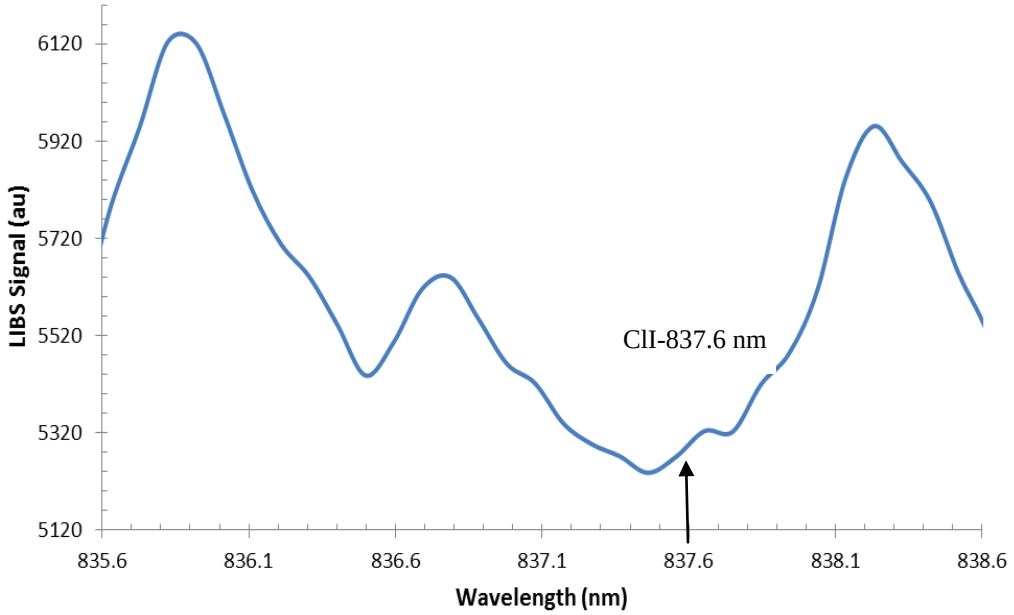

Figure A.65: LIBS spectrum of the cement paste samples using Type (I) cement with silica fume with 2% chloride and 1% sulfate with 837.6 nm atomic transition as a marker.

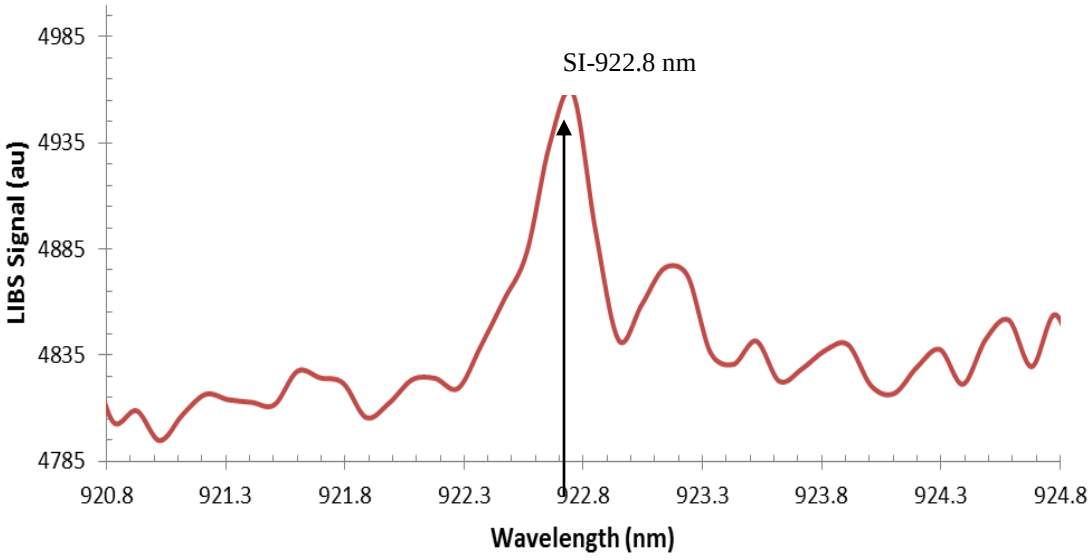

Figure A.66: LIBS spectrum of the cement paste samples using Type (I) cement with silica fume with 0.8% chloride and 0.2% sulfate with 922.8 nm atomic transition as a marker.

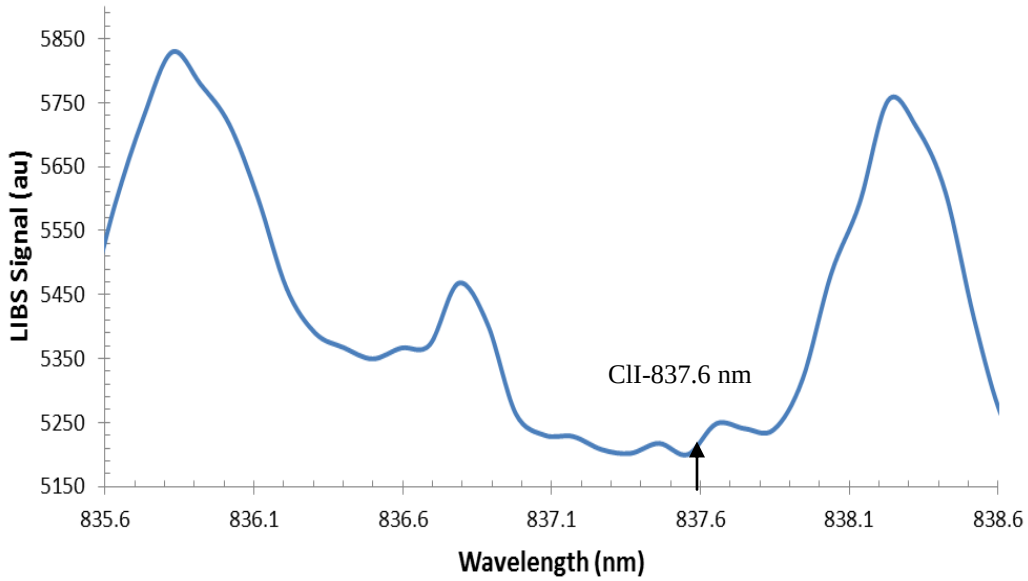

Figure A.67: LIBS spectrum of the cement paste samples using Type (I) cement with silica fume with 3% chloride and 3% sulfate with 837.6 nm atomic transition as a marker.

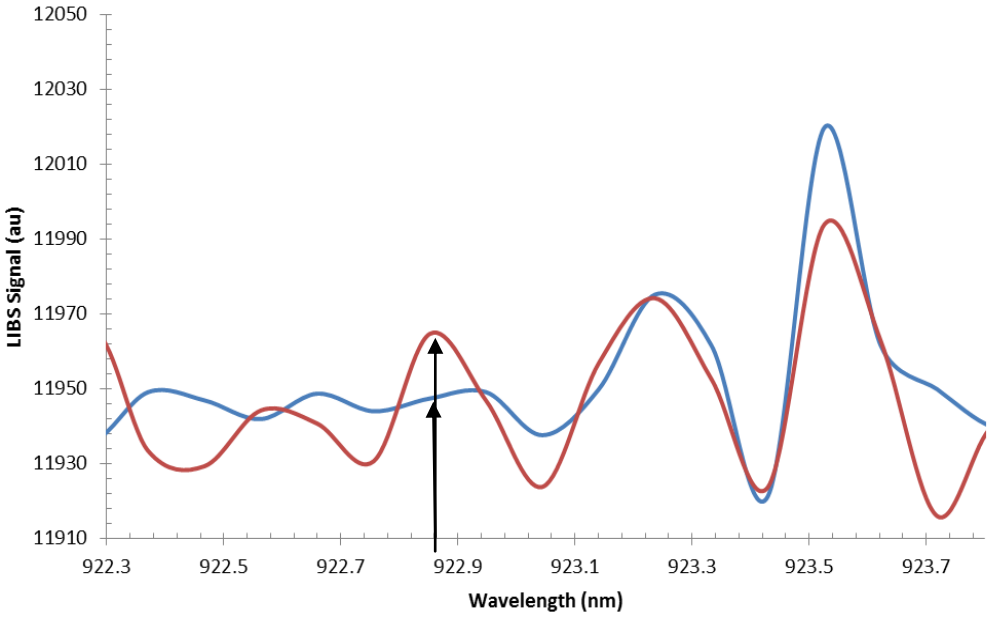

Figure A.68: LIBS spectrum of the cement paste samples using Type (I) cement with fly ash with 0.4% chloride and [0.2% - 0.4%] sulfate with 921.3 nm atomic transition as a marker.

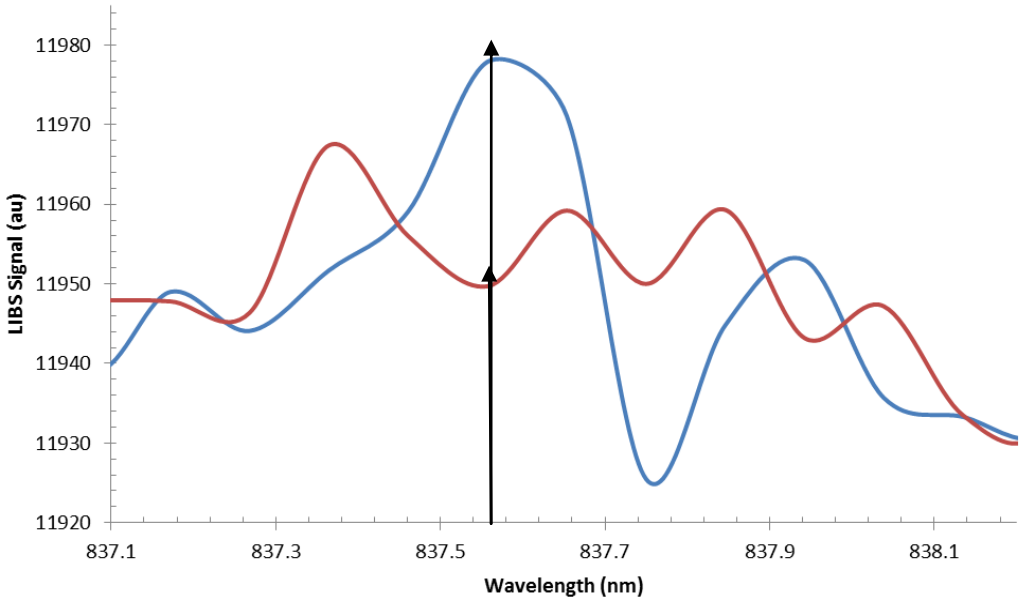

Figure A.69: LIBS spectrum of the cement paste samples using Type (I) cement with silica fume with 0.4% chloride and [0.2% - 0.4%] sulfate with 837.6 nm atomic transition as a marker.

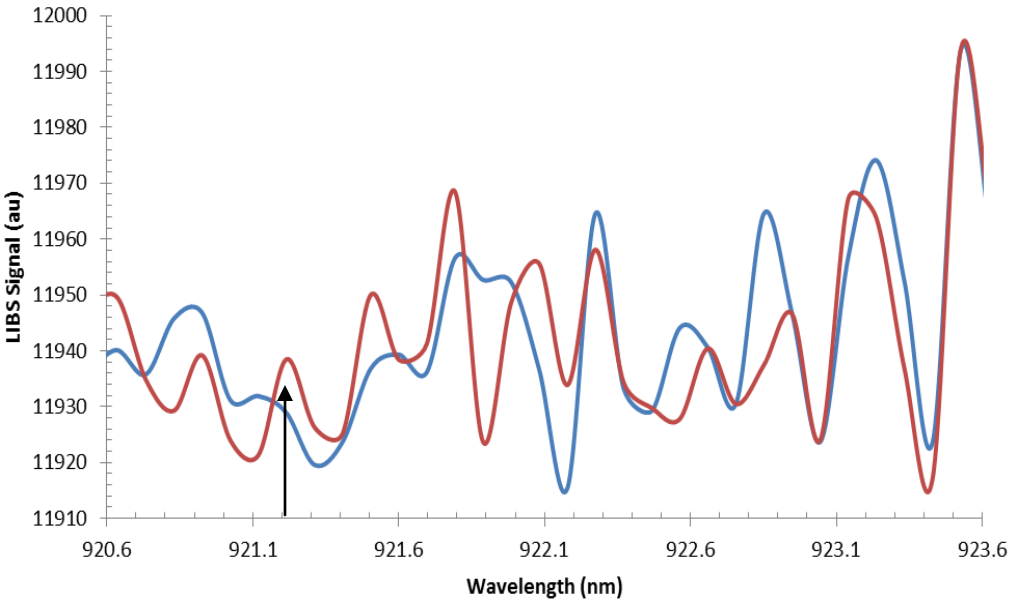

Figure A.70: LIBS spectrum of the cement paste samples using Type (I) cement with silica fume with [0.4% - 0.8%] chloride and 0.4% sulfate with 921.3 nm atomic transition as a marker.

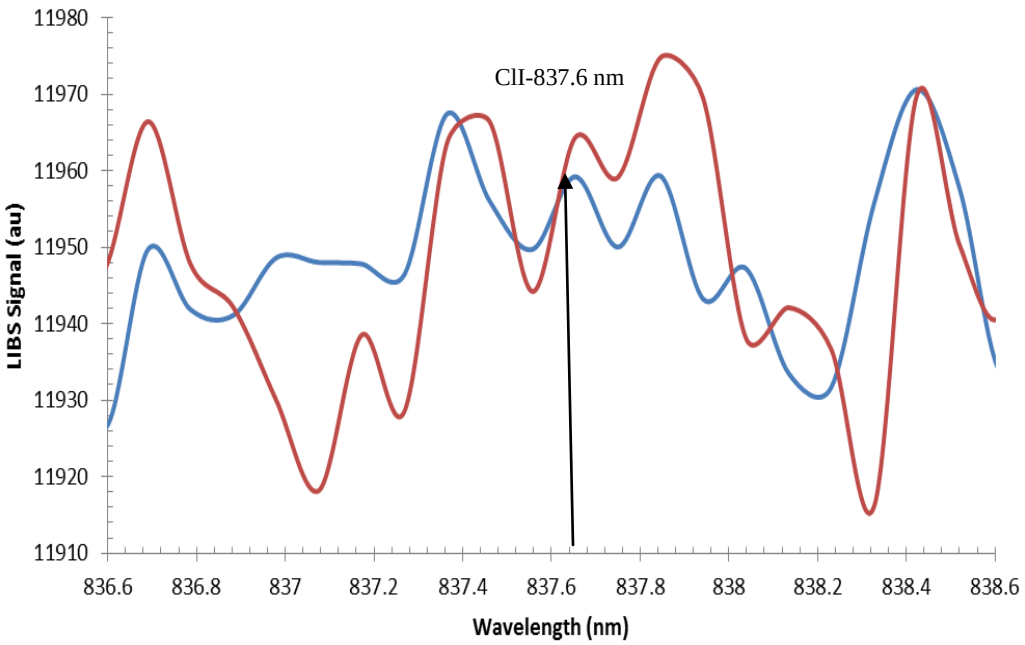

Figure A.71: LIBS spectrum of the cement paste samples using Type (I) cement with silica fume with [0.4% - 0.8%] chloride and 0.4% sulfate with 837.6 nm atomic transition as a marker.

VITAE

NAME: **ABDUL-JABBAR A AL-NAOMI**

NATIONALITY: **YEMENI**

PERMANENT ADDRESS: **THAMAER, YEMEN**

PRESENT ADDRESS: **DHAHRAN, SAUDI ARABIA**

E-MAIL: **alnehmi82@yahoo.com**

g200803780@kfupm.edu.sa

EDUCATION QUALIFICATIONS

Master of Science in Civil Engineering (Structures)

Feb 2008 – Sep 2012

King fahd University of Petroleum and Minerals, Dharan. Saudi Arabia

Bachelor of Engineering (civil)

2002-2006

Thamar University

Frist class with Distinction